

The University of Maine

DigitalCommons@UMaine

Electronic Theses and Dissertations

Fogler Library

Spring 5-5-2023

Feasibility of Thermoplastic Extrusion Welding as a Joining Method For Vacuum-Assisted Additively Manufactured Tooling

Chase C. Flaherty

University of Maine, chase.flaherty@maine.edu

Follow this and additional works at: <https://digitalcommons.library.umaine.edu/etd>



Part of the [Manufacturing Commons](#), and the [Structures and Materials Commons](#)

Recommended Citation

Flaherty, Chase C., "Feasibility of Thermoplastic Extrusion Welding as a Joining Method For Vacuum-Assisted Additively Manufactured Tooling" (2023). *Electronic Theses and Dissertations*. 3772.
<https://digitalcommons.library.umaine.edu/etd/3772>

This Open-Access Thesis is brought to you for free and open access by DigitalCommons@UMaine. It has been accepted for inclusion in Electronic Theses and Dissertations by an authorized administrator of DigitalCommons@UMaine. For more information, please contact um.library.technical.services@maine.edu.

FEASIBILITY OF THERMOPLASTIC EXTRUSION WELDING
AS A JOINING METHOD FOR VACUUM-ASSISTED
ADDITIVELY MANUFACTURED TOOLING

By

Chase Colby Flaherty

B.S. University of Maine, 2021

A THESIS

Submitted in Partial Fulfillment of the

Requirements for the Degree of

Master of Science

(in Mechanical Engineering)

The Graduate School

The University of Maine

May 2023

Advisory Committee:

Dr. Wilhelm Friess, Professor of Mechanical Engineering, Advisor

Dr. Bashir Khoda, Assistant Professor of Mechanical Engineering

Mr. Steve Nolet, Sr. Director for Innovation & Technology, TPI Composites

Copyright 2023

Chase Colby Flaherty

**FEASIBILITY OF THERMOPLASTIC EXTRUSION WELDING
AS A JOINING METHOD FOR VACUUM-ASSISTED
ADDITIVELY MANUFACTURED TOOLING**

By: Chase Colby Flaherty

Thesis Advisor: Dr. Wilhelm Friess

An Abstract of the Thesis Presented
in Partial Fulfillment of the Requirements for the
Degree of Master of Science
In Mechanical Engineering
May 2023

In recent years, additive manufacturing (AM) has been successfully utilized for the production of large-scale composite tooling. Within these endeavors, however, limited research has focused on joining methods between printed sections. This work evaluates the feasibility of thermoplastic extrusion welding as a joining method for additively manufactured tooling structures. This joining method was assessed based on industry specifications of conventional thermoset tooling for wind blade manufacturing utilizing the vacuum-assisted resin transfer molding (VARTM) process. The specifications include requirements for the mechanical strength, vacuum integrity, roughness, and hardness of the tool surface. The feasibility of this welded polymer joint was demonstrated through subscale testing of 1” thick, welded, AM high-impact polystyrene (HIPS) plates. It was found that thermoplastic extrusion welds within AM components can maintain vacuum integrity at 20°C with proper surface preparation and without a surface coating. This met the industry vacuum leakage specification of 10 millibar over 30 minutes with an average loss of 6.61 mbar over 30 minutes through the welded AM plate and bag system. Although beyond the industry specification, the

vacuum leakage was further tested to evaluate performance at an infusion temperature of 80°C. At elevated temperature, the joint and plate lost approximately 26 mbar over 30 minutes. The surface finish was compared with hardness and roughness testing of the welded and machined AM surfaces, showing a decrease in hardness and roughness in the surface of the weld at both temperatures. Standardized ASTM mechanical testing of welded specimens showed an average comparative tensile strength of 80% of the base AM HIPS material. With the addition of undersurface reinforcement within the mold and a surface coating, extrusion welding shows promise for joining large-scale AM tool sections in a manufacturing environment.

DEDICATION

I would like to dedicate this work to my grandfather, Wayne Edward Hilt. Growing up watching his ingenuity and resourcefulness motivated me to pursue a career as an engineer.

Papa, thank you for all you have done for me.

ACKNOWLEDGEMENTS

Many have assisted me throughout this research, I would like to take a moment to thank some of those whose help was imperative to this research.

First and foremost, I would like to thank my graduate advisor, Wilhelm “Alex” Friess, for his attention to detail and responsiveness throughout my research and writing. Your passion for quality work and honest feedback helped me create something I am proud of. I greatly appreciate you for taking this research under your wing. I would still take you up on that sailing trip we discussed!

To my committee member, Steve Nolet, I cannot thank you enough for treating me as a friend and having faith in me from our very first meeting on. I am fortunate to have been able to work with you and learn from your wealth of composites knowledge.

To my committee member, Bashir Khoda, thank you for your friendly positivity and willingness to share you manufacturing knowledge in reviewing this work.

Olivia Murphy, my fiancé and the love of my life, thank you so much for your patience and support in everything that I do. I am so happy with how far we have come together and am so blessed to be spending my life with you beside me.

I must extend an overwhelming thank you to the many staff and students of the UMaine Advanced Structures Composites and Center, whom I have relied on so heavily throughout this endeavor. The ASCC is an amazing conduit for research and learning at the University of Maine. It has been an invaluable experience working with so many talented professionals for the past two years.

John Arimond, my supervisor and project principal investigator, it has been a pleasure working with you. I have learned so much from your management, organization, and crystal clear

communication skills. I am so glad to have been involved with your projects. I wish you and the team the best of luck in the future!

Colby Stokes, my right hand man, thank you for being there for me in and outside the lab for the past two years. Stand tall, and don't ever sell yourself short. You will make an outstanding engineer, my friend.

Justin Willis and Quest Teichman, you both played pivotal roles in making this work come into fruition. Thank you both for your expertise, willingness to help and, of course, for the lighthearted workplace banter.

Trevor Hanson, your professionalism and work quality is impressive, you will make an excellent engineer. Thank you for your support of my work.

Amy Gilman, you played an important role in kick starting my polymer and welding research. Thank you for your hard work and experience in the area.

To other ASCC students like Daniel Wortman, Chris Bock, and Jon Pinkham, thank you for being valuable friends and coworkers. I wish you all the best in your engineering careers.

As I draw this to a close, I would like to thank my family and friends for all they have done for me. I would not have made it this far academically if it were not for their support and encouragement along the way.

TABLE OF CONTENTS

DEDICATION	iii
ACKNOWLEDGEMENTS	iv
TABLE OF CONTENTS	vi
LIST OF TABLES	xi
LIST OF FIGURES	xii
LIST OF EQUATIONS	xv
CHAPTER 1: INTRODUCTION	16
1.1 Project Background	16
1.2 Significance of this Research	16
1.3 Specified Objectives	17
1.4 Thesis Organization	18
CHAPTER 2: REVIEW OF COMPOSITE TOOLING SPECIFICATIONS	19
2.1 Conventional Composite Tooling	19
2.2 Traditional Large-scale Manufacturing Techniques	21
2.3 Tool Requirements for Vacuum Infusion	22
2.3.1 Vacuum Integrity	22
2.3.2 Dimensional Stability	23
2.3.3 Tool Surface Finish	24
2.3.4 Heat Uniformity	25

2.3.5 Tool Functionality	25
2.4 Additively Manufactured Tooling.....	27
2.4.1 Challenges of AM Tooling.....	29
2.4.2 Surface Finish and Durability of AM Tooling	30
2.4.3 Vacuum Integrity of AM Tooling	31
2.4.4 Thermal Expansion and Heat Uniformity of AM Tooling.....	31
2.5 Opportunities and Applications of Large-scale AM Tooling	33
2.5.1 Flexibility within AM material systems	33
2.5.2 AM Tool Heating Systems	34
2.5.3 Sustainability and Environmental Impacts of AM	35
CHAPTER 3: JOINING METHODS	36
3.1 Joining Methods for AM Tooling	36
3.1.1 Potential Joining Techniques.....	36
3.1.2 Adhesives.....	37
3.1.3 Mechanical Fastening	38
3.2 Welding of Thermoplastics	40
3.2.1 Hot Gas Welding	41
3.2.2 Extrusion Welding.....	42
3.2.3 Applications of Extrusion Welding	44
3.2.4 Parameters of Extrusion Welding.....	45

3.3 Weldability of Thermoplastic Materials	46
3.3.1 Models of Polymer Interphases	47
3.3.2 Material: High Impact Polystyrene (HIPS) Thermoplastic	48
3.4 Manufacturing the Thermoplastic Joint	49
3.4.1 Extrusion Welded Joint Design	50
3.4.2 Extrusion Welding Materials and Methods	50
3.4.3 Extrusion Weld Calibration	51
3.4.4 Improving Extrusion Welds.....	54
3.4.5 Selected Joining Method	57
3.4.6 Manufacturing and Welding AM Components for Testing.....	57
CHAPTER 4: EVALUATION OF THE JOINING METHOD	61
4.1 Surface Vacuum Integrity of Welded Components	61
4.1.1 Vacuum Bagging Procedure.....	63
4.1.2 Vacuum Leakage Test Set-up.....	65
4.1.3 Calibration & Processing Test Results	68
4.1.4 Vacuum Leak Rate Behavior.....	69
4.1.5 Baseline Leak Rate in a Solid HIPS Plate	70
4.1.6 Leakage Testing Welded AM Components at 20°C	73
4.1.7 Leak Testing AM Components at 80°C	76
4.2 Surface Finish.....	79

4.2.1 Surface Finish Specification for Thermoset Tooling Surfaces.....	79
4.2.2 Surface Hardness Results	80
4.2.3 Surface Hardness Results at 80°C	82
4.2.4 Comparing Surface Hardness Results at 20°C and 80°C	84
4.2.5 Surface Roughness Results.....	85
4.2.6 Surface Roughness Results at 80°C.....	86
4.2.7 Comparing Surface Roughness Results at 20°C and 80°C.....	87
4.3 Mechanical Testing of 3D Printed Components with Welded Joints	88
4.3.1 Tensile Testing of Welded AM Specimens.....	88
4.3.2 Results of Tensile Testing	91
4.3.3 Tensile Failure	95
4.3.4 Flexural Testing of Welded AM Specimens	98
4.3.5 Results of Flexural Testing.....	99
4.3.6 Flexural Failure.....	103
4.4 Weld Inspection using Microscopy.....	106
4.4.1 Specimen Inspection Preparation	106
4.4.2 Weld Line Inspection.....	108
4.4.3 Porosity Inspection within the Weld	113
CHAPTER 5: CONCLUSIONS AND RECOMMENDATIONS	115
5.1 Conclusions.....	115

5.1.1 Feasibility of the Joining Method Between Tooling Surfaces	115
5.1.2 Recommendation of Full-Scale Welded Joint Design.....	116
5.2 Recommendations for Future Work.....	117
5.2.1 Thermoplastic Composite Materials.....	117
5.2.2 Further Testing of Welded Components	117
5.2.3 Joining other Large-Scale AM Structures.	118
REFERENCES	119
APPENDIX A: LIST OF ABBREVIATIONS	126
APPENDIX B: CALIBRATION	127
APPENDIX C: RECOMMENDED MANUFACTURING PROCEDURE.....	128
APPENDIX D: TECHNICAL DATA SHEETS	133
RESEARCH PERSONNEL.....	Error! Bookmark not defined.
Members of the Committee.....	141
Biography of the Author	142

LIST OF TABLES

Table 1: Vacuum-assisted Tooling specifications and influencing characteristics	27
Table 2: Challenges of Current State Vacuum-assisted AM Tooling.....	33
Table 3: Process Parameters for Extrusion Welding [53].....	45
Table 4: Properties of HIPS Material [66],[67]	49
Table 5: Causes of Defects within Calibration Welds	53
Table 6: TPI Shell Mold Specification Section: Vacuum Integrity [70]	62
Table 7: Leak Rate in Five Vacuum Bags on a Solid Plate over 30 Minutes.....	72
Table 8: Leak Rate of Welded AM HIPS Plate at 20°C	74
Table 9: Surface Specifications for Conventional Thermoset Blade Molds [70].....	79
Table 10: Hardness of HIPS at 20°C	81
Table 11: Average Hardness of Printed and Welded HIPS at 20°C	82
Table 12: Hardness of HIPS at 80°C	83
Table 13: Average Hardness of Printed and Welded HIPS at 80°C	84
Table 14: Roughness of Printed and Welded HIPS at 20°C	85
Table 15: Average Roughness of Printed and Welded HIPS at 80°C	86
Table 16: Tensile Testing Results.....	92
Table 17: Comparative Weld Strength of Tested Specimens	93
Table 18: Failure Modes of Tensile Specimens.....	96
Table 19: Flexural Testing Results	101
Table 20: Comparative Weld Strength in Flexure	102
Table 21: Failure Modes of Flexural Specimens	105
Table 22: Relevant Calibration Information for Mechanical Testing.....	127

LIST OF FIGURES

Figure 1: Plug and Mold Manufacturing	19
Figure 2: Direct to Mold Using AM	20
Figure 3: Large-scale Vacuum Infusion (Provided by TPI Composites Inc.) [10].....	22
Figure 4: ORNL & TPI Inc. 2017 - AM of Wind Turbine Molds [2]	29
Figure 5: ORNL, Large-Scale AM of Self-Heated Molds [48].....	35
Figure 6: Classification of Joining Techniques	36
Figure 7: Classification of Fusion Bonding Techniques.....	40
Figure 8: Set-up and Initial Hot Gas Pendulum Weld	42
Figure 9: Extrusion Welding Process	43
Figure 10: Abbeon Hot Gas Welder, Extrusion Welder, and a Mounted Extruder [59]	44
Figure 11: Molecular Organization of Amorphous and Semi-crystalline Polymers [61].....	46
Figure 12: Intermolecular Healing of Interface [63], [64], [65]	48
Figure 13: Extrusion Weld Design	50
Figure 14: Abbeon HSK26 GSX Extrusion Welder [68]	51
Figure 15: Extrusion Welds conducted for Welder Calibration.	52
Figure 16: Extrusion Welding with Trolley Attached to the Welding foot.	54
Figure 17: Single V Butt Weld Foot [73] Attached to Weld Trolley	55
Figure 18: Compressing Extrudate into Joint Using Silicone Roller.....	56
Figure 19: Post-Calibration Weld in HIPS Plate (left) & Cross-section of Welded Joint.....	56
Figure 20: HIPS Plate Printed on JuggerBot 3D Printer.....	58
Figure 21: Prepared Joint V-Groove in Machined AM Plate	59
Figure 22: Extrusion Welding AM Plate	60

Figure 23: Joint Evaluation.....	61
Figure 24: Evaluation of Vacuum Integrity in a Welded AM Plate	62
Figure 25: Vacuum Bagging Process.....	64
Figure 26: Vacuum Leakage Test Set-up Diagram.....	66
Figure 27: Vacuum Bag over the Welded AM Plate with an Inline Transducer	66
Figure 28: Resin Coated Edges for Improved Surface Seal	67
Figure 29: Data Acquisition Set-up	68
Figure 30: Vacuum Leak Rate Behavior	70
Figure 31: Baseline Vacuum Leak Rate in Solid HIPS Plate	71
Figure 32: Pressure Change due to Leakage of Vacuum in Welded AM HIPS Plate at 20°C	73
Figure 33: Average Leakage due to Permeation through the Welded AM Plate.....	75
Figure 34: Welded AM Plate in Oven at 80°C	77
Figure 35: 25 Millibar Vacuum Loss in Welded AM HIPS Plate at 80°C.....	78
Figure 36: Starrett 3805D Shore D Durometer in use on weld.....	80
Figure 37: Tensile Test Setup	89
Figure 38: Diagram of Material Anisotropy, Welded Joint, and Load Direction.....	90
Figure 39: Force Vs Displacement Response of all Specimens	94
Figure 40: Stress Vs Strain Response for all Welded HIP Tensile Specimens	95
Figure 41: Failure Along Weld line in Tensile Specimen T7.....	97
Figure 42: Failure in Printed Material in Tensile Specimen.....	97
Figure 43: Flexural Test Set-up	98
Figure 44: Load Response of all Specimens in Adapted D790 Flexure	99
Figure 45: Stress Vs Strain Response of all Welded HIPS Flexural Specimens	103

Figure 46: Failure along Weld Bond Line in Flexural Specimen B2	104
Figure 47: Failure in Printed Material in Flexural Specimen	104
Figure 48: Sliced Welded Specimens for Inspection	107
Figure 49: Diagram of the Weld Inspection Locations.....	108
Figure 50: Material Difference at Weld Line in a Failed Specimen.....	109
Figure 51: Weld Bond Line at the Root (x50)	110
Figure 52: Weld Bond Line at the Root (x2000)	111
Figure 53: Porosity at Weld Bond Line near the Top Surface (x100).....	112
Figure 54: Porosity in Weld Surface & AM Surface	113
Figure 55: Porosity at the Root within Weld Material (x200)	114
Figure 56: Joint Design Diagram [68]	116
Figure 57: Render of Welded Joint Between Tooling Segments.....	129
Figure 58: Rear Isometric of Welding Process with Slight Tilt from Operator.....	132

LIST OF EQUATIONS

Equation 1: Absolute Pressure	68
Equation 2: Vacuum Leak Rate due to Permeation of the Welded AM Plate	74
Equation 3: Tensile Strength at Peak Load.....	91
Equation 4: Comparative Weld Strength	92
Equation 5: Flexural Stress at Peak Load	99
Equation 6: Flexural Strain at Peak Load	100

CHAPTER 1: INTRODUCTION

1.1 Project Background

The United States Department of Energy, Office of Energy Efficiency and Renewable Energy (EERE), Advanced Manufacturing Office (AMO) (Award Number: [DE-EE0009401]) awarded the University of Maine Advanced Structures and Composites Center (ASCC) funding to further the development of AM wind blade molds with the goal of a cost and lead time to market reduction of 25%. The partners on this project include TPI Composites, Oak Ridge National Laboratory (ORNL), Siemens Gamesa Renewable Energy (SGRE), Ingersoll Machine Tools, and Techmer Materials.

1.2 Significance of this Research

Current wind blade production is limited by time-consuming plug and mold manufacturing methods which can involve long lead times of 16 to 20 months from plug to finished blade. To innovate in this rapidly developing market to continue to meet the production needs of new wind energy developments, new manufacturing methods are needed to reduce the time to market and the cost of new blades [1].

With the recent advances in large-scale 3D printing technology, AM is poised to revolutionize wind blade product development. By directly manufacturing modular blade shell tooling components in large, joined segments, first-article blades for structural testing and certification can be completed significantly faster.

This modular approach to blade shell fabrication will better enable the manufacturing of families of blades, wherein a common root and mid-span structure can be mated with a variety of tip designs for a variety of site conditions. Segmented tooling also allows for the use of conventional transportation which reduces costs, indirect energy consumption, and greatly reduces the storage space required. This could be particularly advantageous for the wind industry, reducing transportation and manufacturing costs across the board [1].

This approach, however, introduces the challenge of joining the modular AM mold segments. Innovative research in AM joining methods is not only vital to the advancement of this technology in the composite tooling application but has the potential to impact the design of AM structures in a variety of industry applications.

1.3 Specified Objectives

This study has four objectives:

1. To conduct a literature review to understand industry manufacturing specifications and potential joining applications of modern vacuum-assisted composite tooling.
2. To design a joining method for thermoplastic components that meets the determined industrial tooling specifications.
3. To assess the surface vacuum integrity, surface finish, and mechanical properties of the resulting joint design.
4. To make recommendations for the application of the chosen joining method based on the findings of vacuum integrity, strength, surface hardness, and surface roughness.

1.4 Thesis Organization

This thesis is divided into five chapters; Chapter 1 is an introduction to the work, the significance of this research, project background, and its detailed objectives. In Chapter 2 is a literature review of composite tooling, with a focus on the manufacturing methods and specifications of traditional composite tooling, as well as an exploration of the present state of additively manufactured tooling. Chapter 3: Joining methods, is an investigation of various joining methods and the downselection resulting in utilizing thermoplastic extrusion welding as the joining method between mold segments. Chapter 4 presents the results of the testing conducted to evaluate the feasibility of extrusion welding as a joining method for segmented wind blade tooling. The testing includes vacuum leakage testing, hardness and roughness of the surface, ASTM mechanical testing, and weld inspection using microscopy. This chapter also discusses how well this joining method and material meet the project tooling specifications. Finally, Chapter 5: Conclusions & Recommendations, explains to what degree the thesis objectives have been accomplished by presenting the main findings and contributions of the thesis alongside the recommendations for future research.

CHAPTER 2: REVIEW OF COMPOSITE TOOLING SPECIFICATIONS

2.1 Conventional Composite Tooling

Composite tools are designed and manufactured using a variety of materials and methods that often use metals such as steel, invar, and aluminum, or a variety of fiber-reinforced, polymer matrix composites. Metal tools generally have higher durability and can be machined, but are heavier and more expensive, especially for large-scale tools. Composite tools are more difficult to manufacture and are less durable, but are lighter and have the advantage of a similar thermal expansion as the components that are being manufactured.

For large-scale components, it is imperative to leverage the ability of composite molds to consistently reproduce complex components at reasonable lifecycle costs. A very common manufacturing method for large-scale tooling with complex curvatures is the plug-and-mold manufacturing method [2] as shown in Figure 1 below.

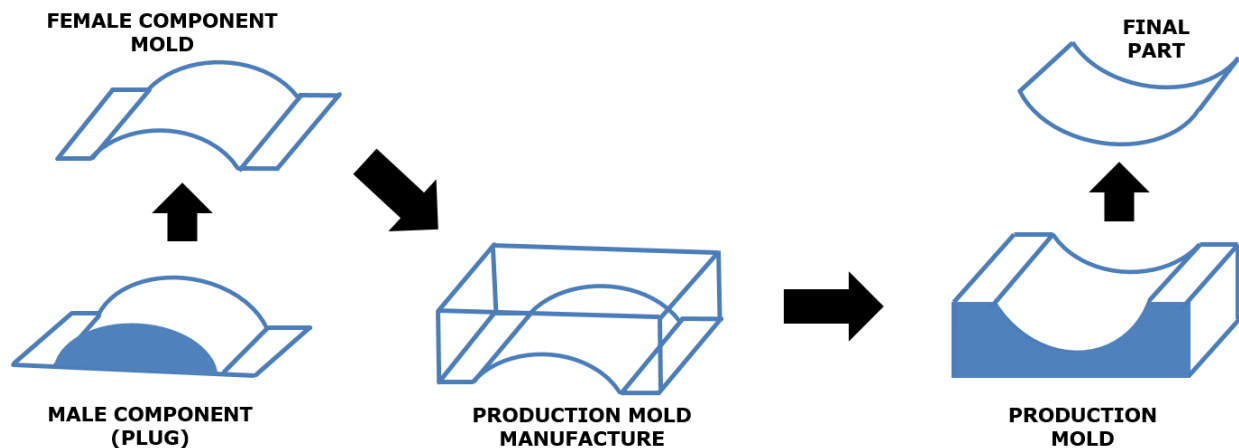


Figure 1: Plug and Mold Manufacturing

This production method involves a plug, or male component, which is created through a labor-intensive highly skilled machining and hand-finishing process to achieve the final surface profile. That profile is then reflected in the paired tooling component; the plug is then used to manufacture

the tooling shell molds, or female tooling components, that will be used in production. This manufacturing method allows for the replication of multiple sets of molds off the single plug or pattern after initial manufacture. The challenge is that this method is costly and limited by long lead times, from months to years, from the manufacture of the first tooling plug to mold to the final part [1]. Thus, there is an ongoing shift from tool and die manufacturers to “eliminate the pattern” or plug via implementing new direct-to-mold manufacturing methods for large-scale components [3]. A diagram direct to mold manufacturing is shown in Figure 2 below.

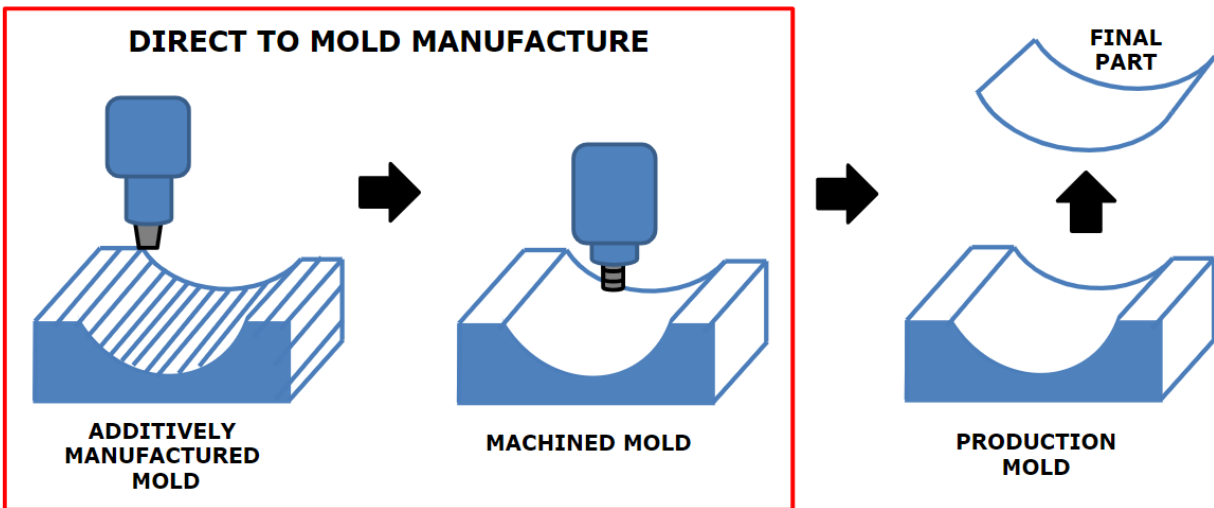


Figure 2: Direct to Mold Using AM

This mold fabrication method involves the significant challenge of fabricating the complex curvature of a mold surface using AM. This practice has been well demonstrated for small-scale component molds [4], but becomes very costly as parts increase in scale [5]. New and improved manufacturing methods are necessary to reduce both costs and the time to market of tooling for new parts in large-scale composites industries, and large-scale AM may be the way to achieve that.

2.2 Traditional Large-scale Manufacturing Techniques

Continuous Fiber-Reinforced Polymer composites (FRP) are prevalent in today's large-scale manufacturing industry. Thermoset-matrix composites, such as glass or carbon fiber reinforced epoxy, phenolic, or polyester-based composites, are utilized in the construction, wind, aerospace, automobile, and marine industries. These composites can be manufactured in a variety of ways, although vacuum infusion processes are preferred for the manufacturing of high-quality large-scale FRP components.

Vacuum-assisted resin transfer molding, or (VARTM), is a well-documented resin infusion process that utilizes a pressure gradient between the reservoir of resin at atmospheric pressure, and the vacuum bag to push the resin through a fiber reinforcement on the tool surface, infusing the part and forming the composite laminate [6]. The Seeman Composites Resin Infusion Molding process (SCRIMP), is a variation of VARTM that incorporates highly permeable distribution media that assists with the continuous flow and consistent distribution of resin across the mold surface [7].

The advantages of this process are reduced labor cost compared to traditional hand lay-up and lower capital costs associated with autoclave consolidation, while producing higher fiber volume fraction laminates leading to improved mechanical properties for large components, and enhanced environmental control of hazardous styrene and volatile organic compound (VOC) emissions involved in the infusion process. This process is easily scalable and flexible, which is particularly important in maintaining affordability in large-composite manufacturing applications that are common in many of today's industries [8]. The standard VARTM manufacturing guidelines are outlined in ASTM D 5687 [9].



Figure 3: Large-scale Vacuum Infusion (Provided by TPI Composites Inc.) [10]

2.3 Tool Requirements for Vacuum Infusion

Composite tools must be designed and fabricated with their intended manufacturing method in mind. Tooling utilizing the VARTM manufacturing process must meet certain requirements to ensure quality in produced components. These requirements include tool surface shape accuracy, vacuum integrity, low thermal expansion, heat uniformity, and surface finish. Since these requirements are largely dependent on the material used, material selection plays a crucial role in determining the overall tool quality and, consequently, the final part quality.

2.3.1 Vacuum Integrity

As the scale of a vacuum infusion increases, the potential for air leakage into the bag increases. As a result, process repeatability and the resulting part quality is heavily dependent on technician experience and skill in addition to the quality of the vacuum bagging equipment used.

Mechanically, Laminate consolidation forces are limited to the pressure difference between the external environment (one atmosphere) and the pressure created under the vacuum bag [6]. As a result, the pressures applied in a VARTM process are much lower than in a closed resin transfer molding or in-autoclave process, thus it is vital to maintain a high degree of vacuum integrity over the surface of the tool to reduce air voids during infusion. VARTM processes can typically achieve fiber volume fractions (FVF) of about 50% [11]. The ASTM standard for composite panel specimen preparation (D 5687) requires tooling surfaces to maintain a minimum vacuum capacity at the lay-up site of at least 75 kPa [750 mbar] with a drop of no more than 3.5 kPa [35 mbar] over 5 minutes. This process requires a pressure tolerance within 5% of the indicated pressure at all times [9]. Modern VARTM applications, such as aerospace and wind blade manufacturing, require far higher vacuum capacity requirements near a complete vacuum with even tighter loss tolerances. This can be a significant challenge for the design of tooling for vacuum infusion processes, especially as composite components grow in scale. To maintain part quality, it is imperative to eliminate leaks in the tooling and vacuum system. Entrained air from vacuum leaks causes improper resin flow and bubbles which leads to defects such as surface porosity and voids in the cured part. The leakage of air can also lead to a significant loss in the pressure needed to obtain the required fiber volume fraction. Typical leak rates in high-performance aerospace industry applications have been reported to be 3-5 mbar per minute during an infusion. These rates can only be achieved with tooling designed for VARTM applications and properly installed bags [7].

2.3.2 Dimensional Stability

Tooling translates its shape to the manufactured parts by undergoing the same thermal loading and cycling as is required to cure the parts. As a result of this relationship, shape accuracy, i.e., the resistance to tool warpage, shrinkage, and part spring-in, is dependent on many complex factors.

These include cure cycle, surface material, surface condition, as well as part geometry [12]. The control of thermal expansion, shrinkage, and tool-part interactions are vital aspects of producing a high-quality dimensionally accurate final part [13]. It is important to have similar or less thermal expansion in the tool than the laminated part to reduce interactions as the composite cures and cools. Tool-part interaction can lead to interfacial shear stresses between the mold and laminate which induce residual stresses in the part during cure. These residual stresses in the laminate may lead to warpage in the final component after the curing cycle completes [14]. Tool part interaction can promote warpage, initiate matrix cracks, and cause delamination. To combat this, a common practice used to eliminate tool-part interactions in the industry is the matching of coefficient of thermal expansion (CTE), where the CTE within the tooling surface is similar or equal to that of the composite part for manufacture [15]. A standard test method for determining CTE is ASTM D696 [16]. Spring-back, or the tendency for a curved part to deform toward a smaller radius of curvature results is an additional thermal stability concern. This results from both the matrix shrink during the curing process and the difference between the CTE of the reinforcement and matrix. This difference in CTE between the fiber and matrix can result in a shrinkage as much as 6% during cross-linking [17]. Both mold and laminate materials and their thickness influence spring-back deformation because of mold part interaction and area moment of inertia respectively. Mold surface material has been shown to affect spring-back, for example, a low CTE invar molds experience ~21% less spring back than a stainless-steel mold material [18].

2.3.3 Tool Surface Finish

The durability and surface finish of the tool affects the service life of the mold and its vacuum integrity. The hardness and roughness of the tool surface determine the ease of part release from the mold, the quality of part surface, as well as the resistance to fatigue and abrasion-induced

fracture of the tools [19]. Roughness that leads to higher parting forces during demolding will negatively impact service life of the mold and require more maintenance. These properties are dependent on the tooling material and surface coatings used to fabricate the surface, which becomes especially important for production tooling. The most common standards for the measurement of surface roughness “Ra” and surface hardness are ISO 4287 [20] and shore D scale as per ASTM D2240 [21], respectively. The ASTM standard for composite panel specimen surface preparation, D 5687, requires surfaces in contact with the laminate to have a maximum average surface roughness of 0.8 μm [32 $\mu\text{in.}$] and preferably 0.4 μm [16 $\mu\text{in.}$] [9]. Advanced applications such as aerospace or wind blade molds often require smoother, harder tooling surfaces for high-quality components.

2.3.4 Heat Uniformity

Tools must be able to withstand elevated temperatures during the curing cycle step of manufacture. Although infusion temperatures are resin specific, the heat uniformity and capacity of the tool are not. ASTM D 5687 dictates that the temperature inside or near the laminate should be used for monitoring temperature during cure. It is recommended that the mold surface should have a tolerance of $\pm 2^\circ\text{C}$ [$\pm 5^\circ\text{F}$] maintained from the specified temperature of the surface in contact with the mold during ramp and hold [9]. Heat uniformity is dependent on the size, thermal conductivity, and heat capacity of the mold material, thus larger thicker laminated components may have a tighter tolerance for maintaining heat over surfaces of high-quality components [22].

2.3.5 Tool Functionality

The functionality of tooling has become a growing topic of interest in recent years. Innovation has led to molds equipped with various temperature-controlled internal heating and cooling systems, sensors for cure monitoring, as well as alignment datums and markings. To achieve elevated tool

surface temperatures during cure, traditional tooling utilizes heated closed molds, or heating within autoclaves or large ovens, however, large-scale tools rarely have the benefit of an autoclave due to the size and cost restrictions of these environmental chambers. Therefore, VARTM and internal self-heating systems are utilized for out-of-autoclave (OOA) applications. Common OOA heating systems include embedded resistive heating elements within the tooling surface such as fabric or wires [23], as well as forced liquid coolant systems utilizing oil, hot air, or water [24]. These systems must be designed to the appropriate heat flux for mold surface zone(s) to maintain uniform heat application and uniformity across mold surfaces. Appropriate insulation is required for the isolation of the tool surface from potential heat sink losses in the frame. Additional functionality of modern molds includes temperature control as well as cure monitoring systems. Most heating systems are PLC or software-controlled, with thermocouples monitoring the process temperature of the tool surface and the limit, or maximum temperature, of internal heating elements within the mold. Additional sensors for flow and cure monitoring include cameras in the case of transparent tooling, electromagnetic sensors, mechanical sensors, thermo-dynamical sensors, etc. Recent studies have focused on embedded monitoring array systems with multiple sensors, namely surface pressure, temperature, and displacement [25] as well as full-field resin flow monitoring using optical reflectometry and fiber optic sensors [26]. Other tooling functionalities include adjustability in the connection of the surface to the mold backing structure, or “egg-crate”, as well as a variety of opening and closing architectures depending on the components that are to be manufactured [2].

Table 1 below summarizes the specifications for vacuum-assisted tooling surfaces, the primary characteristics that influence them, and some relevant standardized test methods for evaluation of these characteristics.

Table 1: Vacuum-assisted Tooling specifications and influencing characteristics

Requirement	Characteristics	Specifications	Relevant Standard(s)
Vacuum Integrity	<i>Surface Finish</i>	Vacuum > 75 kPa [750 mbar],	ASTM D 5687 [9]
	<i>Surface Material</i>	Drop < 3.5 kPa [35 mbar] / 5 min	
	<i>Vacuum System</i>		
Dimensional Stability	<i>Surface Material</i>	CTE matching	ASTM D696 – 16 [16]
	<i>Structural Design</i>	Low anisotropy of CTE	
Durability	<i>Surface Finish</i>	Shore D 80	ASTM D2240 [21], ASTM D 5687 [9], ISO 4287 [20]
	<i>Surface Material</i>	Ra < of 0.8 μm [32 $\mu\text{in.}$]	
Heat Uniformity	<i>Surface Material</i>	Tolerance of $\pm 2^{\circ}\text{C}$ [$\pm 5^{\circ}\text{F}$] across surface	ASTM D 5687 [9] ASTM E1461 – 13 [27]
	<i>Heating System</i>		

2.4 Additively Manufactured Tooling

With the recent advances in large-scale 3D printing technology, AM is poised to revolutionize large-scale composite manufacturing and development. 3D printing is an additive process in which fiber-reinforced polymer material is deposited onto itself to form a final part. Most commonly, fusion deposition modeling (FDM) is a form of 3D printing that involves the melting and extrusion of a heated thermoplastic material into desired shape. AM has been growing in popularity as an innovative solution to manufacture composite tooling [28]. AM allows the direct manufacture of complex shapes and curvatures, including those found in composite molds, thus eliminating the pattern (or plug) manufacturing step in creating first-article parts [3]. Another advancement in many modern AM machines is the simultaneous outfitting for subtractive manufacturing, or machining, allowing high tolerance finishing of surfaces post-print. This can lead to much faster

delivery of first article parts, a reduction of waste due to the elimination of plug manufacturing, and a significant reduction in labor to produce production-ready tooling components.

To quantify this, according to a cost and lead time analysis conducted by ORNL on AM of wind turbine and autoclave molds, AM can reduce manufacturing costs by 10 to 100 times and reduce time to market from months to weeks [29], [33]. This is especially true with the decreasing cost of base materials, higher deposition rates, and expanding print windows of modern large-scale 3D printers. Large-scale AM has significantly widened the applications of the technology, especially in the wind energy and aerospace industries as shown by the AM wind blade mold produced by ORNL in Figure 4. Advances in the size of the print area via large-scale 3D printers, such as Ingersoll Machine Tool's MasterPrint™ [30] or the Cincinnati Machine's "BAAM" [31] can produce much larger structures at a higher deposition rate. In addition to the advantage of size, these large machines can be equipped with attachments that allow 5-axis machining of parts, yielding high-tolerance surfaces on directly printed parts.



Figure 4: ORNL & TPI Inc. 2017 - AM of Wind Turbine Molds [2]

AM tooling technologies are being researched and employed in many sectors. At the large scale, these primarily include wind energy systems [1], [2], marine manufacturing in the form of watercraft layup tooling [32], the construction of precast concrete molds [33], as well as high-tolerance molds for hybrid aerospace components [3]. As AM develops further and material costs are reduced, the application of this technology will widen to further industries as it competes with current state manufacturing methods.

2.4.1 Challenges of AM Tooling

AM has potential opportunities for application in many industries, however, this new mold manufacturing technique still has material and design challenges to overcome. The primary challenges for vacuum-assisted AM tooling are meeting requirements for durability, vacuum integrity, and anisotropy of thermal expansion for production quality tools.

2.4.2 Surface Finish and Durability of AM Tooling

The hardness and roughness of the tool surface are properties that determine the resistance to fatigue and abrasion-induced fracture of the tooling surface as well as part release from the mold [19]. Within AM components, there is an inverse relationship between the deposition rate and surface finish; the faster the deposition rate, the poorer the surface finish [34]. This is due to the unavoidable stepped formation inherent in layer-by-layer material deposition [35]. However, the finish machining capabilities of large gantry systems have drastically improved the surface finish of AM tooling. The two common methods to address surface finish in AM tooling are over-depositing material and CNC machining to the exact dimensions of the target surface profile, or over-machining the surface to leave a specified tolerance for layer(s) of coating to be applied to achieve the target surface profile [36]. Oak Ridge National Laboratory demonstrated the validity of AM tools for in-autoclave applications, aerospace-quality carbon fiber epoxy parts with less than 0.1 mm (0.004 in) deformation within the layup area on uncoated AM surfaces. These parts also achieved an as-machined surface roughness of under 64 μin [37]. However, this tool did not satisfy recommended vacuum integrity requirements without surface coatings.

An additional challenge in polymer-based AM tools is a low material hardness which causes them to be prone to scratching during part production. It has been reported that uncoated AM molds sustain visible scratches in less than 10 curing cycles, and various surface defects were caused by the mold surface gradually deteriorating from each part production, raising durability concerns for 3D printed composite molds [38]. Uncoated AM molds have only been shown to be an effective approach for limited production runs of fiber-reinforced composite parts [39], however, recent work has shown that machined and coated tooling surfaces have the capability of producing more than 10 parts without surface degradation [36], [40]. Although this is far from the service life of

conventional thermoset wind blade production molds, which are specified for the production of 1000 parts [2].

2.4.3 Vacuum Integrity of AM Tooling

Most applications of AM tooling rely on surface coating to achieve the required finish characteristics for production. By post-machining the printed surface and finishing with a polishable gel coating, the surface porosity can be reduced, yielding a higher quality surface than printing and post-machining alone. This is especially important for vacuum-assisted AM tooling due to the potential for high porosity in deposited thermoplastic materials that may lead to significant vacuum loss during elevated cure temperatures and pressures. Another significant challenge to vacuum integrity is layer-to-layer bead adhesion. Studies have found that a heated bed can assist with initial layer adhesion [41]. In addition to this, maintaining and monitoring the substrate temperature above the glass transition temperature (T_g) of the printed material provides improved layer-to-layer adhesion, resulting in higher strengths in the Z -direction [36]. While vacuum integrity poses a significant challenge for AM tooling, Bell Aerospace reportedly manufactured a large-scale carbon fiber reinforced ABS vacuum trim tool for helicopter rotor blades on Ingersoll's MasterPrint that is vacuum-tight post-machining [42]. As the large format machining of AM components develops, surface vacuum integrity continues to be of particular interest to tool manufacturers.

2.4.4 Thermal Expansion and Heat Uniformity of AM Tooling

The thermal expansion of thermoplastic resins is generally larger than that of thermoset resins, which in the AM tooling application can significantly affect manufacturing tolerances [19]. Filled thermoplastics display high anisotropy of thermal expansion in the extruded material. This is the nature of extrusion and layer-by-layer printing; however, this anisotropy is amplified by the alignment of feedstock additives that affect these properties. These factors can lead to expansion

or contraction differences of 5-10 times greater in the z-axis than in the x and y-printing axes [43]. This CTE challenge is further exacerbated in large tooling components, with significant work required to alter polymer material systems to reduce tool-part interaction because of tool expansion. As mentioned earlier, the primary solution to this problem is for the CTE of the tool to be the same or below the CTE of the part, especially for large-scale components that are typically fabricated via VARTM processes with large temperature differentials from cure to demolding. As a result, low-expansion materials are chosen for the mold to maintain the dimensional tolerance of the part itself and are measured as per ASTM D696 [16].

The elevated temperatures during the curing cycle step of manufacture can be a challenge for thermoplastic materials involved in AM as opposed to high-temperature-resistant thermoset materials. The thermal parameters of concern include heat capacity, glass transition temperature (T_g), and melt temperature (T_m), however, for tooling molds, the heat distortion temperature (HDT), becomes important when considering a polymer tooling surface subjected to elevated temperatures and pressures. HDT is a measure of a polymer's resistance to non-recoverable deformation under a given load at an elevated temperature. The standard test method for heat deflection temperature of plastics is ASTM D648-18 [44]. Additives to the polymer can have a significant effect on thermal properties in AM materials. Specifically, carbon fiber is an ideal reinforcement for increasing thermal conductivity and stiffness in the composite, thereby improving heat uniformity, and increasing heat deflection temperature. A standard test method for thermal conductivity is ASTM E1461 – 13 [27].

Table 2 below shows the challenges for AM to meet the production requirements of vacuum-assisted tooling for composites manufacturing, the characteristics related to those requirements, and some relevant standardized test methods for evaluation of these characteristics.

Table 2: Challenges of Current State Vacuum-assisted AM Tooling

Requirement	Characteristics	Challenge(s)	Relevant Standard(s)
Vacuum Integrity	<i>Surface Finish</i>	Staircase effect	
	<i>Surface Material</i>	Inter-bead adhesion/ high porosity	ASTM D 5687 [9]
	<i>Vacuum System</i>		
Dimensional Stability	<i>Surface Material</i>	High CTE	ASTM D696 – 16 [16]
	<i>Structural Design</i>	High anisotropy of CTE	
Durability	<i>Surface Finish</i>	Low hardness polymers	ASTM D2240 [21], ASTM D 5687 [9], ISO 4287 [20]
	<i>Surface Material</i>	High roughness	
Heat Uniformity	<i>Surface Material</i>	HDT, T _g , and T _m of Polymers	ASTM D648 – 18 [44], ASTM D 5687 [9]
	<i>Heating System</i>	Low thermal conductivity without additives	ASTM E1461 – 13 [27]

2.5 Opportunities and Applications of Large-scale AM Tooling

AM of tooling has multiple additional opportunities including flexibility in material systems, innovative new heating systems, and reduced environmental impact. The technology has been successfully utilized to manufacture boat hulls, wind blade tooling molds, and concrete girders and has the potential to be utilized in many more industry applications across a variety of industries [2], [32].

2.5.1 Flexibility within AM material systems

Polymers can be engineered with additives, creating a fiber reinforced polymer composite tool with enhanced properties. This process is called fiber-reinforced additive manufacturing (FRAM). While there are many possible polymer additives, the two fiber reinforcements that are primarily considered in composite tooling applications are glass and carbon fibers [45]. Glass and carbon

fibers have been shown to positively impact expansion/contraction, thermal conductivity, print warpage, internal residual stresses, and as a result, the dimensional accuracy of printed parts [46]. Glass fibers are high-strength low-cost reinforcement materials. The addition of short glass fibers to polymer feedstock leads to increased tensile and compressive strength. However, glass fibers have drawbacks that limit their scope of application including a low modulus, low abrasion resistance, high density, and low fatigue resistance [46]. Additionally, glass fibers are not ideal for the tooling application due to their insulating properties, reducing thermal conductivity. Although expensive, carbon fibers are a common polymer reinforcement additive due to their enhancement of material properties. The addition of 20 percent volume carbon fiber to a polymer feedstock leads to an increase in thermal conductivity, a decrease in thermal expansion, substantially reduced warping in larger prints, a reduction in residual stresses within the part, and an increase in the dimensional accuracy of AM parts. This addition of strength and stiffness in carbon-reinforced polymers has greatly increased the potential of AM for end-use components beyond the application of prototyping alone [47].

2.5.2 AM Tool Heating Systems

A variety of AM-specific heating systems are under development for composite molding operations. A demonstrated example of an AM-specific heating system is a closed-loop forced hot air, or water, mold with heating and cooling channels with an arrangement of integrated heating units under the mold surface [2]. Another candidate is the co-extrusion of heating wires within the 3D-printed bead material [55]. This can be achieved with a wire co-extrusion tool attached to a large format printer that feeds wire directly into the part during the printing process. While this practice is only a recent development, it shows significant promise for self-heated AM tooling applications. The flexibility of AM has increased the possibilities of tool heating systems resulting

in a variety of new research in this area; however, further work needs to be conducted before this AM functionality can be commercialized.

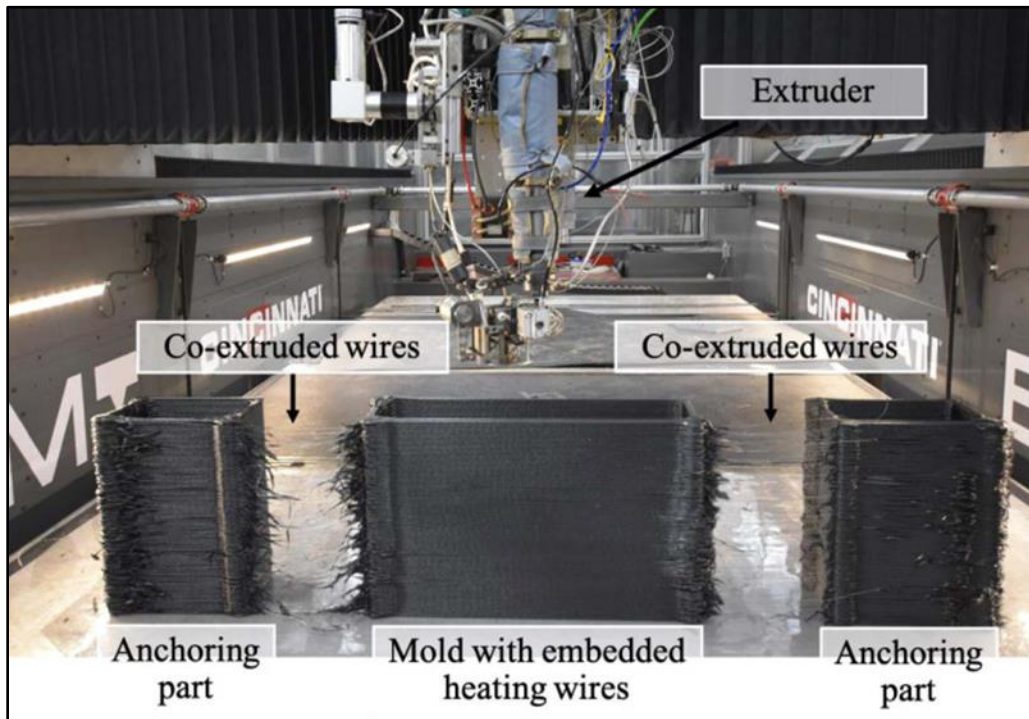


Figure 5: ORNL, Large-Scale AM of Self-Heated Molds [48]

2.5.3 Sustainability and Environmental Impacts of AM

AM tooling has the potential to be a more sustainable solution in a variety of industries. AM is more sustainable than subtractive manufacturing because of waste and material reduction. However, a more significant component of the impact of AM is the energy consumption required for the manufacturing process. The energy consumption in the FDM process is comparable to traditional subtractive manufacturing [57]. Recent life cycle assessments showed that AM has the potential to reduce consumption and environmental impact when compared to conventional methods. Particularly, AM has significant potential to reduce indirect consumption, such as energy and emissions due to the transport phase of materials and components [50].

CHAPTER 3: JOINING METHODS

3.1 Joining Methods for AM Tooling

This study investigates various joining and sealing techniques for the tooling joints in large-scale segmented AM tooling. Following the down-selection shown below in Figure 6, thermoplastic extrusion welding was selected for demonstration in AM tooling components.

3.1.1 Potential Joining Techniques

The Handbook of Plastics Joining: A Practical Guide [49] was utilized for this down-selection of joining techniques. Figure 6 provides a classification of joining techniques that were considered for this research.

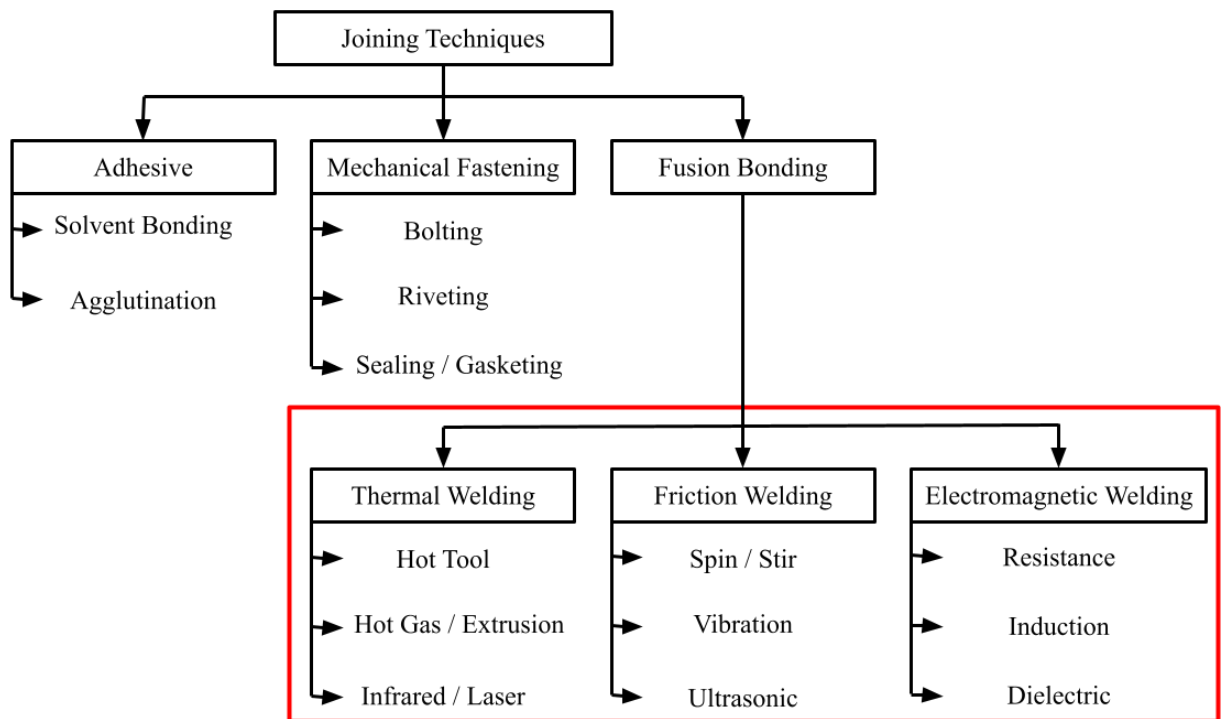


Figure 6: Classification of Joining Techniques

Adhesive joining, mechanical fastening, and fusion bonding were considered, and ultimately, fusion bonding, or welding, was selected for further investigation.

The feasibility of these joining options was assessed based on design criteria from Robert Flitney's Seals and Sealing Handbook [50], including:

- Integrity of sealing required
- Temperature and pressure range
- Industry standards and practice
- Durability and life requirement
- Material of counter faces
- Movement between counter faces
- Assembly method
- Fluids to be sealed.
- Environment
- Maintenance requirement
- Testing and inspection criteria
- Manufacturing volume

Primary attention was given to the temperature and pressure range, vacuum integrity of capability, and durability life requirements involved in conventional large-scale composite manufacturing.

3.1.2 Adhesives

A sealing option that was explored for this joint design involved the use of adhesives, such as one and two-part epoxies, structural acrylics, UV curable, cyanoacrylates, and solvent bonding depending on the base polymer. However, this joining option presented challenges, such as limited operating temperature range, potential health concerns during preparation, rigorous surface preparation and large bond area requirements, in addition to a discontinuous mold surface seam

between segments across the joint [49]. While industrial adhesives are available for high-temperature ranges, thermal expansion within the joint during cure is still a significant issue. Additionally, adhesives require lapped or flat butted bond surfaces that require rigorous preparation, which rarely create a seamless joint without meticulous preparation.

ORNL demonstrated an adhesive joining technique for AM boat hull tooling, where threaded rods were used to hold the assembly together and the sections were adhered with PlioGrip Plastic Repair epoxy. This approach successfully manufactured a composite boat hull, however, “pneumatic cracks” evidence of air leaks was observed [32], suggesting difficulty meeting the surface and vacuum integrity requirements of tooling surfaces. As a result of these difficulties in previous research, the adhesive joining technique was not chosen for further evaluation in large-scale segmented AM tooling.

3.1.3 Mechanical Fastening

Another sealing option considered for this joint design includes mechanical sealing elements such as O-rings, profiles with various geometries, sheet, and disc gaskets, as well as expansion spring-loaded joints secured with fasteners such as bolts or rivets that could be de-mated for transport or changeover of tooling sections. The challenges with these joining options were low thermal performance and operating temperatures of elastomer materials, complicated reinforcement design, and the resulting surface finish across the joint. Elastomeric seals are susceptible to leakage due to the cycling of elevated temperatures during part production which may lead to failures requiring additional maintenance.

In addition to the research on adhesive joining, ORNL demonstrated an O-ring joining technique in AM molds that achieved vacuum integrity with losses of less than 1.5 cm Hg/5min (~20.3

mbar/5min) at elevated temperatures of 20 – 200 °C [51]. This vacuum loss is still not tolerable in specifications for vacuum infusion processes within the industry. Two primary concerns were cited in this work: first, the need to minimize the seam line between mold segments to meet surface quality requirements for the final components, and secondly, the importance of carefully machining the tool surface to enhance the seal and vacuum integrity of the AM tool surface. Due to these findings, the mechanical fastening joining technique was not chosen for further evaluation in large-scale segmented AM tooling.

3.2 Welding of Thermoplastics

Thermoplastic welding is a process involving the fusion of thermoplastic material through heating, pressurizing, and cooling, or melting thermoplastic material into a groove or joint, similar to conventional arc welding. This joining method creates a flexible, high-strength bond, that has great fatigue properties [49]. Figure 7 shows the three primary fusion bonding classifications within relevant literature [52], [53], [54].

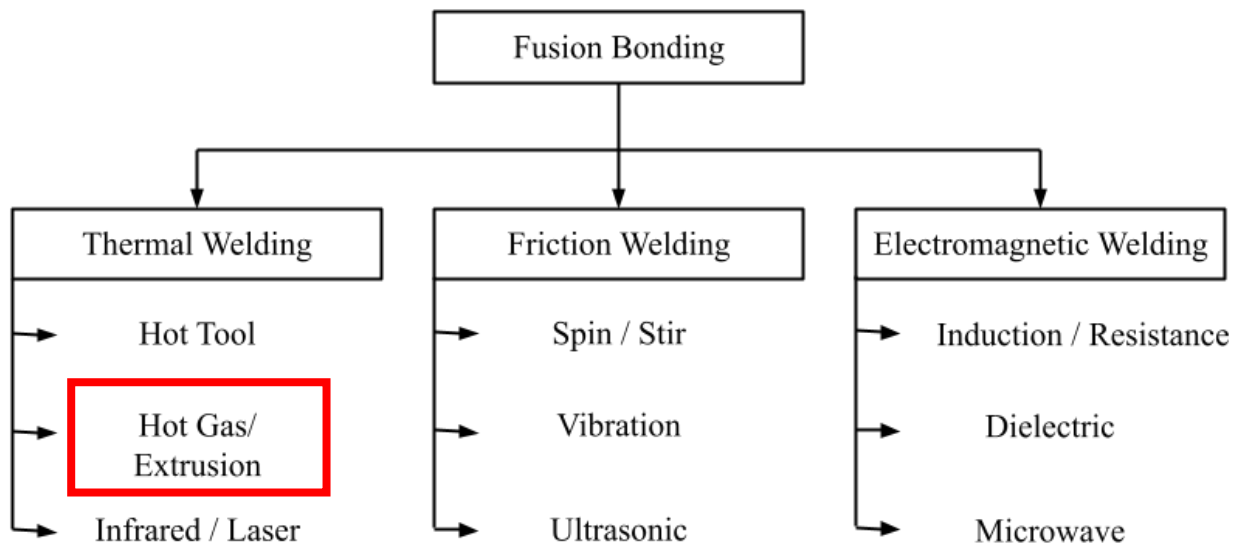


Figure 7: Classification of Fusion Bonding Techniques

In this work, polymer welding methods from all three classifications were investigated. This work focuses on thermal welding solutions for joining large-scale AM components, specifically hot gas, and extrusion welding techniques which have been demonstrated for joining large thermoplastic structures [53]. Due to joint design requirements and size limitations, friction and electromagnetic welding techniques were not considered for this work. This is primarily due to the scale of equipment needed to manufacture the joint and the required surface finish within the tool. For example, stir welding techniques have difficulty achieving the required surface finish across the joint in a tool surface [55], [56]. Additionally, vibration, ultrasonic, and dielectric polymer welding

techniques are limited by the size of their welding systems and do not scale well to joining operations that are potentially several meters in length [49], [53].

3.2.1 Hot Gas Welding

Hot gas welding, which involves blowing air into the joint to heat and melt a filler rod and base material, is a flexible joining process capable of a range of applications including welding of small components, large structures, or tanks [53]. This technique has also been demonstrated for plastics repair at ORNL, by backfilling voids in carbon fiber-ABS mold surfaces to improve surface finish [33].

To investigate the feasibility of using hot gas welding for joining large-scale AM components, a Leister Diode S hot air tool [57] was used to conduct preliminary test welds on a small-scale base material of flat polystyrene plates. Initial pendulum welding was utilized to join 1/4" polystyrene (PS) plates with a beveled edge as shown in Figure 8 below.



Figure 8: Set-up and Initial Hot Gas Pendulum Weld

Process parameters such as temperature, orientation of the material, and welding speed were varied to better understand their effect on the weld. Although these initial welds were of low quality and not suitable for tooling surfaces, they did demonstrate the importance of both joint preparation, and matching the weld material to the base polymer and for a high-quality, well-fused joint. This was observed when a PS filament material from a different supplier failed to fuse with the base material, however, a strip of base material fused into the joint well as shown in Figure 8. It was also evident from these initial welds that a larger welder with a higher extrusion rate would be necessary to join the planned large-scale thick AM components.

3.2.2 Extrusion Welding

Extrusion welding is similar to 3D printing in that it involves preheating the faying surfaces of an engineered joint with a hot gas blower, and then plasticizing or extruding fully molten material

through a shoe at the desired weld temperature while the welder is moved along the groove [58]. The infeed material can be fed into the extruder either via rolls of filament material on an external spool that is ground internally into granulate or pelleted granulate material fed via a hopper. An electric motor feeds the extruder with the pelleted material, which melts and is extruded through the welding foot into the prepared weld cavity, as shown in Figure 9.

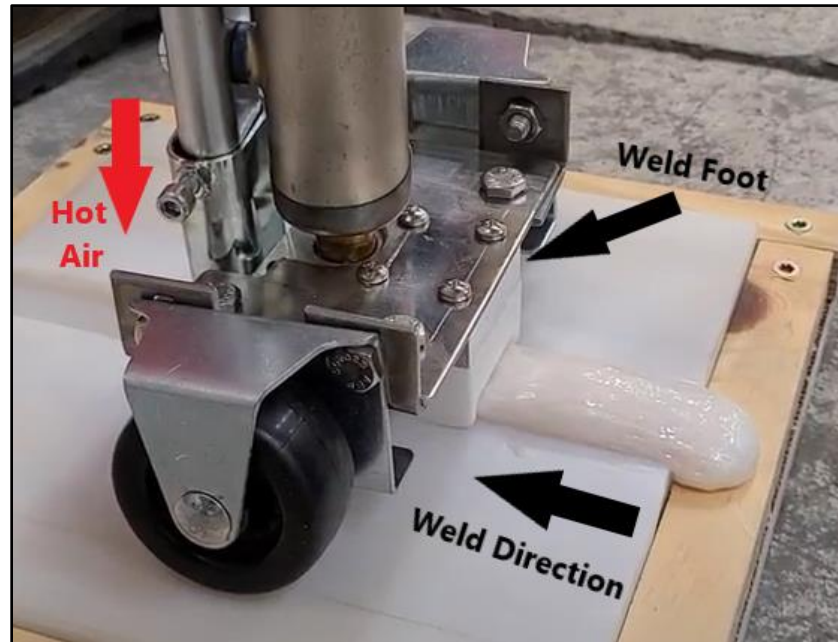


Figure 9: Extrusion Welding Process

Extrusion welding utilizes a welding foot to apply pressure, guiding the extrudate into the groove while reducing squeeze out. The weld shoe is either made or coated with Teflon (PTFE) to reduce friction and minimize sticking to the welding foot [53].

Compared to filament fed hot gas welding, extrusion welding allows for shorter fabrication times because a larger joint volume can be filled in a single pass. Moreover, the ability to control extrusion feed rates within the motorized extruder reduces the number of process parameters, making extrusion welding easier to perform consistently than hot gas welding [57]. Using the same

feedstock material also ensures that the weld material matches the mold material, which subsequently matches the coefficient of thermal expansion with the tool.

When working with smaller extrudate volumes or on-site projects where a large extruder is not accessible, a handheld extrusion welder is used. However, these handheld extruders can be large and heavy, making them cumbersome to use for longer welding operations [53]. In contrast, for welding thicker materials in an industrial setting, a stationary extruder on wheels with a lightweight movable weld shoe nozzle is preferred. Figure 10 below shows examples of hot gas and extrusion welders alongside a mounted single screw extruder manufactured by Abbeon Cal Inc [59].



Figure 10: Abbeon Hot Gas Welder, Extrusion Welder, and a Mounted Extruder [59]

3.2.3 Applications of Extrusion Welding

Extrusion welding is a relatively slow and labor-intensive process, which limits its use for high-production rates where other thermoplastic joining techniques are superior. However, it scales well to large components over three meters in size, where other techniques would be limited by their equipment [53]. Extrusion welding is commonly employed in joining large drainage pipe sections, composite tanks or vessels, roofing, pool, and landfill sheet liners, as well as sealing geomembranes [49]. Common materials for extrusion welding include Polypropylene (PP) and Polyethylene (PE), however, specific equipment can be used to weld PVC and a few other materials for custom applications [60].

3.2.4 Parameters of Extrusion Welding

Extrusion welding requires careful consideration of several important process parameters, including the temperature of the extrudate, the temperature of the pre-heat air, the extrusion rate, the welding travel speed, the weld force, the composition of filler, and the welding shoe utilized. Polymer welded joints need to be specifically designed to the attached welding foot to allow for a variety of engineered joint types, such as butted, lapped, grooved, and filleted edges. Table 3 details some of the key parameters for extrusion welding.

Table 3: Process Parameters for Extrusion Welding [53]

Process Parameters	Description
Temperature	Temperature of extrudate existing weld foot and blower air
Weld Material	Composition of filler material, diameter geometry (filament or pellets)
Travel Speed	Rate at which the welder is moved along
Extrusion Rate	Rate at which material exits the nozzle
Weld Force	Amount of force applied to the filler rod
Shoe/Foot	Design and size of welding nozzle

The temperature the extrudate is governed by the melt temperature range of the chosen filler, or weld, material chosen. The weld material can be in filament or pellet form depending on the equipment utilized and generally is matched to the base polymer surfaces that are to be welded. Typical extrusion welding speeds of 0.5 – 1.0 meter / minute (1.6 – 3.3 feet / minute) can be achieved depending on material thickness and extruder size. However, as with traditional welding, the quality of the resulting joint heavily depends on the operator's experience [49]. Travel speed is dictated by joint volume and the extrusion rate at which the joint is filled, therefore a higher extrusion rate is needed to fill a larger joint, or to fill the same joint at a higher speed. Weld force

is directly related to the weight of the welder as it compresses the material into the joint under the weld foot or shoe during extrusion.

3.3 Weldability of Thermoplastic Materials

Understanding the formability and weldability of the chosen polymer is fundamental for designing a thermoplastic joint. The crystallinity of a polymer, which refers to its degree of structural organization, plays a significant role in the bonding of polymers. Figure 11 illustrates a simple model that compares amorphous or unorganized polymers to semi-crystalline or semi-organized polymers.

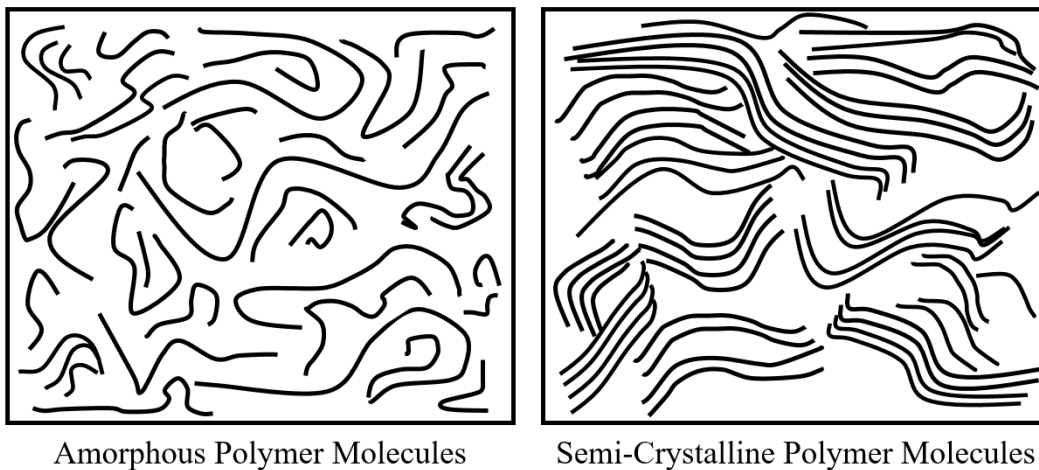


Figure 11: Molecular Organization of Amorphous and Semi-crystalline Polymers [61]

Amorphous polymers, which have low crystallinity, are easier to weld due to their random or low molecular organization. When heated beyond their glass transition temperature, amorphous polymers melt together at the molecular level. Semi-crystalline polymers, on the other hand, have highly ordered molecular structures that result in a sharp melting point instead of gradual softening, making them more challenging to weld [61]. To weld thermoplastics, the materials must be heated above their glass transition temperature (T_g) into their melt temperature range (T_{melt}), which is a

larger range for amorphous polymers than it is for semi-crystalline polymers. Appendix D contains a technical reference utilized for this work, the Tangram Technology Periodic Table of Thermoplastics [62]. This technical reference displays various commodity-grade to engineering-grade plastics on a scale of increasing crystallinity. Moving down the table, crystallinity increases, and subsequently, the weldability of the thermoplastic material decreases.

3.3.1 Models of Polymer Interphases

There are multiple theoretical models of polymer bonding interphases including heat transfer, kinetics, and autohesion (healing) models [63]. However, these models do not fully capture the phenomena of polymer fusion. This section will focus on a simplistic model of the polymer healing process.

When two similar polymer interphases come into contact at a temperature higher than their glass transition temperatures, the contact surface gradually bonds through polymer healing, resulting in slowly increasing mechanical strength at the polymer-polymer interface [54], [64]. Figure 12 illustrates two distinct interphases adjacent to one another in part A. During welding, these interphases are heated beyond their glass transition temperature and brought into contact as shown in part B. At this point, polymer healing begins as the interphase collapses through inter-diffusion in part C [63]. The collapse of the interphase between polymers results in an increasing number of intersections between polymer chains across the contact region, leading to increased mechanical strength based on the degree of healing.

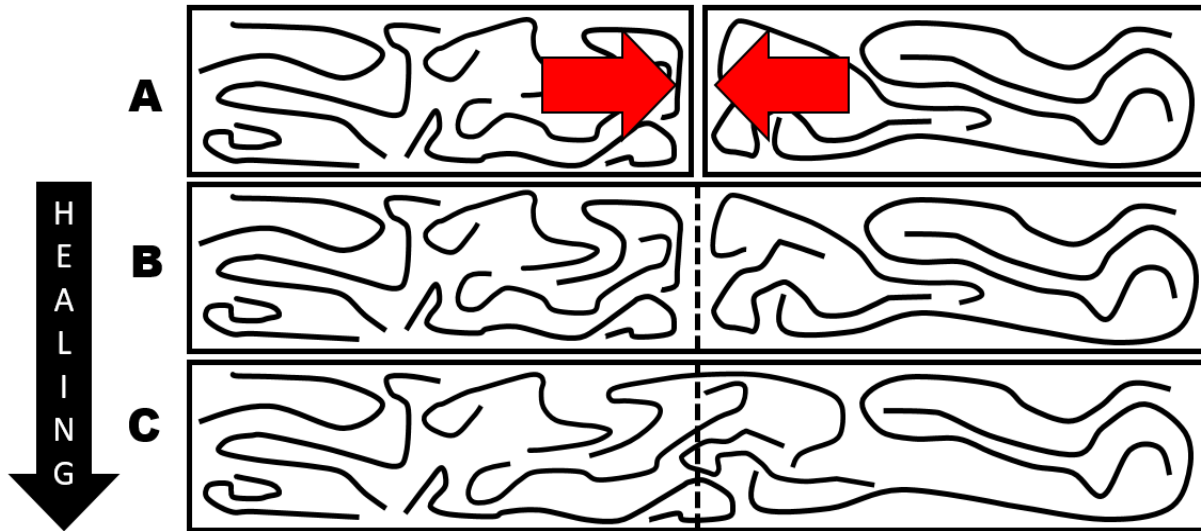


Figure 12: Intermolecular Healing of Interface [63], [64], [65]

While this is a simple model, it provides a molecular interpretation of the phenomenon of self-diffusion in the bulk polymer and encompasses the fundamentals of bond line fusion occurring during the welding of thermoplastic materials.

3.3.2 Material: High Impact Polystyrene (HIPS) Thermoplastic

High Impact Polystyrene (HIPS) was chosen for evaluation of extrusion welds. Although it is not a common welding material, HIPS is an amorphous polymer that is highly formable and easy to weld. HIPS has good chemical and water resistance and a high surface hardness, but it is sensitive to UV radiation. Polystyrene (PS) is clear like glass and impact-sensitive, but high-impact varieties contain additives that increase their durability, toughness, and impact resistance, as well as giving them an opaque white color. The melting point of HIPS is between 240°C and 270°C and the continuous use temperature is -60°C to +80°C [66].

HIPS was selected for evaluating the feasibility of polymer welded joints in tooling surfaces due to its cost, thermo-mechanical characteristics (specifically its HDT), and durability. Throughout this study, the plates and welds that join them were made of neat, unfilled Unigel HIPS. Table 4

below shows the properties of HIPS material relevant to this research. For more material information, see the material data sheet and safety data sheet for the HIPS material utilized in the appendix D.

Table 4: Properties of HIPS Material [66],[67]

Property	Test Method	Value	Unit of Measure
Tensile Strength	ASTM D638	3,000	(psi)
Tensile Modulus		240,000	
Flexural Strength	ASTM D790	8,700	
Flexural Modulus		280,000	
Density	ASTM D792	0.038	$\left(\frac{\text{lb}}{\text{in}^3}\right)$
Coefficient of Thermal Expansion	ASTM D696	4.2	$\times 10^{-5}$ (in./in./°F)
Melt Temperature Range		240 - 270	(°C)
Heat Deflection Temperature	ASTM D648	92	(°C) at 264 psi
		195	(°F) at 264 psi

3.4 Manufacturing the Thermoplastic Joint

This section describes the process used to manufacture the welds between components. This process involved calibrating the welder specifically for the HIPS material, making improvements to the welding process, and manufacturing specimens to evaluate the feasibility of joints for use in a large-scale tooling application.

3.4.1 Extrusion Welded Joint Design

The initial joint design drew inspiration from the extrusion welding industry's application of pipe and tank welding, where two beveled surfaces are joined using a single groove "V" or double groove "X" weld [49]. The fundamental principle is that the welder preheats and fills the groove with some flash or squeeze-out on the opposite side of the joint. Figure 13 depicts the design of a straightforward extrusion welded 60° V-groove joint that joins two 1 in plates. The plates used in the design are intended to simulate the thickness of the additively manufactured tooling surface. Thus, this simple welded plate represents a joint between two AM mold surfaces.

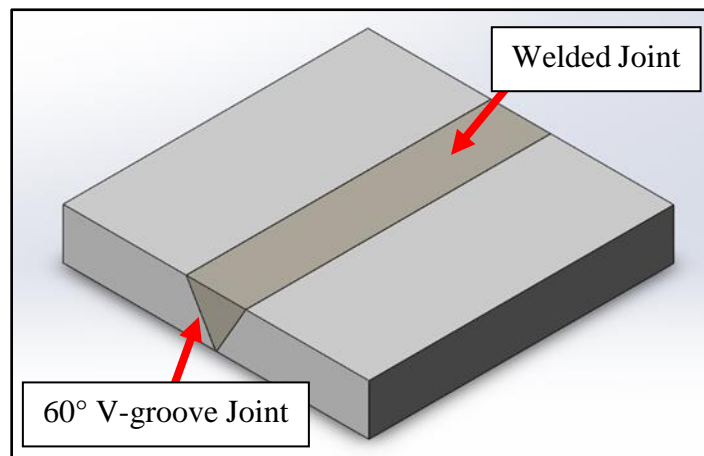


Figure 13: Extrusion Weld Design

3.4.2 Extrusion Welding Materials and Methods

This study employed an Abbeon HSK26 GSX extrusion welder [68] as shown in Figure 14 below. The HSK26 comes equipped with a hopper that gravity-feeds pellet or granulate material. The pelleted material falls into the extrusion drive screw, which pushes the material into the melt chamber, compounding the pellets and melting them into extrudate that exits the weld nozzle. The welder features temperature control for both the extrudate and blower air, as well as extrusion speed control. Although marketed primarily for welding PE, PP, and TPU, it was also used for the HIPS material in this study.

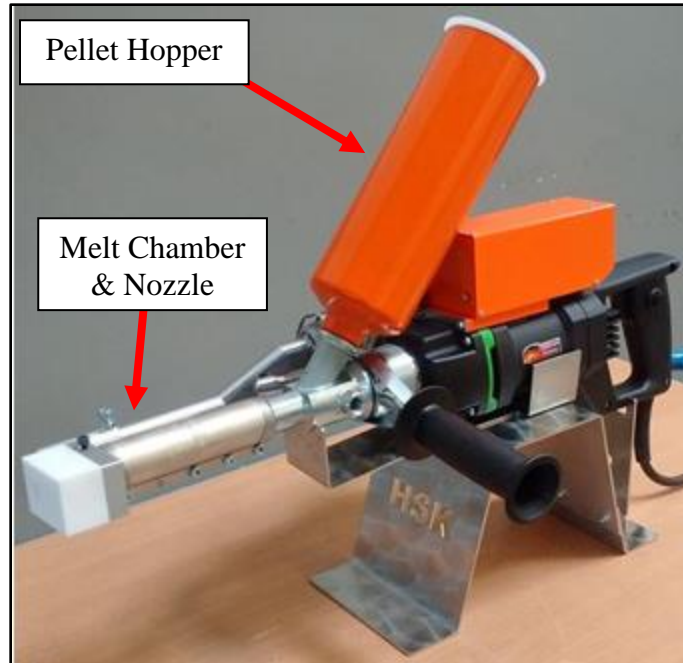


Figure 14: Abbeon HSK26 GSX Extrusion Welder [68]

To ensure safe operation of the welder, appropriate personal protective equipment was utilized in the lab. Welding gloves, a welding jacket, and a face shield were always worn while operating this equipment.

3.4.3 Extrusion Weld Calibration

To better understand the optimal welding parameters for granulated HIPS material and improve weld quality, calibration test welds were conducted using the Abbeon extrusion welder. This required adjusting multiple process parameters to find suitable temperature and flow rate settings. The welder has two temperature adjustments. The first control is the plasticizer temperature, which regulates the temperature of the granulate being extruded through the screw in the weld barrel and out of the welding foot. The second adjustment controls the temperature of the hot air blower, which preheats the joint to improve the bond with the softened fairing surfaces. Another crucial adjustment is the extrusion rate of the welder's internal screw, which plasticizes and extrudes

material out of the foot of the welder. Five 6 in long 60-degree V-grooves were cut, following the weld design and a 1 in V-groove router bit to allow for a series of calibration welds in a single fastened plate, as illustrated in Figure 15 below.



Figure 15: Extrusion Welds conducted for Welder Calibration.

Process parameters were incrementally adjusted between welds as shown in Table 5 below. The parameters adjusted were extrudate temperature, blower air temperature, and extrusion rate. During these welds, the operator moved too quickly to adequately fill the v-groove joint as can be seen across all welds. This resulted in a concave welded face shape that provides an inadequate surface for the intended application. Table 5 shows the defects noticed within these five welds and their potential causes.

Table 5: Causes of Defects within Calibration Welds

Extrudate & (Blower) Temperatures	~ Extrusion Rate (lbs/hr)	Defect(s)	Cause(s)
265°C (280°C)	0.92		Poor Technique (Operator speed too fast/ Extrusion rate too slow)
260°C (280°C)	1.83	Discontinuous weld bead Under filled joint Poor bonding	
260°C (270°C)	2.76		
250°C (260°C)	3.68	Under filled Joint	Operator speed too fast
260°C (260°C)	3.68	(Concave weld face)	

The calibrated process parameters for a high-quality HIPS weld were determined to be a plasticizer temperature of 260°C and a blower air temperature of 280°C or higher. The base material softened noticeably more in the first two welds, indicating that a higher blower temperature could further improve the process. A moderate to high extrusion rate, above half of the maximum screw speed, was found to best match the rate at which the operator moved the welder along the joint. This ideal speed created a flow ahead of the welding foot that added compression to the extruded material. As shown in Figure 15, the welds conducted at higher speeds fill the joint with additional material compared to the lower extrusion speed welds. After improving the process parameters via this test, longer continuous welds were manufactured for bench testing.

3.4.4 Improving Extrusion Welds

In vertical applications perpendicular to the joint, a wheeled trolley was designed and attached to the welder as shown in Figure 16. The trolley allowed for height adjustment to ensure proper flying height and was compliant, flexing as the operator moved along the joint, and served as a guide for the welder. This simple welding trolley improved consistency in welds, easing the strain on the operator and improved joint quality.

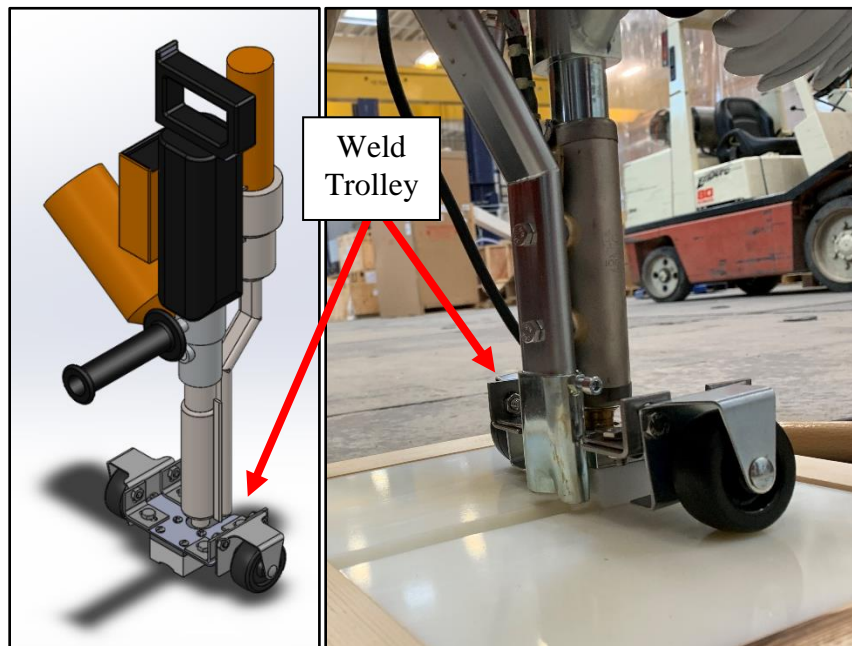


Figure 16: Extrusion Welding with Trolley Attached to the Welding foot.

Additional welded joints were manufactured using the process parameters determined above and with the addition of a 1 in single V weld nozzle in conjunction with the welding trolley as shown in Figure 17 below. A higher extrusion rate was found to improve the quality of the welded joint and was utilized for all future welds in thick HIPS plates.

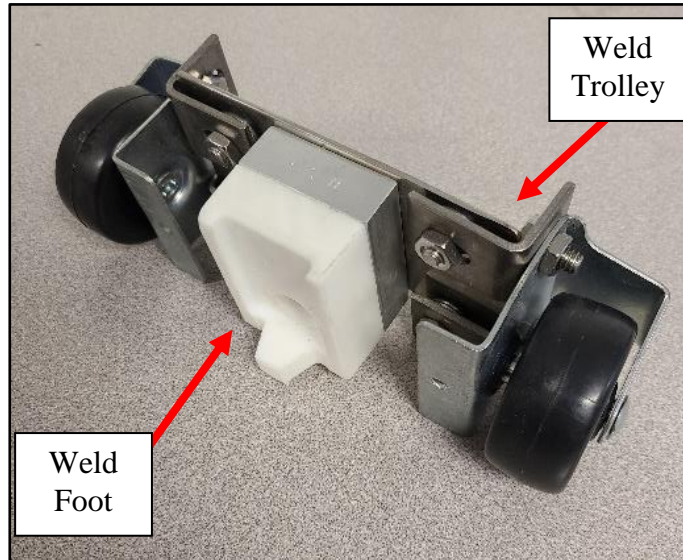


Figure 17: Single V Butt Weld Foot [73] Attached to Weld Trolley

The welding trolley attachment noticeably improved weld consistency by allowing the compression of material under the weld foot to push the welder along the joint. This made the welding process as simple as allowing the set extrusion rate of the welder to dictate the speed the operator moved along the joint. As the welds progressed, another operator utilized a silicone roller, also supplied by Abbeon, to compress the melted weld material into the joint as shown in Figure 18. Rolling the welds has been demonstrated to improve the contact between weld and base material, subsequently improving the resulting welds [54].

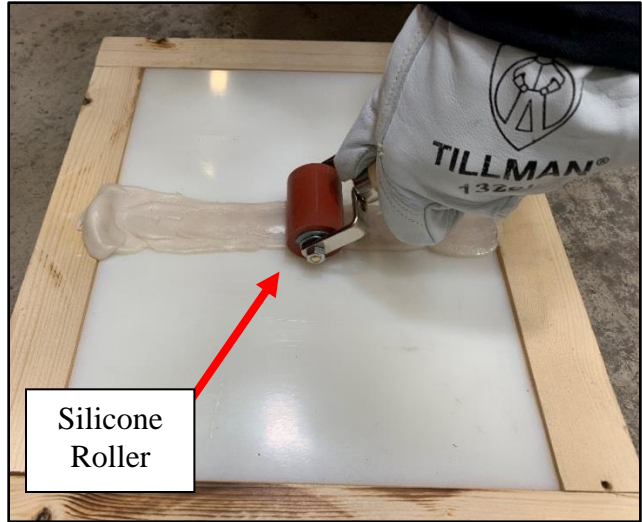


Figure 18: Compressing Extrudate into Joint Using Silicone Roller

After allowing the welded plates to cool for over an hour, their surfaces were milled flat and then sanded with 220-grit sandpaper. An example of the improved welds after surface finishing is shown in Figure 19, along with a cross-sectional view of the welded joint.

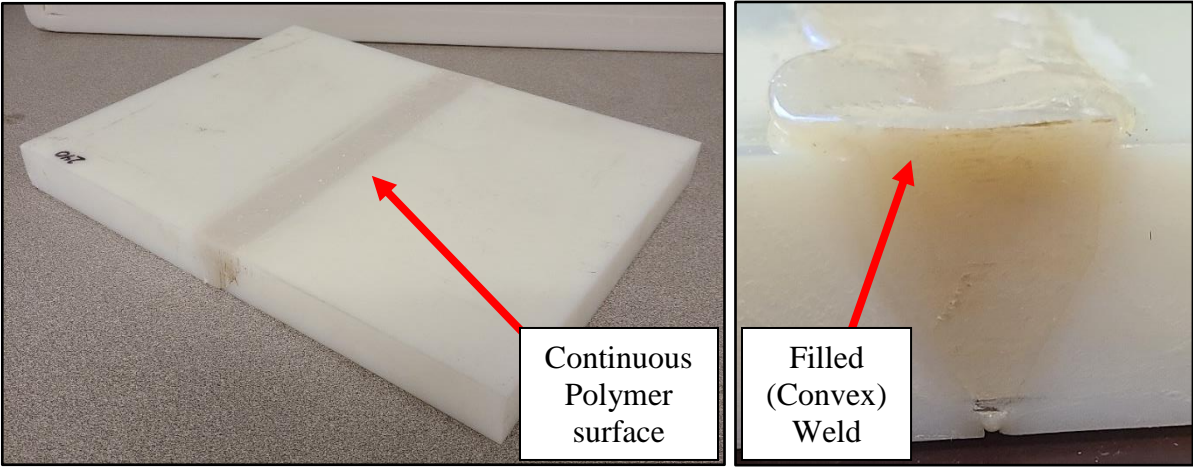


Figure 19: Post-Calibration Weld in HIPS Plate (left) & Cross-section of Welded Joint

3.4.5 Selected Joining Method

After calibrating the HIPS material for extrusion welding, the thermoplastic welds shown were adequately filled, which resulted in a convex weld face that could be finished into a continuous polymer surface. This continuity across the welded joint satisfies a key requirement for tooling surfaces that adhesives and mechanical seals did not. As a result of this improvement and the novelty of this application of this technology, thermoplastic extrusion welding was chosen to be further evaluated as a joining method for segmented AM tooling components. Thermoplastic extrusion welding offers several advantages for large-scale demonstrations, particularly in terms of compatibility with 3D-printed polymer surfaces. The use of polymer welds allows for a seamless match with the material of the AM tool surface, avoiding potential issues related to thermal expansion between segments. The joint can be extruded directly into a machined single “V” butt joint between AM components, which can then be finished by hand or via CNC machining and coated or sealed if desired. The absence of alignment issues associated with other mechanical sealing elements is another benefit, as these welded joints can be manufactured to meet the adjustment needs of both fairing surfaces. This joint design can also be reinforced under the tooling surface, relying on a steel frame for additional axial and out-of-plane support. This maintains the structural advantages of the steel frame in conventional thermoset glass-fiber tooling. Overall, the use of thermoplastic extrusion welding for segmented AM tooling offers a promising joining solution for this application.

3.4.6 Manufacturing and Welding AM Components for Testing

This section details the manufacturing process of the welded AM HIPS plates. The plates were produced using a Juggerbot3D Tradesman Series P3-44 industrial 3D printer [69]. The plates were designed to be unidirectional prints, with dimensions of 24 x 12 x 1 (in). These plates were printed

at 220°C in all zones of the extruder, with the print bed maintained at 100°C to reduce warping. The bead size from this print nozzle was 0.6 in wide and 0.15 in tall, resulting in printed dimensions of 12.21 x 23.82 x 1.26 (in). The oversized plate allowed for surface machining without reducing the plate thickness below 1 in. Figure 20 shows a HIPS plate being printed on the JuggerBot Tradesman 3D printer. The full plate was fully printed in about 45 minutes.

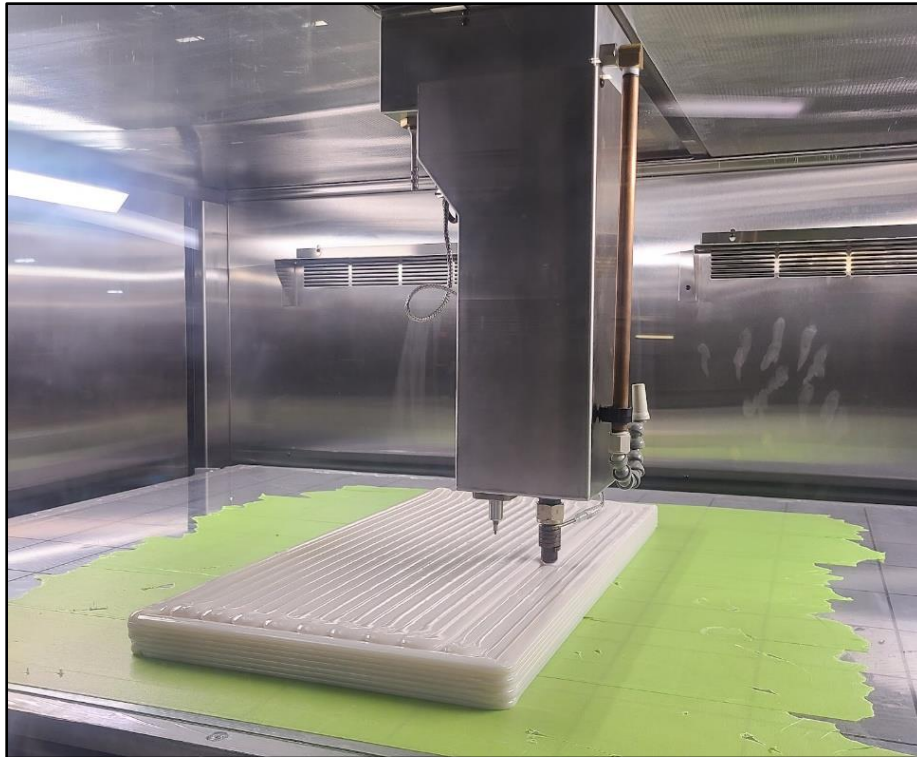


Figure 20: HIPS Plate Printed on JuggerBot 3D Printer

Once the prints had cooled, the top surface was machined flat to ~1 in thickness halfway the height of a bead layer of AM material. To improve the surface quality of the AM plates.

This step was important to achieving vacuum integrity and surface finish in the AM components. The fairing surfaces of the joints were then manufactured with a 1in v-groove router bit, sanded with 150 to 220 grit sandpaper, and cleaned to prepare the plates to receive a weld. Figure 21 shows the prepared fairing surfaces in an AM plate.

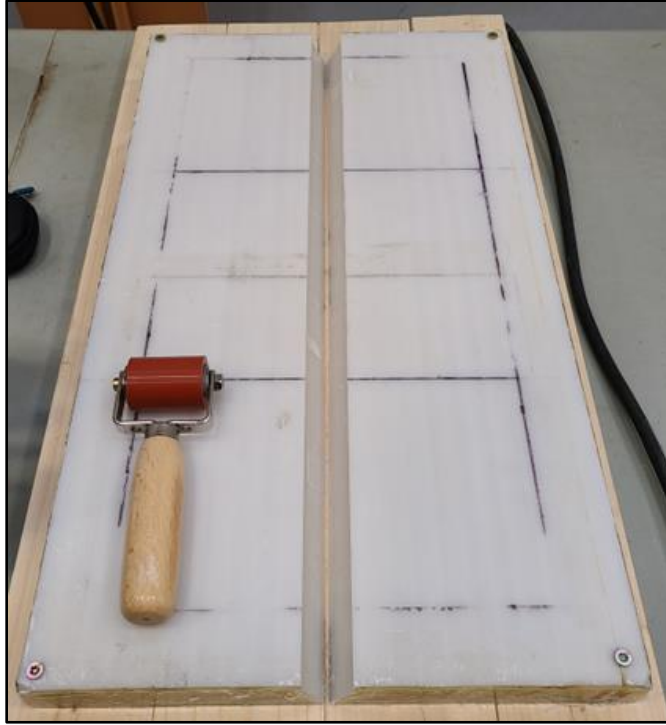


Figure 21: Prepared Joint V-Groove in Machined AM Plate

Before welding, the plates were fixed down onto a wooden backer board. This served multiple purposes, including holding the plates in alignment and restricting any potential movement during the welding process as well as after the welding was completed and that plate was cooling. The wood also provided a backing surface that allowed extrudate to build pressure against the wood and fairing surfaces of the joint during welding and when rolled flat. As a result of this, it is recommended that any welds manufactured in plates have a backing to improve compaction into the joint.

The AM plates were then welded with an Abbeon HSK26 thermoplastic welder. The plasticizer temperature was set to 260°C, and the blower air temperature was set to 300°C. Careful attention was paid to the welding rate to ensure that adequate material was plasticized into the groove to fill uniformly, as shown in Figure 22. Again, the weld was rolled with a silicone roller while it was still hot to compact it into the joint.



Figure 22: Extrusion Welding AM Plate

Once the welds had sufficiently cooled to room temperature in a stable environment, the weld surfaces were finish machined with a fly-cutting end mill yielding a flat, consistent polymer surface across the welded joint. Significant porosity was observed in the weld material, this is inspected in further sections.

CHAPTER 4: EVALUATION OF THE JOINING METHOD

To evaluate the feasibility of thermoplastic welding as a joining method between AM tooling segments, three aspects of the welded joint were investigated as shown in Figure 23 below.

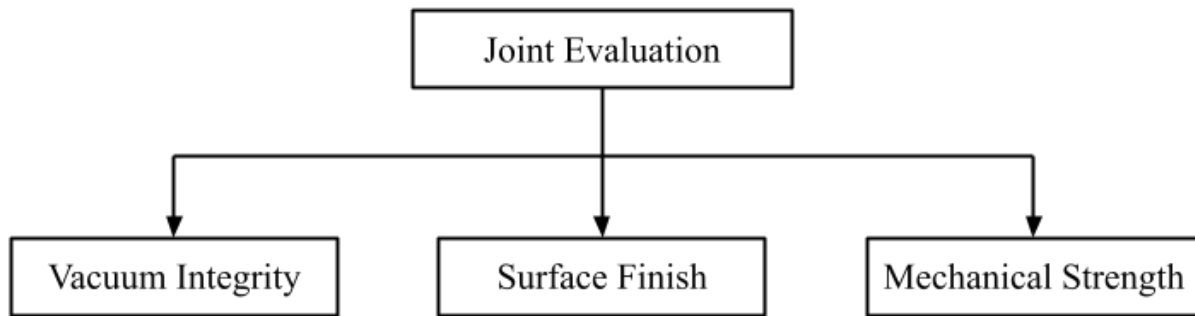


Figure 23: Joint Evaluation

The vacuum integrity has been evaluated by testing the vacuum leakage through a welded joint in an AM plate and comparing it to the loss through a baseline solid HIPS plate. The surface finish has been evaluated by measuring and comparing the surface hardness and surface roughness of the weld bead and the base AM material. Mechanical strength was evaluated through ASTM tensile and flexural testing of welded joints and comparing resulting failure stresses to that of the base material.

4.1 Surface Vacuum Integrity of Welded Components

In this section, the vacuum leak rate through an extrusion welded AM plate is measured. The leak rate will then be compared with the industry specification for vacuum integrity in a wind blade mold. During a vacuum leakage test, air enters the system increasing the total pressure. The change in pressure is then measured as vacuum loss. These air leaks can be from two sources: the bag system, or permeation of the part. A solid HIPS plate was leak tested to obtain a baseline leakage through the bag system. A welded AM plate was then leak tested to measure the leakage through

the welded joint and AM surface. These leak rates were then compared, as shown in Figure 24 below, to determine the leak rate due to permeation through the welded AM plate.

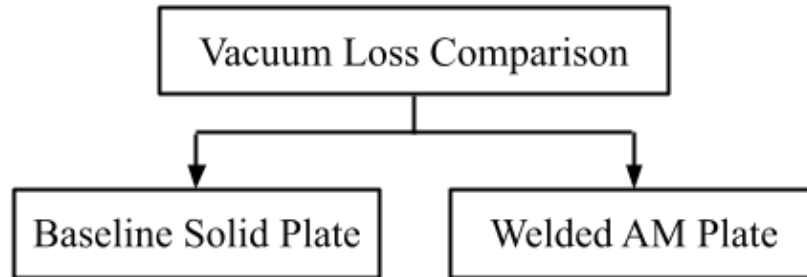


Figure 24: Evaluation of Vacuum Integrity in a Welded AM Plate

For the work presented here, vacuum leakage testing was only conducted on uncoated AM plates. The goal of this testing was to quantify the leakage through the welded joint within a tooling surface, not the leakage through a coated AM surface. Coating a mold surface seals it and eliminates imperfection as a result of surface porosity. This leads to enhanced vacuum integrity and surface finish within the mold [36].

The surface vacuum integrity specification for the welds has been established with input from the project partner, TPI Composites, based on the manufacturing requirements of conventional thermoset wind-blade shell molds shown in Table 6 below [70].

Table 6: TPI Shell Mold Specification Section: Vacuum Integrity [70]

Tool / Test	Temperature	Vacuum ^{*)}	Vacuum Drop
All molds	No Heating	≤ 20 mbar (absolute) (alternatively less than or equal to -0.980 bar gauge pressure)	10 mbar/ 30 min

*) stabilized value to start of drop test

4.1.1 Vacuum Bagging Procedure

The consistency within the leak testing results is dependent on the seal of the bag. Therefore, careful attention was paid when bagging to ensure a good seal was achieved. This process is shown step by step in Figure 25 below.

To prepare for bagging, the first step was to clean the surface of any dust and debris and marked, outlining the area that is to be bagged. Then all bagging materials were cut to size, and test fit. The materials for vacuum bagging include:

- Vacuum Bag Sealant Tape [71]
- Polyethylene Vacuum Bag [72]
- Felt-based Bleeder Media [73]
- 3/8-in Spiral tubing
- 3/8-in Tube tee

To begin bagging, vacuum bag sealant tape was applied to the surface in a consistent square area without removing the backing tape. Four to five-inch lengths of tape were cut and folded to create two pleats that were added to the sealant tape, each in line with the outlet of the setup as shown in step two of Figure 25 below.

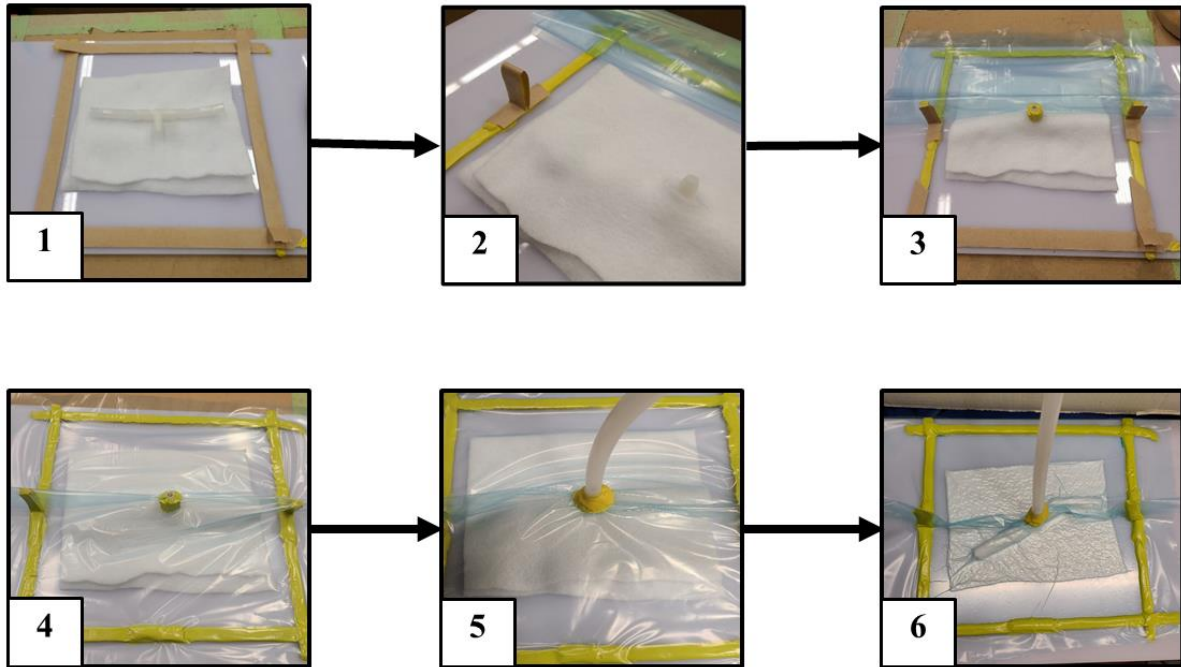


Figure 25: Vacuum Bagging Process

The vacuum bag was then added in the third step, and close attention was paid to ensure it was laid flat and into the corners of the tape to avoid leaks at the seams. This was achieved by progressively removing the tape backing while working the vacuum bag down each side. The bag must be carefully adhered and across the added pleats, as these are the area's most susceptible to leakage. Once the vacuum outlet reached the top of the pleats, a small circumference length of sealant tape was applied around the tee, or vacuum port, to seal the bag to the tee connection from the inside.

In step four, the bagging process was completed, and a small bump of sealant tape was added at the bottom center of the bag to catch remaining bag, preventing creases.

Once the bag was sealed, a small pinhole was added within the tee connection to allow the bag to stretch around the fitting. The tubing leading to the vacuum pump required for the leakage testing was then attached to the tee connection, stretching the bag over the tee within the tubing

as shown in step five. The connection was then sealed from the exterior with a wrap of sealant tape.

To verify the bag was sealed down well and is without large leaks, the system was given a thorough check to ensure vacuum integrity before the leak testing. Step six shows an example of a final bagged plate during the initial leakage test. This was achieved by applying a vacuum from the pump through a valve to evacuate the air from the bag gradually, allowing adjustment of the bag to get a good seal and resolve potential leaks. Any leaks that were found were pressed firmly against the tape to seal them further. To maintain good practice, the sealant tape was pressed down firmly, squeezing it between the bag and the surface with significant hand pressure or with a silicone roller. These initial tests were held for multiple minutes to compress the sealant tape and ensure the plate was not leaking.

4.1.2 Vacuum Leakage Test Set-up

Vacuum leakage testing applies a vacuum in the same manner as the industrial infusion process, however with the aim of testing the leakage rate through the welded joint using an in-line pressure transducer. Figure 26 depicts a diagram of the vacuum leakage test setup, which includes the instrumentation, bag system, and the test component.

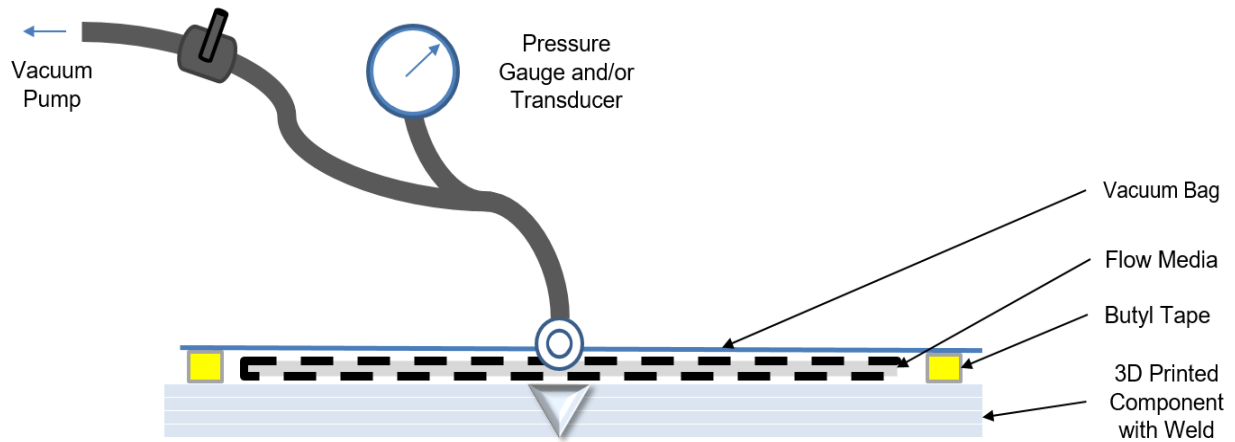


Figure 26: Vacuum Leakage Test Set-up Diagram

The transducer and digital vacuum gauge were placed in line with the vacuum bag to record the loss in the bag through the plate after the valve closes off the rest of the vacuum system that leads back to the pump as shown in Figure 27.

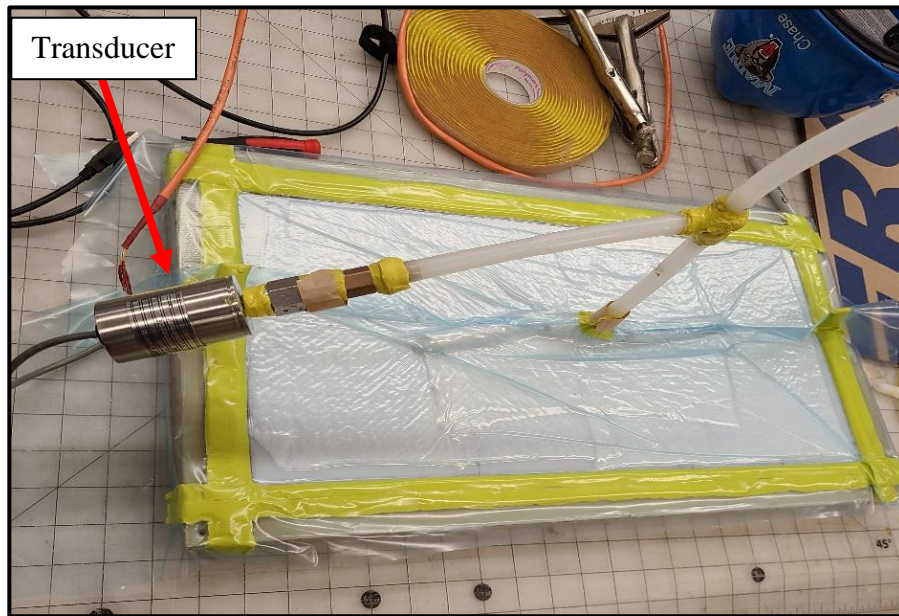


Figure 27: Vacuum Bag over the Welded AM Plate with an Inline Transducer

After machining the plates to be tested, grooves between beads in the 3D printed surface and at the weld lines created additional challenges for vacuum bagging. The grooved surfaces allowed

significant leakage across the surface under the bag. To solve this, multiple layers of Derakane 8804 epoxy vinyl-ester resin [74] were applied around the plate sides about ~ 2 in around the top, sides, and bottom faces as shown in Figure 28. During this coating, close attention was paid to leaving the area within the bag uncoated. The coating isolates vacuum leakage through the weld and plate by removing the potential loss under the sealant tape due to surface imperfections within the 3D printed part.

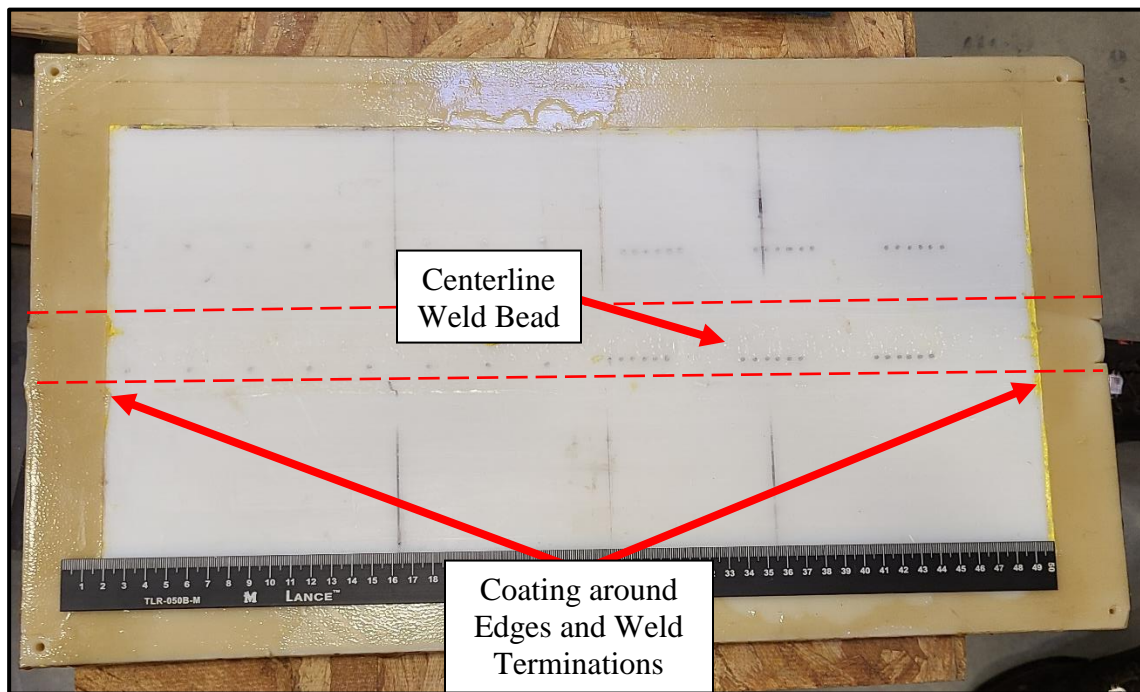


Figure 28: Resin Coated Edges for Improved Surface Seal

To measure the negative pressure of a vacuum infusion mold over time, an Omega PX-613 pressure transducer [75] (range -15 to +30 psi) with 1 to 5 Vdc output was used. The sensitivity of the transducer was verified as 784 mBar/V using a calibrated Ashcroft DG2531N1NAM02L0IM&V vacuum pressure gauge. The transducer was powered by a stable 24 VDC excitation from a Rigol DP711 programmable power supply wired to a 24-bit NI 9202 analog input Compact DAQ card [76]. This card was connected to a laptop running LabVIEW 2022 to

display and log this data, as shown in Figure 29 below. All data was collected at 200 Hz, averaged, and logged at 2 Hz.

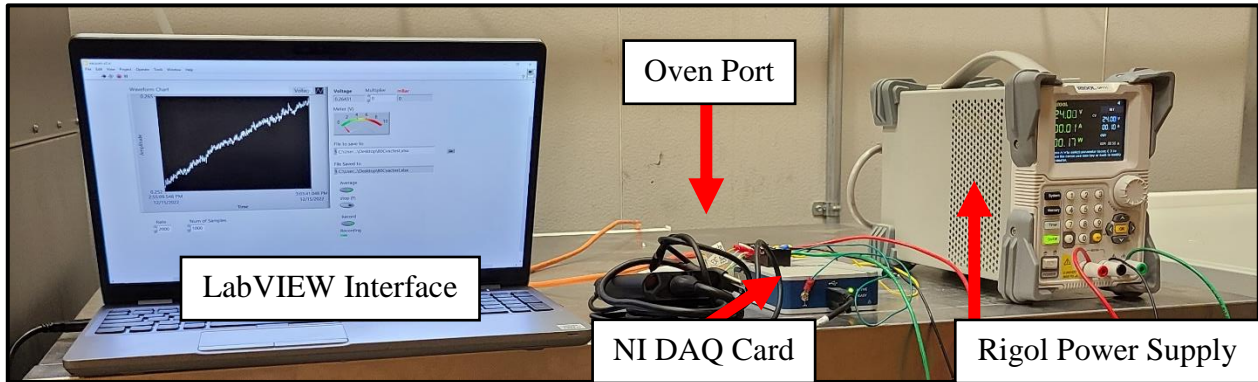


Figure 29: Data Acquisition Set-up

This data acquisition set-up was improved multiple times before data of sufficient quality for this work was captured. The power supply was upgraded to improve the stability of supplied excitation voltage to the setup. The DAQ card was also upgraded from 12-bit to 24-bit, greatly improving the resulting resolution of captured data.

4.1.3 Calibration & Processing Test Results

Atmospheric pressure was recorded using a wall-mounted barometer made by White instruments Inc. Additionally, an Ashcroft digital pressure gauge was zeroed to atmospheric pressure at the start of each test and then used to record the maximum vacuum pressure achieved at the beginning of the test. The results of this study are given in terms of absolute pressure, governed by Equation 1 below where atmospheric pressure and gauge pressure (in this case, vacuum pressure) are known and recorded at the start of each test.

$$P_{abs} = P_{atm} - P_{vac} \quad (1)$$

- Absolute Pressure (P_{abs}) is defined relative to absolute vacuum where absolute pressure is zero.
- Atmospheric pressure (P_{atm}) is defined as the pressure in the surrounding air.
- Vacuum pressure (P_{vac}) is defined as the difference between the system and the surrounding atmosphere.

In this work, all pressure measurements are reported in terms of absolute pressure with complete vacuum defined as zero pressure.

To convert the output of the transducer to a pressure readout in units of millibar, voltage readings were recorded at known pressures and then averaged to establish a two-point best fit straight line calibration. The first voltage measurement was taken under open-air atmospheric conditions, while the second measurement was recorded after the vacuum pump had run for at least three minutes to ensure the system was at maximum vacuum pressure. This calibration was conducted before each round of vacuum leakage tests to account for any differences in atmospheric pressure and the maximum pressure of the vacuum pump on the day of testing.

4.1.4 Vacuum Leak Rate Behavior

In vacuum bagged systems, the leak rate is not constant and initially occurs nonlinearly. After a length of time (t_{ss}), the leak rate reaches a linear, steady state region. This vacuum leak rate behavior is shown below in Figure 30, where region I represents the nonlinear region and region II represents the steady-state region. The cause of the nonlinearity of region I is likely due to consolidation and settling within the bag and flow media, causing an initial pressure change. As a result of this, the non-linear region is brief, lasting approximately five minutes for most 30 minute tests.

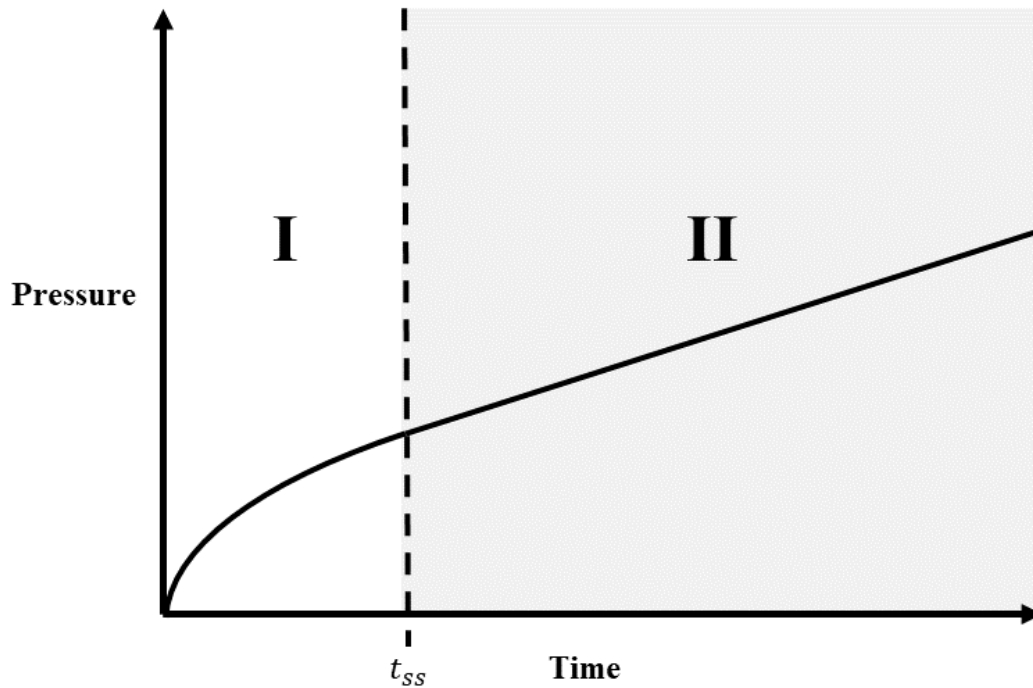


Figure 30: Vacuum Leak Rate Behavior

To improve the approximation of the steady state leak rate, this study will use a line of best fit to approximate the leak rate only in the steady-state region (region II).

4.1.5 Baseline Leak Rate in a Solid HIPS Plate

To measure the leak rates through joined AM specimens, the baseline leak rate of the test setup was first measured, which included the vacuum bag, tubing, and various tubing connections.

To achieve this, repeatable tests on solid ¼” HIPS plates were performed. The assumption was made that the solid polymer plate was impermeable to any vacuum loss. Therefore, any measured vacuum loss could be attributed solely to the bag system.

Five thirty-minute vacuum leakage tests were performed on the same area of a solid plate, using different bags each time. The vacuum system, transducer, connected tubing, and valves remained

the same throughout these tests. Figure 31 below shows the resulting change in pressure across the five tests.

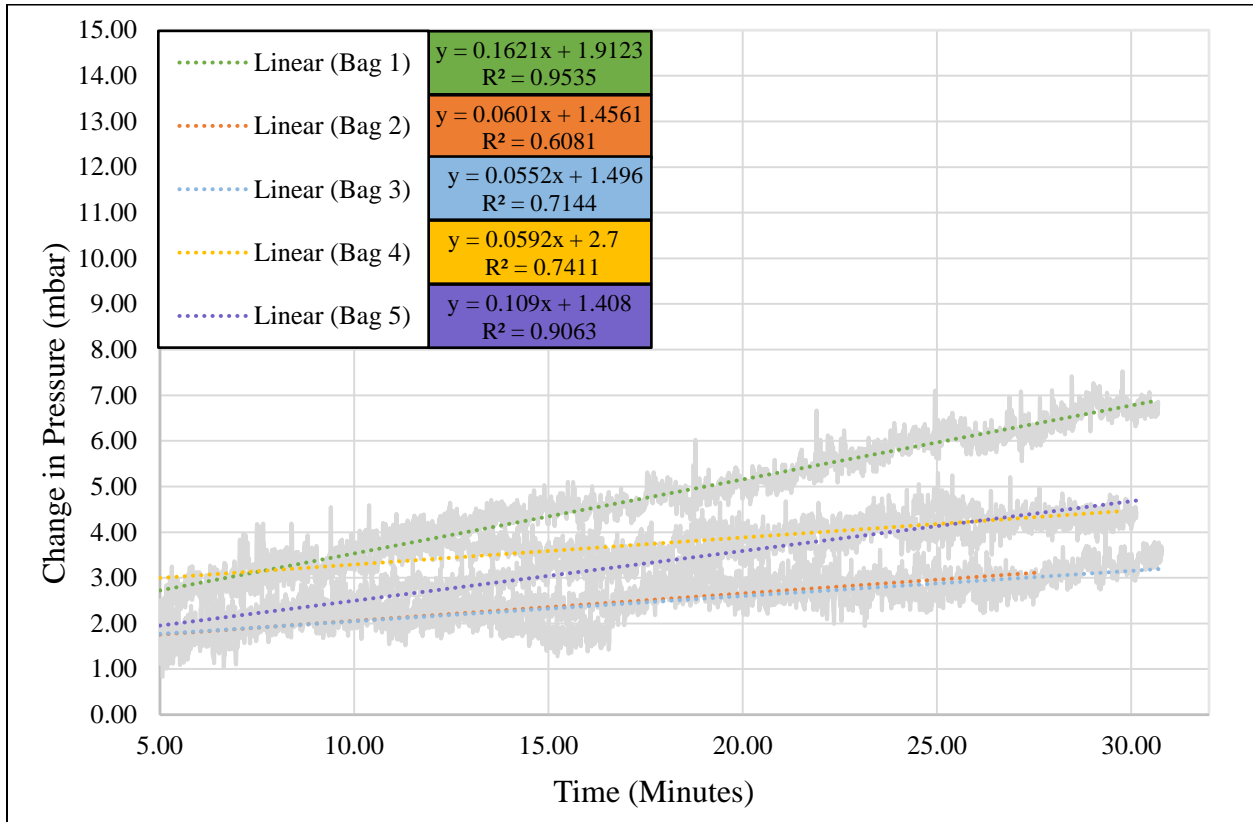


Figure 31: Baseline Vacuum Leak Rate in Solid HIPS Plate

Figure 31 shows the normalized pressure data for each test in grey, the best-fit lines for the linear portion of the pressure data, as well as their corresponding equations and R^2 correlation values. The slope of the change in pressure, or the rate of change in pressure, is the resulting vacuum leak rate for each test. The best-fit lines have an average R^2 value of 0.78, suggesting an acceptable correlation with the leakage data. The following Table 7 displays the vacuum pressure loss (ΔP) and corresponding linear leak rates for each of the five bags during the 30-minute test.

Table 7: Leak Rate in Five Vacuum Bags on a Solid Plate over 30 Minutes

Bag/Test	ΔP (mbar)	Leak Rate (mbar/min)
1	6.78	0.23
2	3.26	0.11
3	4.68	0.16
4	4.48	0.15
5	3.15	0.11
Average	4.47	0.15
Standard Deviation	1.46	0.05
Coefficient of Variation		33%

The leak rates across all five bags range from 3.15 mbar to 6.78 mbar over 30 minutes, with an average vacuum loss of 4.47 mbar, a standard deviation of 1.46 mbar, and a coefficient of variation of 33%. Although the coefficient of variation is high, it is within an acceptable and expected range considering the potential for variability in the vacuum bagging process. The average vacuum loss of 4.47 mbar indicates that almost half of the allowable 10 millibar leakage within the industry specification may be due to the vacuum bag and tubing system itself, rather than permeation through the testing surface.

Potential sources of variability between bags include induced human error within the bagging process and the accuracy of the testing equipment. The Omega PX- 613 transducer [75] has a general accuracy of ± 2.76 mbar over the calibrated one atmosphere scale, including non-linearity, hysteresis, and non-repeatability errors. Additional noise may be induced by instability in the excitation voltage from the power supply or the data acquisition card.

4.1.6 Leakage Testing Welded AM Components at 20°C

Leakage testing was conducted on the welded AM plate at a room temperature of approximately 20°C. All tests were performed using a consistent vacuum bagging procedure and included the Derakane vinyl-ester epoxy coating [74] on the plate's edges and sides.

Figure 32 illustrates the normalized vacuum leakage over 30 minute period, represented as the change in pressure in units of millibar. The rate of pressure change corresponds to the leak rate of the bag system, the AM plate, and the weld. The pressure data have been normalized to demonstrate the change in pressure during the test. Furthermore, all tests were initiated below the specification requirement of 20 mbar (0.59 inHg) absolute pressure.

Figure 34 shows the change in pressure in units of millibar for the four tests, presented in grayscale. The best-fit lines and correlation are provided for each test. The red bold line indicates the project specification requirement of a maximum leak rate of 10 mbar over a 30-minute period.

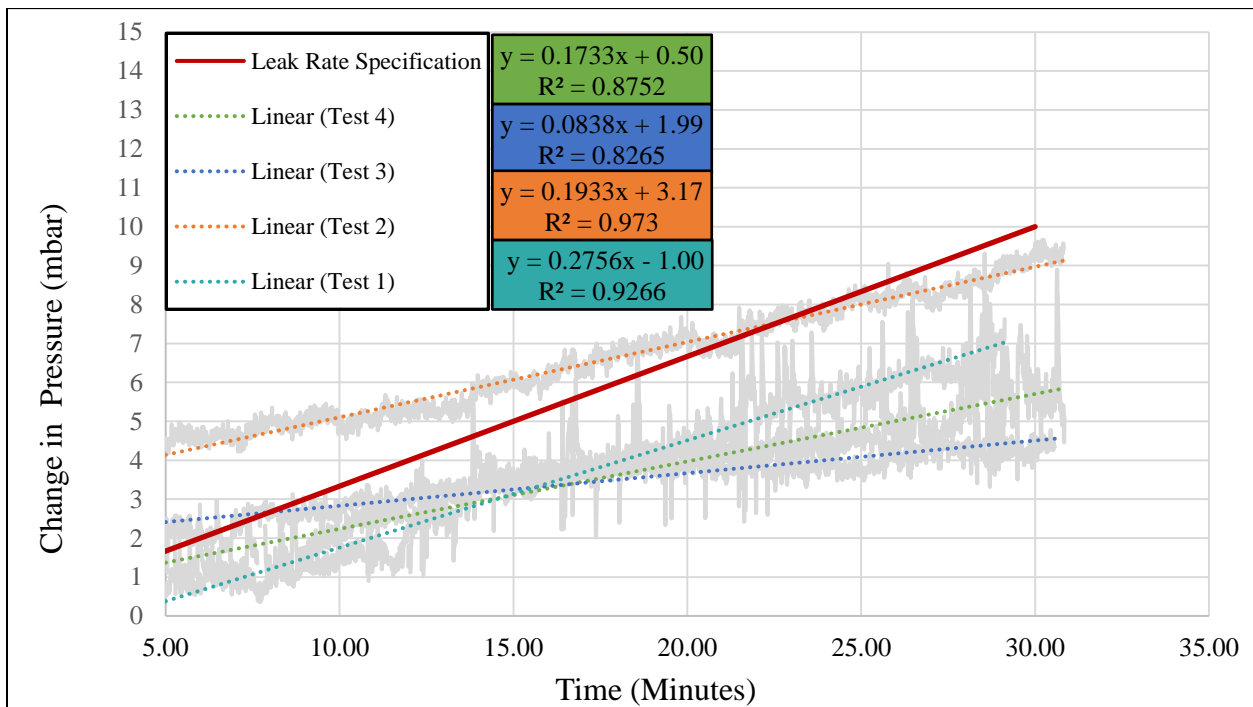


Figure 32: Pressure Change due to Leakage of Vacuum in Welded AM HIPS Plate at 20°C

Table 8 shows the pressure change and the leak rate of the welded AM plate. The best-fit lines exhibit a strong correlation with the leakage data, as indicated by an average R^2 value of 0.90.

Table 8: Leak Rate of Welded AM HIPS Plate at 20°C

Bag/Test	ΔP (mbar)	Leak Rate (mbar/min)
1	5.70	0.24
2	4.51	0.30
3	8.97	0.15
4	7.27	0.19
Average	6.61	0.22
Standard Deviation	1.94	0.06
Coefficient of Variation		29%

The leak rates over 30 minutes for the welded AM plate at 20°C range from 4.51 mbar to 8.97 mbar, with an average leak rate of 6.61 mbar, a standard deviation of 1.94 mbar, and a coefficient of variation of 29%. This variation is considered acceptable given the high potential for variability in the vacuum bagging process. However, tests three and four exhibit some noise not observed in the other tests, which may be attributed to vibration or additional current draw from on-site work that affected the transducer's excitation voltage.

To isolate the vacuum leakage due to permeation of the welded AM plate from the vacuum leakage of the baseline bag system, the baseline leak rate will be deducted from the AM joint leak rate as shown below in Equation 2.

$$\frac{dP_{\text{Permiation}}}{dt} = \frac{dP_{\text{Total}}}{dt} - \frac{dP_{\text{Baseline}}}{dt} \quad (2)$$

$\frac{dP_{Permiation}}{dt}$ is defined as the vacuum leak rate due to permeation of the welded AM plate.

$\frac{dP_{Total}}{dt}$ is defined as the total vacuum leak rate through the bag system and Welded AM plate.

$\frac{dP_{Baseline}}{dt}$ is defined as the vacuum leak rate through the bag system.

Equation 2, was used to separate the leakage of the welded AM plate from that of the bag system, as depicted in Figure 33 below. The results showed that, at 20°C, the welded AM plate had an average leakage of 2.14 millibar over a 30-minute test. This value is represented by the grey area in Figure 33, which is the difference between the total leakage and the baseline leakage. The region below the baseline represents the average measured leakage through the bag system.

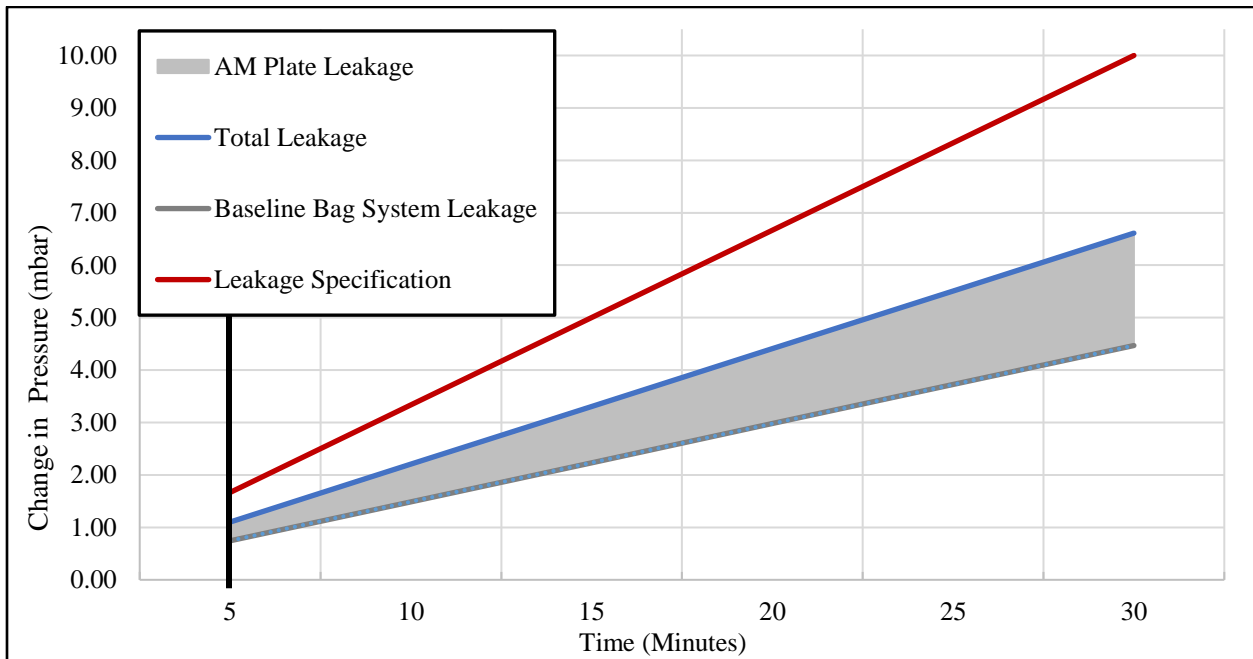


Figure 33: Average Leakage due to Permeation through the Welded AM Plate

Based on these results, the isolated leak rate of the welded AM plate satisfies the surface vacuum integrity requirement for AM tooling surfaces at 20°C. However, it is important to note that the vacuum loss through the bag system is just as high as the leakage through the welded AM plate.

To summarize, the vacuum leakage testing of the welded AM plates met the conventional thermoset mold surface vacuum integrity requirement for vacuum infusion of wind turbine blades. This was achieved by satisfying both the initial maximum vacuum requirement of less than 20 millibar and the maximum leak rate specification of 10 mbar over 30 minutes.

4.1.7 Leak Testing AM Components at 80°C

Heated molds are used in the VARTM process to improve resin curing. For wind blade manufacturing, the specified infusion temperature is 80°C. However, the industry vacuum integrity specification is conducted at room temperature and not at the infusion temperature. Thus, meeting the vacuum integrity specification is not required at 80°C during the initial vacuum integrity check of the surface and bag system. This is because the mold will be heated during the infusion while the pump is running. Evaluating the vacuum integrity at the infusion temperature provides valuable insight into how the welded AM plate behaves at elevated temperatures, even if it is beyond the specification.

To test the vacuum integrity of the welded joint within an AM surface at infusion temperatures, vacuum leakage testing was conducted in ASCC Oven #2 (AS# 4283) at 80°C, as shown in Figure 36 below.

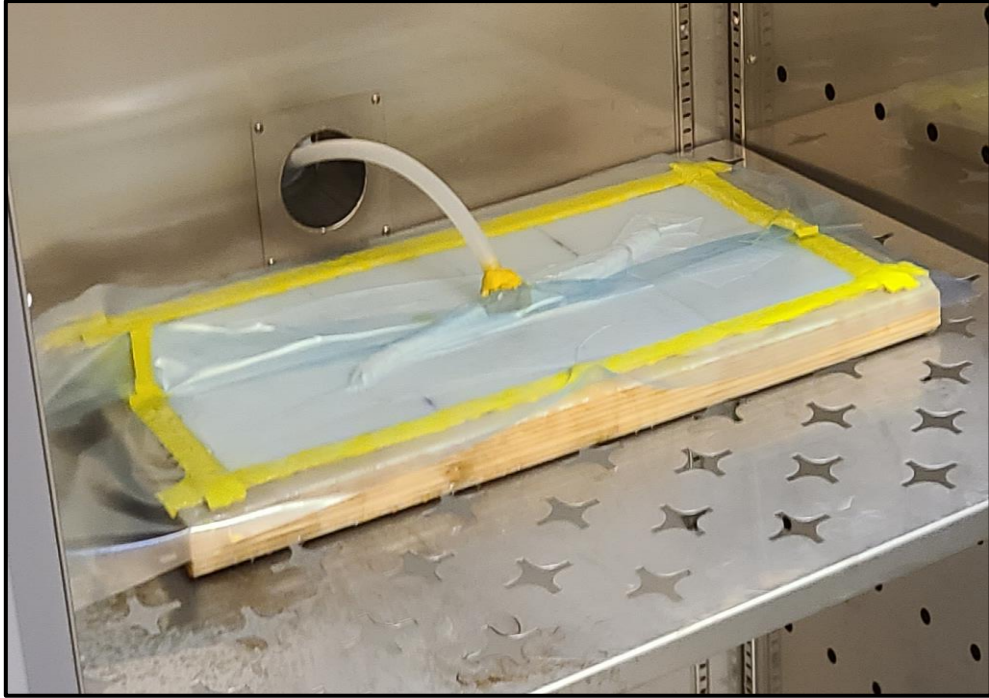


Figure 34: Welded AM Plate in Oven at 80°C

All vacuum leakage tests presented at 80°C were conducted multiple times and bagged repeatably following the vacuum bagging procedure. The same vacuum pump used for the other tests was utilized, and the vacuum line was directed through a port at the rear of the oven. To maintain consistency, the tubing length from the bag to the shutoff valve and the transducer remained unchanged, with only the distance between the shutoff valve and the vacuum pump being adjusted. This ensured that the same system was used for the 80°C testing as for the 20°C testing.

Figure 35 shows that at 80°C, the welded plate and bag system experienced a total vacuum loss of approximately 27 mbar over two 30-minute tests. The additional vacuum loss observed could have originated from either the part surface or the bag system, but the latter is considered more likely. This is because the vacuum sealant tape appeared to have softened at 80°C, despite being rated for operational use up to 204°C. This softening may have weakened the seal between the part surface and the tape, resulting in increased vacuum loss through the bag system. Within this testing, the

vacuum loss through the bag system was not tested as it was during the 20°C testing, therefore the leakage difference of the part and bag system was not measured. Further testing is recommended to analyze and isolate the vacuum leakage sources at 80°C.

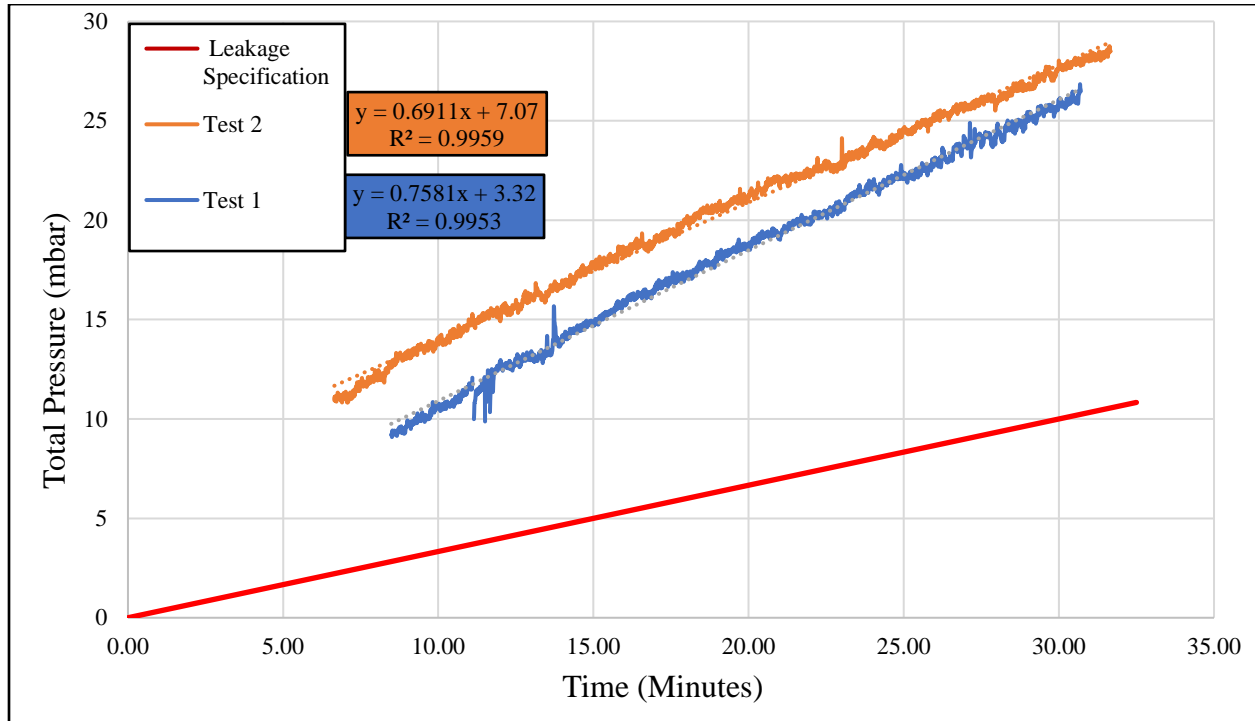


Figure 35: 25 Millibar Vacuum Loss in Welded AM HIPS Plate at 80°C

Evaluating vacuum integrity in the welded AM plate at elevated temperatures provides valuable insights into its performance within a tooling structure. These large-scale composite joints will experience significant thermal loads during part infusion and cure. Therefore, elevated temperature testing further confirms that the welded joint can maintain vacuum integrity with the vacuum pump running during the resin infusion manufacturing process. This is especially important in thermoplastic tooling surfaces, where the coefficient of linear thermal expansion can be significantly higher than that of thermoset composite surfaces.

4.2 Surface Finish

To assess the surface quality of the machined 3D printed HIPS material and the machined welded surface, hardness and roughness data were collected for each case. A Starrett 3805D Shore D Durometer [77] with a digital readout and a deviation of less than 1% was utilized following the manufacturers standard procedure. A Mitutoyo SJ-210 Portable Surface Roughness Tester [78] with a measuring force of 4mN, an axis range of 0.7 in, and a tip radius of 5 μ m was utilized to evaluate roughness following the standard procedure provided by the manufacturer. Specification sheets for both instruments can be found in Appendix D.

4.2.1 Surface Finish Specification for Thermoset Tooling Surfaces

Table 10 below shows the project goals set for the surface finish, which were defined based on conventional glass fiber-reinforced epoxy thermoset tooling surface specifications for the manufacturing of wind blade molds.

Table 9: Surface Specifications for Conventional Thermoset Blade Molds [70]

Surface Criteria	Specification
Hardness	Shore D 80
Roughness	< 5 μ m (196.85 μ in)

Surface hardness is a material property. Therefore, HIPS, an unfilled amorphous thermoplastic, will have a lower hardness than a filled engineering grade thermoplastic. As a result, a lower hardness is expected in the HIPS surface. Surface hardness varies between thermosets and thermoplastics, with thermosets typically having a higher surface hardness than thermoplastics. Depending on the surface coating chosen, a change in the hardness specification may be warranted.

In addition, surface roughness can be improved in thermoplastics by sanding and polishing, leading to a significant enhancement in the surface finish.

4.2.2 Surface Hardness Results

A total of 18 surface hardness data points were recorded in three sets of six measurements, spaced 0.25 in apart, on both the 3D printed and welded HIPS. Measurements were taken along the weld and bead direction as shown in Figure 36 below.



Figure 36: Starrett 3805D Shore D Durometer in use on weld

Table 10 below shows the mean, standard deviation, and coefficient of variation for each set of six of indentations. To account for potential variations in hardness along the length of the weld, three sets of indentations were recorded.

Table 10: Hardness of HIPS at 20°C

HIPS	3DP (Machined)	Extrusion Welded
Indentation	Hardness (Shore D)	
1.1	80.5	60
1.2	81	81
1.3	80.5	79.5
1.4	81.5	54
1.5	81.5	77.5
1.6	80.5	75.5
Mean	80.92	71.25
SD	0.449	10.363
CV	0.55%	14.54%
2.1	81.0	65.5
2.2	80.5	72
2.3	81.0	79
2.4	80.5	56.5
2.5	81.0	79.5
2.6	81.0	61.5
Mean	80.83	69
SD	0.236	8.602
CV	0.29%	12.47%
3.1	81.5	80
3.2	80.0	79.5
3.3	81.0	79.5
3.4	81.5	74
3.5	79.5	80.5
3.6	80.5	76.5
Mean	80.67	78.33
SD	0.745	2.321
CV	0.92%	2.96%

Table 11 below shows the mean, standard deviation, and coefficient of variation in hardness along the length of the weld. The 3D printed and machined HIPS surface measured an average shore D hardness of 80.81, 5.17% higher than the measured average shore D hardness of 72.86 in the

welded surface. All hardness measurements showed low variation and deviation. However, the weld data showed higher deviation and variance in hardness compared to the printed surface.

Table 11: Average Hardness of Printed and Welded HIPS at 20°C

Hardness (Shore D)		
	3DP (Machined)	Extrusion Welded
Mean	80.81	72.86
Standard Deviation	0.531	8.836
Covariance	0.66%	12.13%
Percent Difference	10.34%	

The 3D-printed HIPS surface was found to be 10.34% harder than the welded surface, despite being manufactured with the same feedstock and machined at the same time with the same end mill. This difference in hardness may be attributed to the different processing temperatures, extrusion nozzle, or pressure during extrusion welding and 3D printing, which could affect the resulting density and finish of the surface.

The finished weld shore D hardness of 72.86 did not meet the hardness specification of shore D 80 for conventional production tooling surfaces as shown in Table 9. This decrease in hardness was expected for a thermoplastic tooling surface when compared to cured thermoset tooling surfaces. This is material dependent and does not include a surface tooling coating, which may affect the surface finish.

4.2.3 Surface Hardness Results at 80°C

To gain a comparison at infusion temperatures of 80°C, the surface finish was tested after placing the welded plate in an oven at 80°C for one hour. Again, following the standard hardness testing procedure as shown in Table 12 below.

Table 12: Hardness of HIPS at 80°C

HIPS	3DP (Machined)	Extrusion Welded
Indentation	Hardness (Shore D)	
1.1	78	70.5
1.2	77	77
1.3	77.5	77.5
1.4	77.5	76.5
1.5	78.5	56.5
1.6	75	71.5
Mean	77.25	71.583
SD	1.109	7.271
CV	1.44%	10.16%
2.1	77.5	72
2.2	77.5	51.5
2.3	78.0	75
2.4	76.5	45.5
2.5	77.5	64
2.6	78.0	76
Mean	77.50	64
SD	0.500	11.744
CV	0.65%	18.35%
3.1	72.5	67
3.2	77.0	60
3.3	77.5	66.5
3.4	76.5	77
3.5	77.5	71.5
3.6	77.5	76
Mean	76.42	69.67
SD	1.789	5.885
CV	2.34%	8.45%

The mean, standard deviation, and coefficient of variation for all tests at 80°C are compared below in Table 13. The 3D printed and machined HIPS surface measured an average shore D hardness of 77.06, 11.88% higher than the measured average shore D hardness of 68.42 in the welded surface. The printed surface shows low variation and deviation at 1.73%, however, the weld data showed higher deviation and variance in hardness than the printed surface at 13.52%.

Table 13: Average Hardness of Printed and Welded HIPS at 80°C

Hardness (Shore D)		
	3DP (Machined)	Extrusion Welded
Mean	77.06	68.42
Standard Deviation	1.332	9.247
Covariance	1.73%	13.52%
Percent Difference	11.88%	

The 3D printed HIPS surface at 80°C was 11.88% harder than the welded surface despite being manufactured with the same feedstock and machined at the same time with the same end mill. This may have been a result of the different processing temperatures, the extrusion nozzle difference, or pressure during extrusion welding and 3D printing affecting the resulting density and finish of the surface.

4.2.4 Comparing Surface Hardness Results at 20°C and 80°C

As anticipated, the hardness of thermoplastic surfaces decreases when tested at elevated temperatures, as a result of the softening of the polymer surface material. Specifically, a reduction in hardness from 72.86 at 20°C to 68.42 at 80°C was observed, representing a 6% difference in measured weld surface hardness between room temperature and infusion temperatures.

The finished HIPS weld does not meet the hardness specifications of shore D 80 for conventional production tooling surfaces as defined in Table 9. This decrease in hardness is expected for a thermoplastic surface when compared to cured thermoset surfaces. It is important to note that this material-dependent result does not consider the potential effect of a surface tooling coating, which may improve the surface finish. While the weld surface and printed surface do not meet the same

specification, their performance is similar when exposed to a 60°C temperature increase that occurs during resin infusion on large-scale components.

4.2.5 Surface Roughness Results

For the 3D printed and welded HIPS, eight data points were captured for surface roughness measurements along the weld and bead direction. The mean, standard deviation, and coefficient of variation are shown in Table 14 below. The 3D printed and machined HIPS surface measured an average surface roughness of 50.18 μin and the machined weld had an average surface roughness of 38.93 μin . The roughness measurements showed a standard deviation between 10.18 and 13.86 from the mean, which yielded a coefficient of variation of 20.3% for the 3D printed surface and 35.6% for the weld surface.

Table 14: Roughness of Printed and Welded HIPS at 20°C

HIPS:	3DP (Machined)	Extrusion Welded
Trial	Roughness "Ra" (μin)	
1	57.09	62.66
2	72.87	50.25
3	42.75	18.03
4	45.76	39.22
5	47.35	22.51
6	40.92	49.14
7	53.8	34.08
8	40.93	35.56
Mean	50.18	38.93
Standard Deviation	10.18	13.86
Covariance	20.3%	35.6%
Percent Difference	25.25%	

With a surface roughness of 38.93 μin , the welded HIPS was 25.25% smoother than the machined 3D printed surface. This difference may be due to the nozzle diameter of the welder being larger than that of the 3D printer, resulting in a wider weld and larger solid surface area for the roughness

tester stylus to pull across. In contrast, the 3D printed part is composed of many smaller beads, potentially leading to a higher overall roughness.

4.2.6 Surface Roughness Results at 80°C

At 80°C, surface roughness was measured in the 3D printed and welded HIPS following the same procedure as above. Table 15 below shows the mean, standard deviation, and coefficient of variation of the average roughness of the printed and welded HIPS.

Table 15: Average Roughness of Printed and Welded HIPS at 80°C

HIPS:	3DP (Machined)	Extrusion Welded
Trial	Roughness "Ra" (µin)	
1	38.44	32.3
2	50.89	45.2
3	39.18	37.57
4	49.24	38.6
5	49.84	33.34
6	42.12	60.73
7	76.16	52.01
8	47.33	69.87
Mean	49.15	46.20
Standard Deviation	11.18	12.73
Covariance	22.7%	27.6%
Percent Difference	6.18%	

At 80°C, the 3D printed and machined HIPS had an average surface roughness of 49.15 µin, while the machined weld had an average surface roughness of 46.20 µin, making it a 6.18% smoother surface. The roughness measurements had a standard deviation of 11.18 and 12.73 from the mean, which resulted in a coefficient of variation of 22.7% for the 3D printed surface and 27.6% for the weld surface.

4.2.7 Comparing Surface Roughness Results at 20°C and 80°C

At both 20°C and 80°C, the surface roughness of the weld increased, while that of the printed surface decreased slightly. Specifically, the roughness of the weld increased from 38.93 μin at 20°C to 46.20 μin at 80°C, representing a 16% difference in the measured surface roughness between room temperature and infusion temperatures. Additionally, the roughness measurements of the two materials converged at 80°C, with only a 6.18% difference in roughness compared to a 25.25% difference at 20°C. While this convergence could be due to variability in the roughness measurement data, it may also indicate different surface responses between the two materials due to the 60°C increases in temperature.

The data also showed higher deviation and variance in roughness for the weld compared to the printed surface at both temperatures. This could be attributed to surface imperfections such as voids, bead line irregularities, and machining chatter marks, which are common in roughness measurements.

The weld roughness post-machining of 38.93 μin at 20°C and 46.20 μin at 80°C met the roughness specifications of less than 196 μin for conventional production tools, as shown in *Table 9*. Although machining was the only finishing step performed, roughness could be further improved with additional finishing steps such as sanding and polishing.

4.3 Mechanical Testing of 3D Printed Components with Welded Joints

To evaluate the mechanical strength of the welded joint, standardized ASTM tests were conducted on welded AM coupons. Two tests were performed to quantify mechanical strength in these welded coupons: ASTM D638, the Standard Test Method for Tensile Properties of Plastics, and ASTM D790, the Standard Test Method for Flexural Properties of Unreinforced and Reinforced Plastics and Electrical Insulating Materials [79], [80]. These tests were conducted at controlled atmospheric conditions following the specimen and laboratory conditioning standard ASTM D618, Standard Practice for Conditioning Plastics for Testing [81]. The one-inch-thick specimens were conditioned at 21°C – 25°C in a 40% - 60% relative humidity for longer than the required 88-hour period in preparation for mechanical testing. The calibration information for the universal testing machines and load cells utilized in this testing are shown in Appendix A.

4.3.1 Tensile Testing of Welded AM Specimens

Tensile testing was conducted on EM #3 an Instron 68FM – 100 (AS4397) electro-mechanical universal testing machine with a 22-kip load cell (AS4396) as depicted in Figure 37. The ten specimens were cut on a flow waterjet, with type 3 dimensions following ASTM D638.

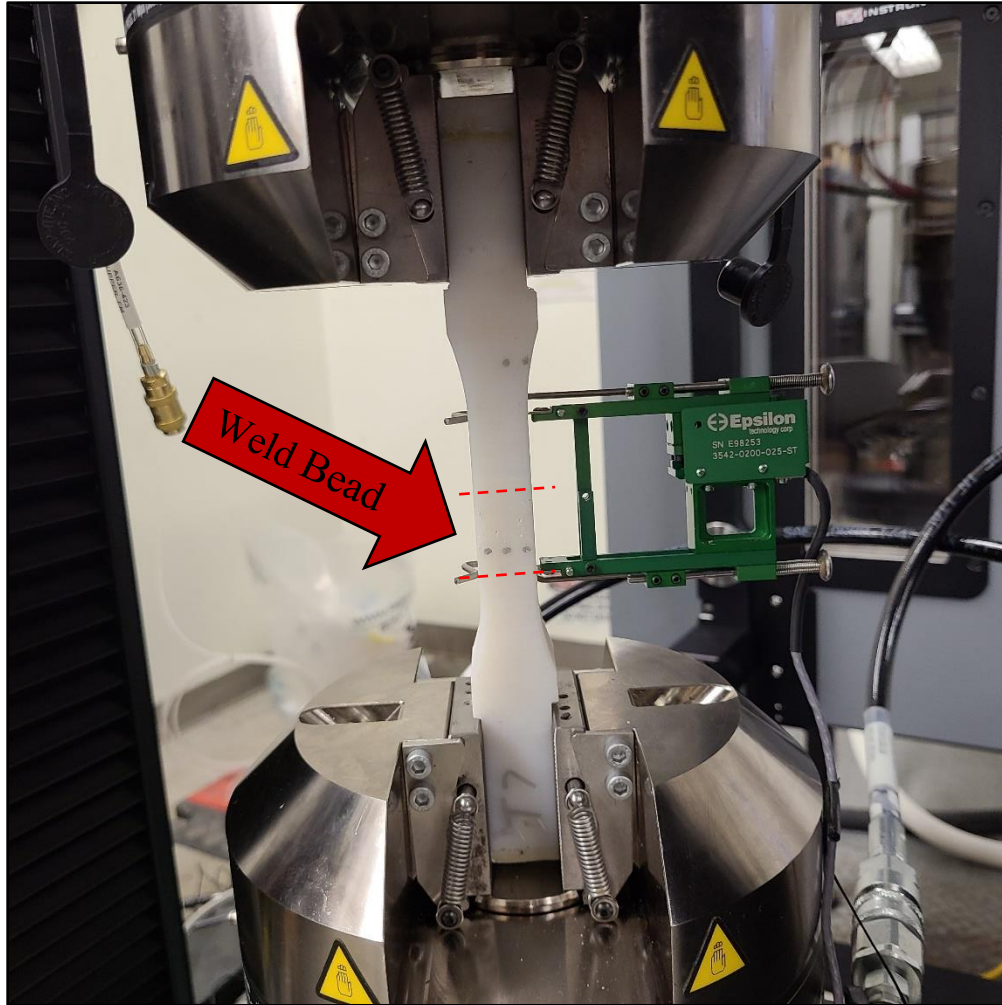


Figure 37: Tensile Test Setup

The ASTM D638 standard tensile test method was adapted to accommodate the increased 1-inch plate thickness across the welded joint within the AM plate. The material thickness within the grips was reduced to enable the Instron grips to hold the ends of the thick specimens, as shown in the above image.

The average measured gauge area of these specimens is 0.88 in^2 , following the type 3 dimensions for width but adapting the specimen thickness. Strain, or percent elongation, was captured using an Epsilon axial extensometer attached to the specimen.

These specimens were tested in what is considered to be the weak material print direction [82], which is transverse to the bead and weld direction as illustrated in Figure 38 below. This was a deliberate choice aimed at assessing the more probable transverse failure within the joint if welded parallel to the print direction. This print and weld orientation represents the lowest strength implementation of this joining method in an AM component [82].

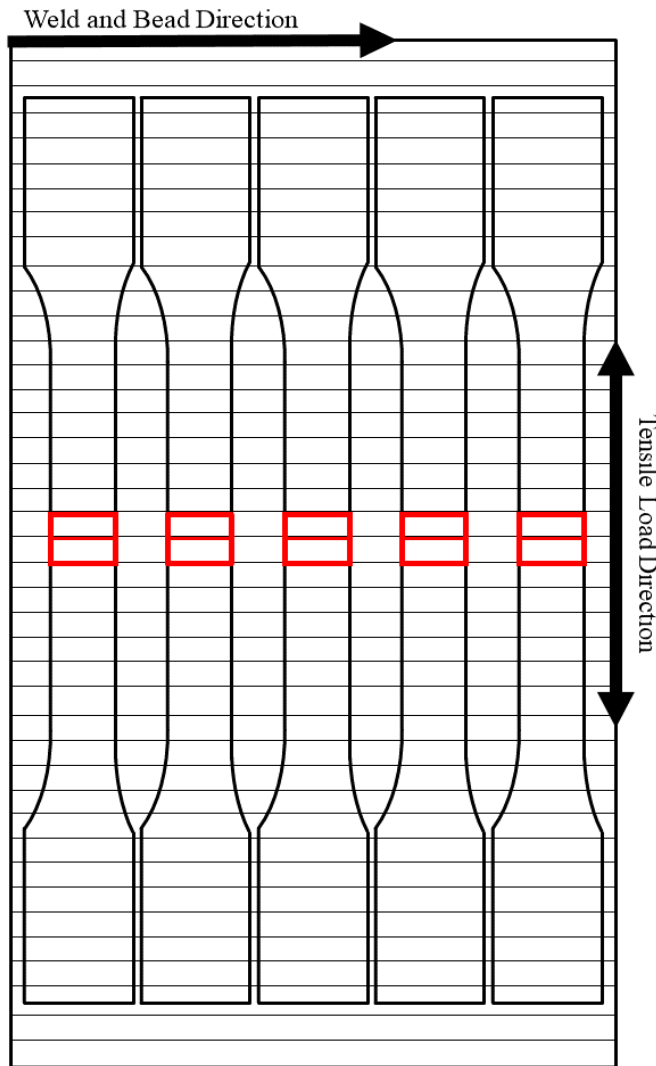


Figure 38: Diagram of Material Anisotropy, Welded Joint, and Load Direction

To compare the welded specimen strength with the base AM material, an assumption was made to compare the bulk strength of injection molded HIPS with the transverse, or 90 degree, strength of AM HIPS specimens. Literature has shown that AM ABS specimens with various layer orientations have failed between 50 percent and 83 percent of the injection molded ABS's strength across ten ASTM D638 tests [83]. For this work, a conservative base AM material tensile strength of 1800 psi or 60 percent of the bulk HIPS polymer strength, shown in Table 4, will be used.

4.3.2 Results of Tensile Testing

The Instron machine provided time, force, and displacement data. The attached extensometer provided strain data. This data was utilized in accordance with ASTM D638 to calculate the strength and modulus of each specimen. The tensile stress at failure was calculated using Equation 3 below.

$$\sigma_{weld} = \frac{Max\ Force}{Gauge\ Area} \quad (3)$$

- Max Force is defined as the maximum load experienced during the test.
- Gauge Area is the measured specimen thickness times its width in the specimen gauge region.

Equation 3 shows that, on average, these welded specimens failed at a tensile stress of 1435 psi, with a standard deviation of 301.4 psi and a coefficient of variation of 21%. The resulting failure stress, strain at failure stress, and chord modulus was tabulated for each tensile load for specimen in Table 16 below. Unfortunately, the strain data captured from the attached extensometer showed significant error due to a portion of the elongation occurring outside the extensometer within the AM part. To resolve this, bulk strain was captured following the ASTM D638 standard using the displacement and gauge length of the type three specimens. Chord modulus was calculated using

a two point slope approximation of the stress-strain curve shown below in Figure 40 again following the D638 standard.

Table 16: Tensile Testing Results

Specimen	Maximum Force (lb)	Maximum Stress (psi)	Tensile Strain at peak load (%)	Chord Modulus (psi)
T1	1639	1843	2.70	68,165
T2	1540	1766	2.33	75,779
T3	1218	1404	1.71	82,358
T4	940.6	1073	1.41	76,080
T5	907.7	1017	2.30	55,966
T6	1434	1629	2.05	79,471
T7	1401	1568	1.98	79,377
T8	1236	1411	1.73	81,788
T9	1455	1669	2.19	76,377
T10	861.3	972	1.15	84,485
Average	1263	1435	1.95	75,983
SD	264.1	301.4	0.38	79,52
CV		21%	19.6%	10.5%

To evaluate the strength of the welds within the specimens, weld factor (f_w) [54] was calculated using the assumed ultimate tensile strength of the base AM material. The weld factor, or comparative weld strength, is defined in Equation 4.

$$f_w = \frac{\sigma_{weld}}{\sigma_{base}} \quad (4)$$

- σ_{weld} is defined as the maximum tensile strength seen during the test.
- σ_{base} is defined as the tensile strength of the HIPS base material, or 60% of bulk HIPS material tensile strength.

These weld factors were calculated using an assumed base material strength of 60% the bulk HIPS material tensile strength from Table 4 and tabulated for comparison below in Table 17.

Table 17: Comparative Weld Strength of Tested Specimens

Specimen	Maximum Stress (psi)	Tensile Weld factor (f_w)
T1	1843	1.02
T2	1766	0.98
T3	1404	0.78
T4	1073	0.60
T5	1017	0.56
T6	1629	0.91
T7	1568	0.87
T8	1411	0.78
T9	1669	0.93
T10	972	0.54
Average	1435	0.80
SD	301.4	0.17
CV		21%

Table 17 shows that, on average, these welded specimens failed at 80% of the tensile strength of the HIPS base material, with a standard deviation of 17% and a coefficient of variation of 21%. This variation in maximum stress for polymer welds suggests that the welded joint has a relatively

consistent mechanical strength along its length. Although the results indicate that the welded joint's strength is lower than the base material, there are other factors that affect the strength of these welded specimens, which are further discussed in the next section.

The load responses are shown in Figure 39 below, showing a rather linear loading response until failure within all specimens except T5. Specimen T5 shows significant inelasticity as it is loaded until failure in the print material.

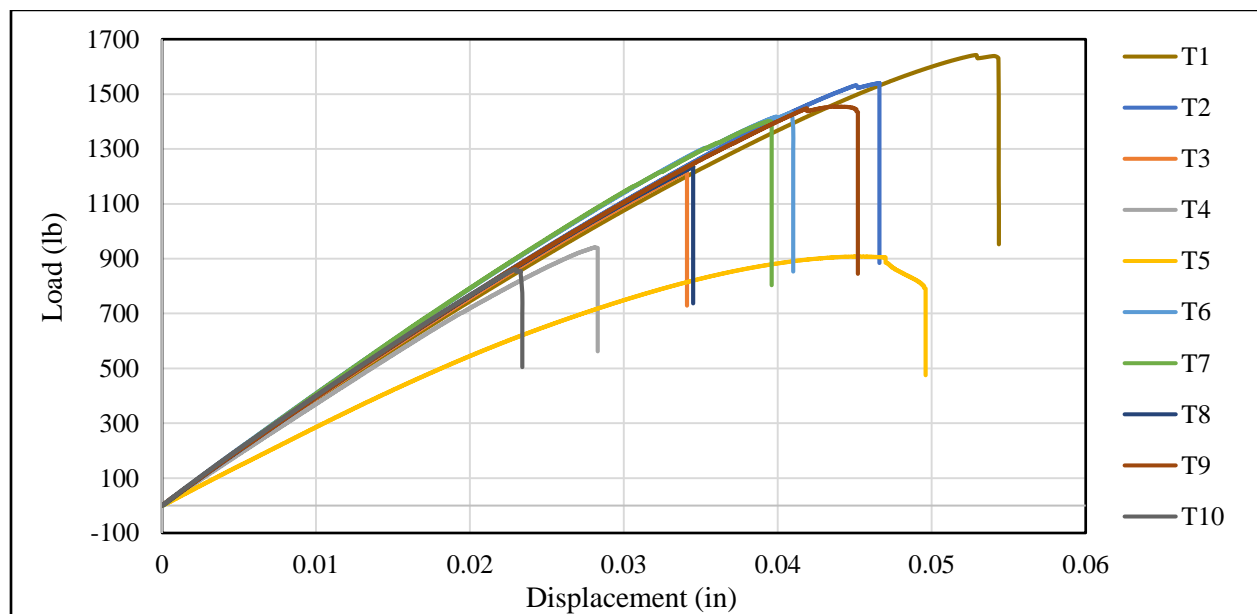


Figure 39: Force Vs Displacement Response of all Specimens

The stress vs strain response of all ten tensile specimens is shown in Figure 40 below. Just as observed in Figure 39, the response of all specimens is reasonably linear until failure, except specimen T5 which shows significant elasticity as evidenced by the change in slope of the curve, or change in modulus, before failure. Specimen T5 displays a very different tensile response than the others which is the leading source of deviation in the mechanical testing results.

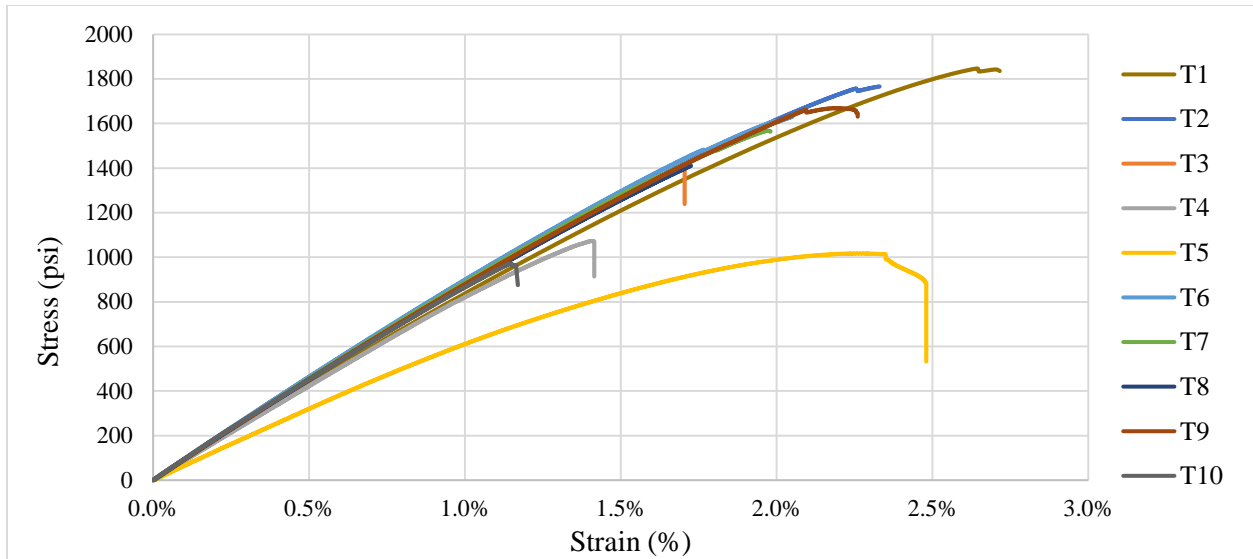


Figure 40: Stress Vs Strain Response for all Welded HIP Tensile Specimens

The average chord modulus of elasticity of these specimens was 75,984 psi, which is approximately a 104% difference from the modulus tabulated for the bulk HIPS polymer in Table 4. This represents a significant reduction in stiffness in an AM welded specimen from the reported stiffness of the bulk polymer, or an injection molded specimen. Figure 40 also shows a far lower percent elongation in the welded AM specimens than bulk polymer. This shows the welded AM specimens experienced embrittlement as a result of the AM and welding processes. This is consistent with relevant literature, showing that the AM process results in a reduction in specimen tensile strength, strain until fracture, and resulting elastic modulus compared to the properties of the bulk polymer manufactured via injection molding [84].

4.3.3 Tensile Failure

The resulting tensile strength in the joint is lower than the expected strengths of polymer hot gas welds in literature, although these strengths were obtained for different materials [54]. Moreover, the strength of these specimens is affected by the material anisotropy inherent in AM components that results in a variety of failure modes. The exhibited failure modes include:

- Failure within the weld material
- Failure within the printed material
- Multimodal, failure in both materials across the weld line

This indicates that the failure is not solely occurring at the welded joint, but the printed material is also failing, suggesting that the Juggerbot printed plate is comparable in strength to the welded joint. Table 18 below summarizes the failure modes of these tensile specimens.

Table 18: Failure Modes of Tensile Specimens

Specimen	Failure Mode
T1	Weld Line
T2	Multimodal
T3	Multimodal
T4	Weld Line
T5	Print Material
T6	Print Material
T7	Weld Line
T8	Print Material
T9	Print Material
T10	Multimodal

Figure 41 below shows failed tensile specimen “T7” that failed predominantly along the weld line, beginning at the top surface of the weld. However, this failure is multimodal, as it also failed vertically into the base material near the root of the weld instead of following the weld line diagonally as indicated by the red dashed line following the weld line.

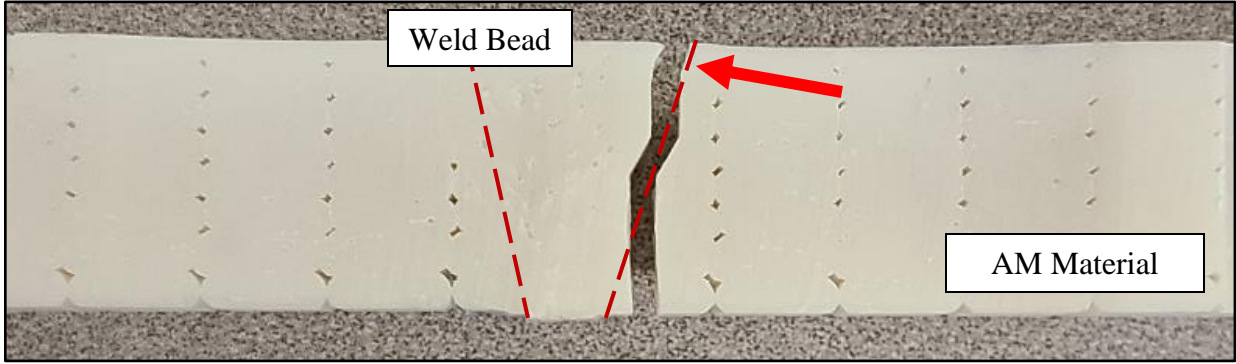


Figure 41: Failure Along Weld line in Tensile Specimen T7

Figure 42 below shows a tensile specimen that failed in the print material. This failure propagated from void to void between beads through the printed part.

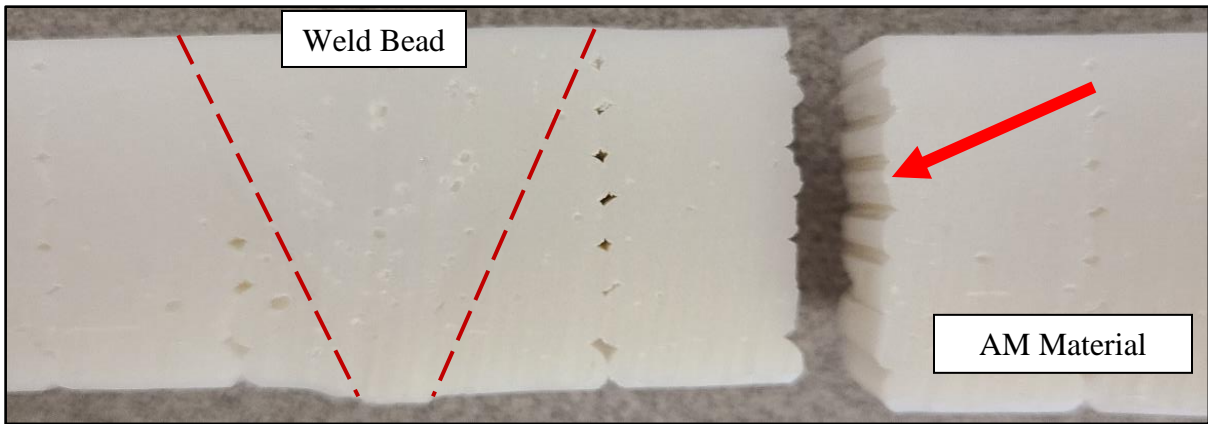


Figure 42: Failure in Printed Material in Tensile Specimen

4.3.4 Flexural Testing of Welded AM Specimens

Flexural testing was conducted on MTL #5 an Instron 8800 series 6” rotary stroke servo hydraulic universal testing machine (AS512) with a 25kN load cell (AS518) following ASTM D790. Eight specimens were cut on a flow waterjet. The ASTM D790 standard test method was again adapted to accommodate the increased 1 in plate thickness across the welded joint within the AM plate. To ensure adequate loading in bending and reduce the likelihood of shear-dominated failure within the specimens, the specimens were cut as long as possible with the available material. The three-point bend test set-up had an 11 in total span, or 5.5 in from the support to the load applicator as shown in Figure 43 below. Unfortunately, with an average measured cross-sectional area of 1.22 in^2 , not enough material was present to span the full 16:1 span-to-depth ratio suggested in the standard. This adaptation to ASTM D790 has been done previously within the lab for 3D printed specimens with larger bead sizes and has yielded acceptable results.

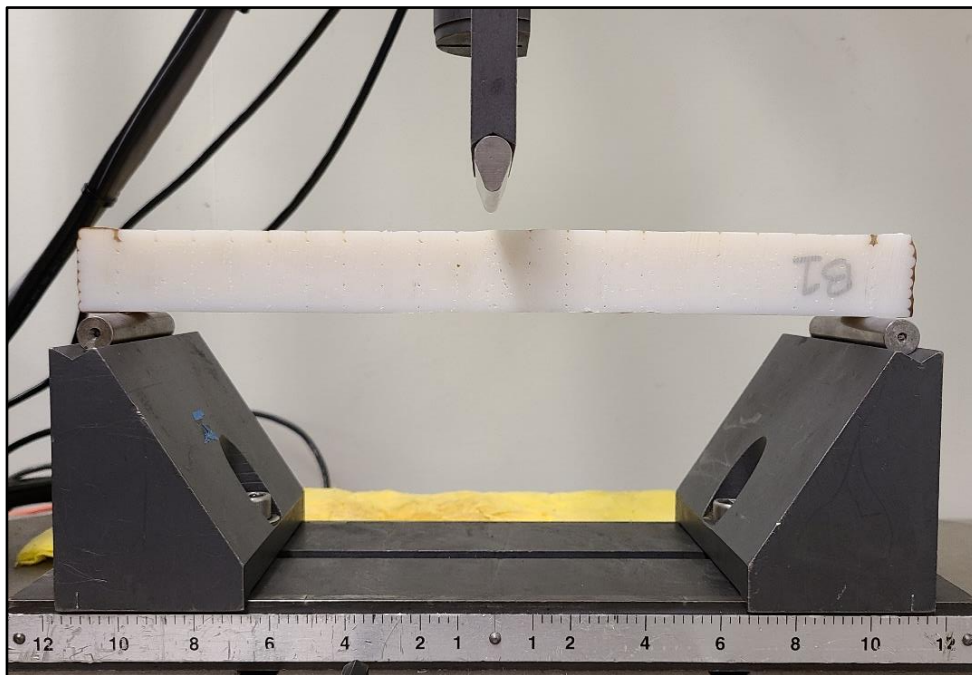


Figure 43: Flexural Test Set-up

4.3.5 Results of Flexural Testing

The Instron outputs load and position data that were used to graph load vs displacement graphs are shown in Figure 44.

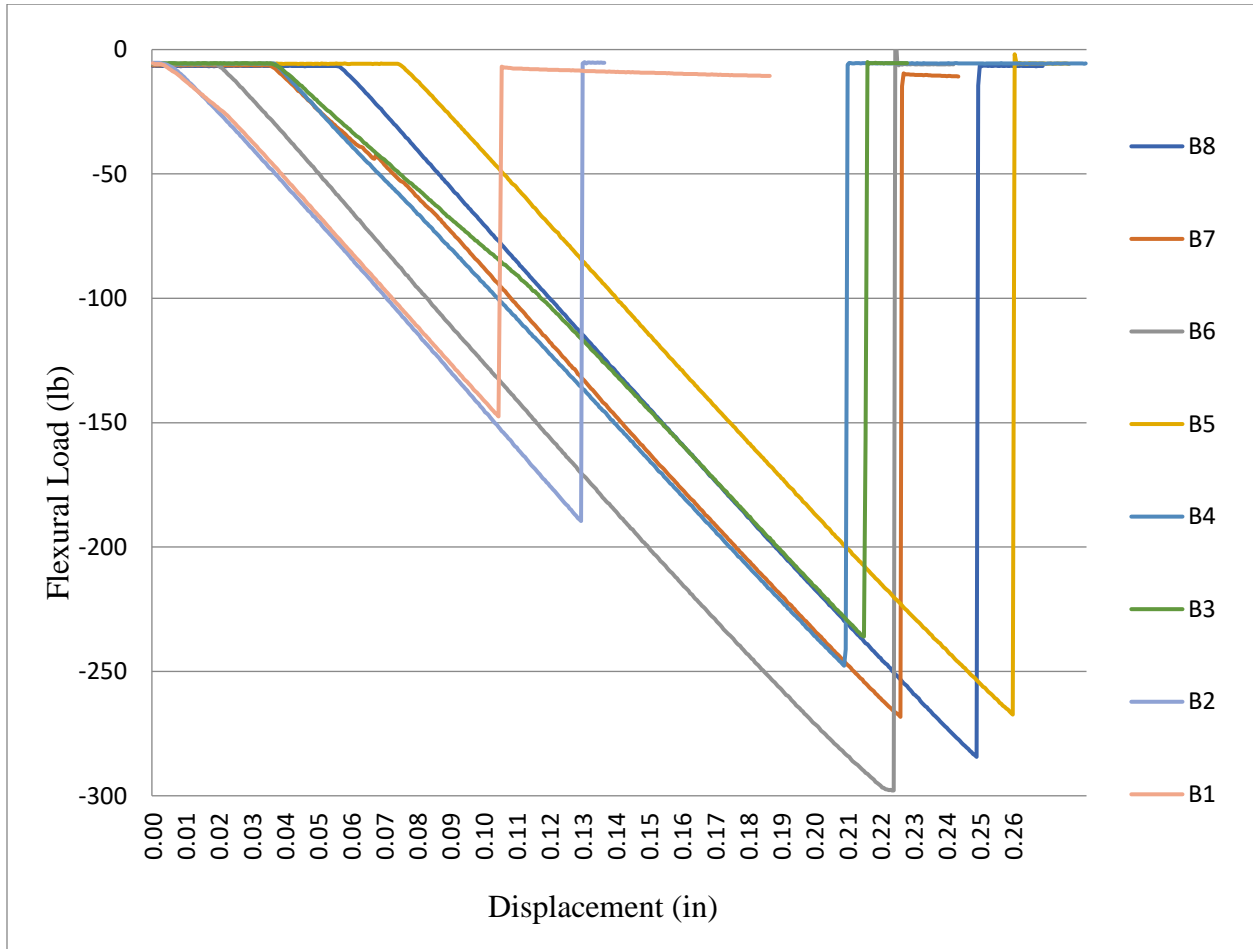


Figure 44: Load Response of all Specimens in Adapted D790 Flexure

Following ASTM D790, the flexural strength, flexural strain, and modulus of elasticity were calculated for each specimen. The flexural stress at failure was calculated using Equation 5 below.

$$\sigma_f = \frac{3PL}{2bd^2} \quad (5)$$

- σ_f is defined as the stress in the outer fibers at the midpoint in psi.
- P is defined as the peak load in pounds force.
- L is defined as the support span in inches.
- b is defined as the width of the specimen tested in inches.
- d is defined as the thickness of the plate tested in inches.

The flexural strain at failure was calculated using Equation 6 below.

$$\varepsilon_f = \frac{6Dd}{L^2} \quad (6)$$

- ε_f is defined as the strain in the outer surface (in./in.)
- D is defined as the maximum deflection of the center of the specimen in inches

The failure load, stress, and strain are tabulated for each flexural specimen in Table 19 below.

Table 19: Flexural Testing Results

Specimen	Maximum Load (lb)	Max Flexural Stress (psi)	Flexural Strain at Max Stress (%)	Chord Flexural Modulus (psi)
B1	147.5	1631	0.62	261,102
B2	189.6	2172	0.79	259,145
B3	235.9	2617	1.30	195,826
B4	247.7	2754	1.27	212,615
B5	267.4	2981	1.57	185,292
B6	297.8	3325	1.34	241,299
B7	268.3	2985	1.37	213,106
B8	284.4	3142	1.51	202,707
Average	242.3	2701	1.22	221,387
SD	47.4	521.6	0.32	27,042
CV	20%	19%	26%	12%

The average flexural stress at failure was found to be 2700 psi, with a standard deviation of 521.6 psi and a covariance of 19%. This level of variation is consistent with the variability observed in the tensile strength results.

To assess the strength of the welds within the specimens in comparison to the HIPS base material, Equation 4 and 5 were calculated using the estimated flexural strength of an AM HIPS base

material of 5220 psi, or 60% the strength of the bulk polymer. These comparative weld strengths were then tabulated for comparison below in Table 20.

Table 20: Comparative Weld Strength in Flexure

Specimen	Flexural Stress (psi)	Comparative Weld Flexural Strength
B1	1631	0.31
B2	2172	0.42
B3	2617	0.50
B4	2754	0.53
B5	2981	0.57
B6	3325	0.64
B7	2985	0.57
B8	3142	0.60
Average	2701	0.52
SD	521.6	0.10
CV		19%

Table 20 shows a significant difference between the comparative strength in flexure in the tested specimens and the base material with an average comparative weld strength of 52% of the base polymer and a covariance of 10%. This performance indicated a poor performance in flexure as compared to the 80% comparative weld strength of the welded AM specimens in tension.

The stress vs strain response of all eight flexural specimens is shown in Figure 45 below. Just as observed in Figure 40, the response of all specimens is reasonably linear until failure, except specimen T5 which shows significant elasticity as evidenced by the change in slope of the curve, or change in modulus, before failure.

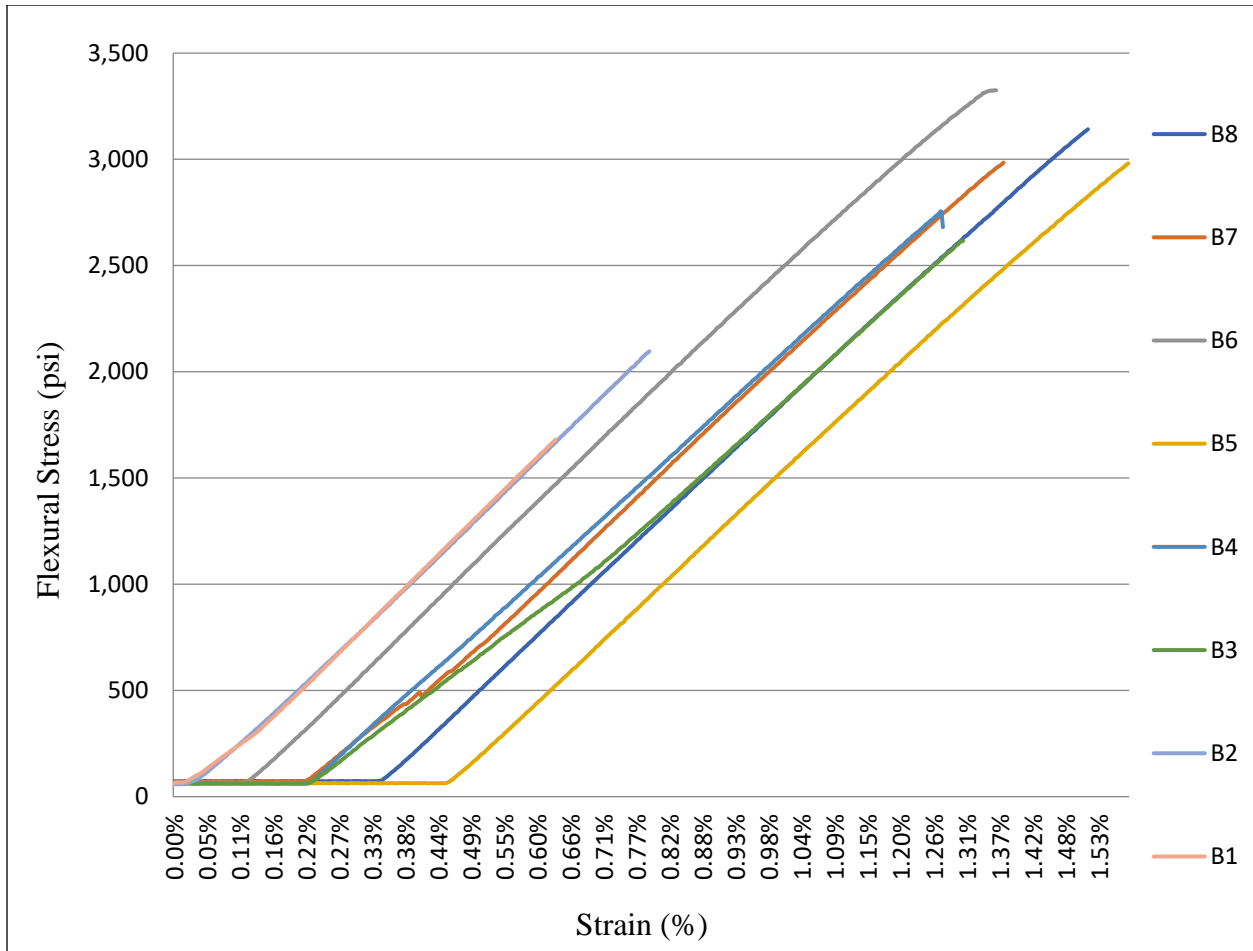


Figure 45: Stress Vs Strain Response of all Welded HIPS Flexural Specimens

The average chord flexural modulus of elasticity of these specimens was 221,386 psi, which is 23.38% less than the tabulated flexural modulus of the bulk HIPS polymer in Table 4. This represents a reduction in stiffness in an AM welded specimen from an injection molded specimen, however, this is a smaller reduction in stiffness in flexure than that was measured in tension.

4.3.6 Flexural Failure

The results of the flexural testing are similar to the tensile testing, with varying failure modes across the specimens. This suggests that the failure is not exclusively occurring at the welded joint and that the Juggernaut printed plate is comparable in bending strength to the welded joint.

Figure 46 below shows failed flexural specimen “B2” which failed predominantly along the weld line, beginning at the top surface of the weld, and then following the weld line.

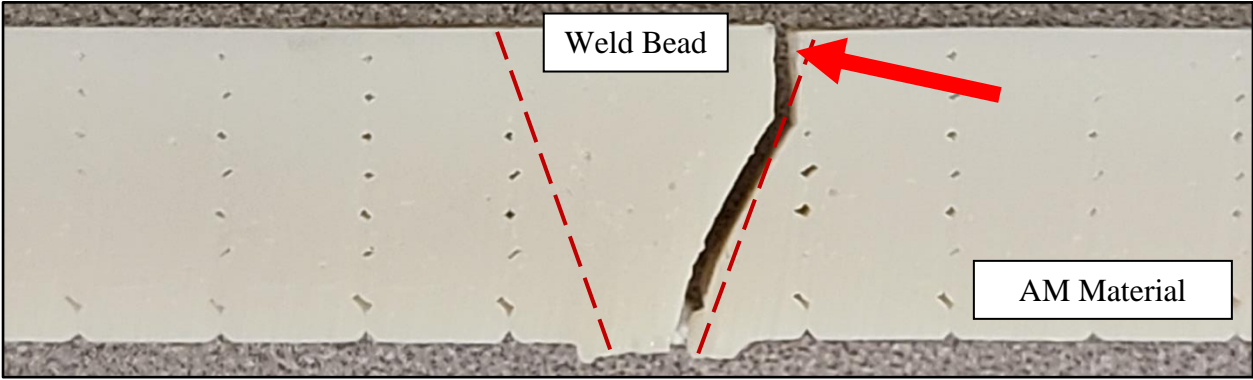


Figure 46: Failure along Weld Bond Line in Flexural Specimen B2

Figure 47 below shows an alternative failure mode in a flexural specimen that failed through the print material between beads, propagating from void to void between beads.

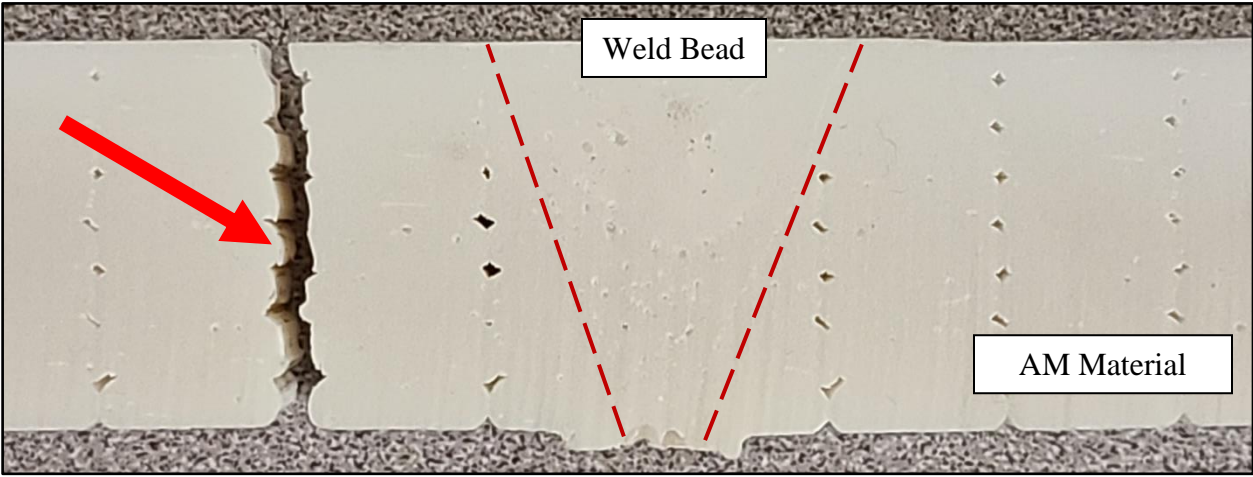


Figure 47: Failure in Printed Material in Flexural Specimen

While the failure shows the weld is stronger than the printed material in flexure, it is a less conclusive result and not an accurate approach to calculating the mechanical strength of the weld.

Table 21 below shows the failure modes of all flexural specimens tested.

Table 21: Failure Modes of Flexural Specimens

Specimen	Failure Mode
B1	Weld Line
B2	Weld Line
B3	Weld Line
B4	Print Material
B5	Print Material
B6	Multimodal
B7	Multimodal
B8	Multimodal

It can be observed that failure in many of the specimens appears to begin and propagate from the top surface of the welded material but does not fully follow the weld line through the entire cross-section. This will be further investigated in the next section of this work.

4.4 Weld Inspection using Microscopy

This section focuses on inspection of the welds to gain a better understanding of the bond between the weld material and the AM fairing surface. The welds were sectioned using a specimen saw and then examined with a Hitachi TM3000 tabletop scanning electron microscope. This microscope is capable of 50 to 2000 times magnification and imaging [85].

4.4.1 Specimen Inspection Preparation

The specimens were sliced through the weld and plate thickness using a Preciso CL50 Low-Speed Diamond Specimen Saw (AS4204) [86]. These slices were obtained from leftover material between tensile "dog bone" specimens, taken from the middle portion along the weld. The slices had a width of 0.1 in, with the 0.02 in thick blade between each slice taken into consideration, as shown in Figure 48.

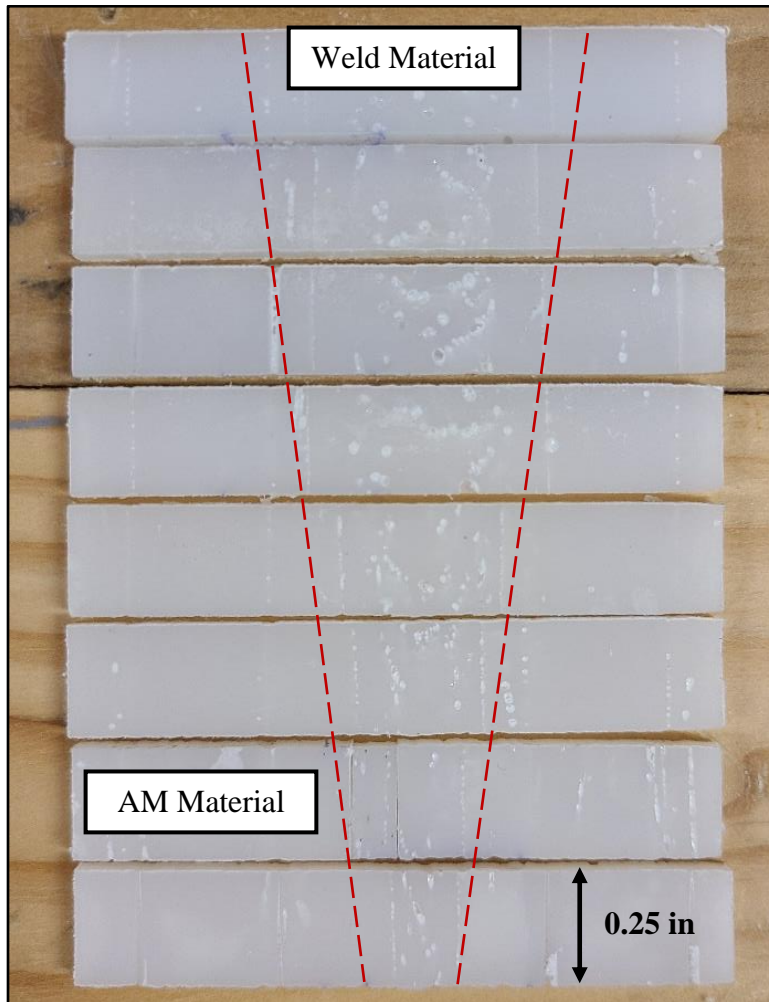


Figure 48: Sliced Welded Specimens for Inspection

The specimens were cut to image various locations within the cross-section for inspection, as shown in Figure 49. Both the root and top sections of the weld line were inspected, and a slice was

taken parallel to the weld bead at the top surface to inspect internal porosity in the weld. material.

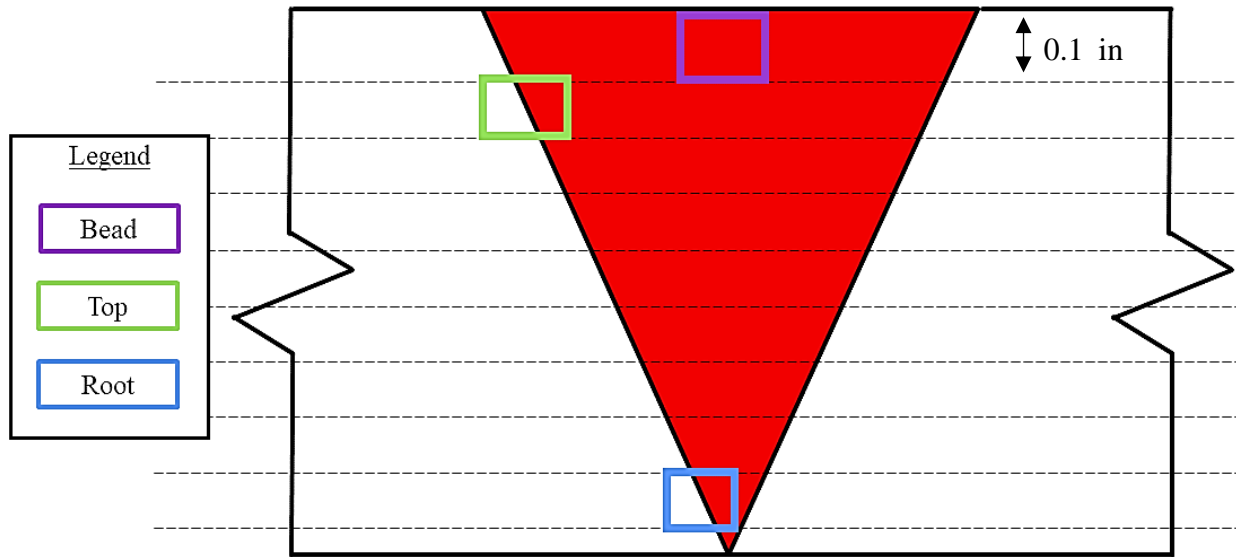


Figure 49: Diagram of the Weld Inspection Locations

4.4.2 Weld Line Inspection

To understand the material morphology at the bond line of the weld, cross-sectional specimens were inspected at both the root and top sections of the weld. Figure 50 shows a clear difference in material alignment and porosity between the two materials separated by a bond line in a failed flexural specimen. The material above the bond line is extruded weld material and the material below the bond line is AM HIPS.

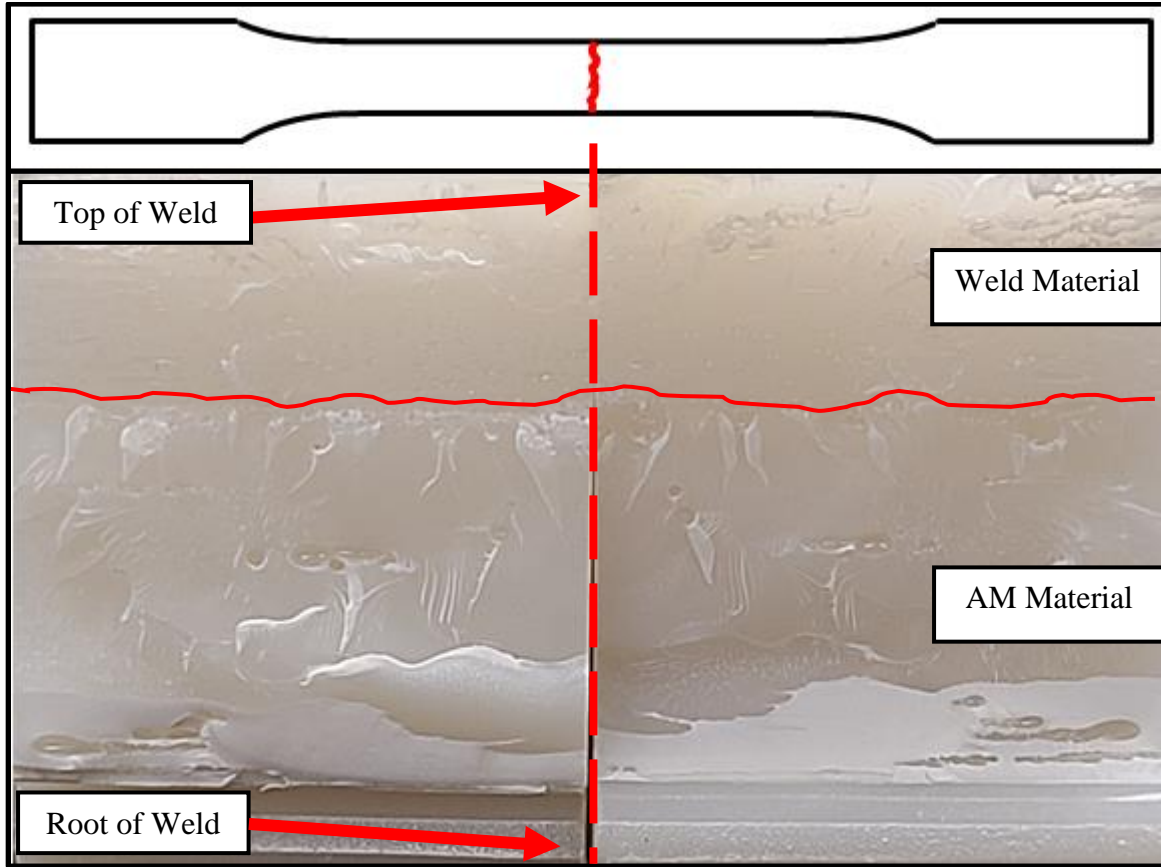


Figure 50: Material Difference at Weld Line in a Failed Specimen

To capture what is occurring in the material at the bond line of the weld, cross-sectional specimens were inspected in the root and top sections of the weld. The weld line within the root section was imaged at 50 times magnification as shown in Figure 51 below.

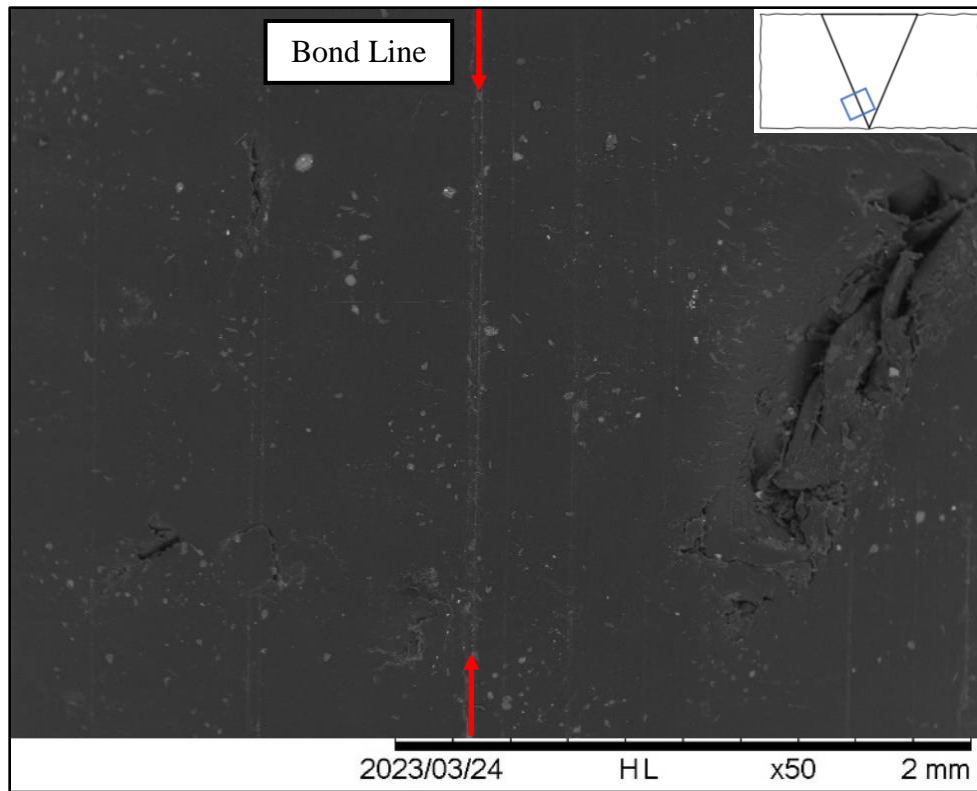


Figure 51: Weld Bond Line at the Root (x50)

Figure 51 shows a clear difference in the porosity of the two materials separated by a clear bond line. The material on the left is printed HIPS, while the material on the right is extruded weld material. There is a clear interphase region at the weld bond line. Figure 52 shows the same region as above Figure 51, however, at 2000 times magnification. Within this region, there is a clear heat-affected zone in the root of the weld that is approximately $60 \mu\text{m}$ across.

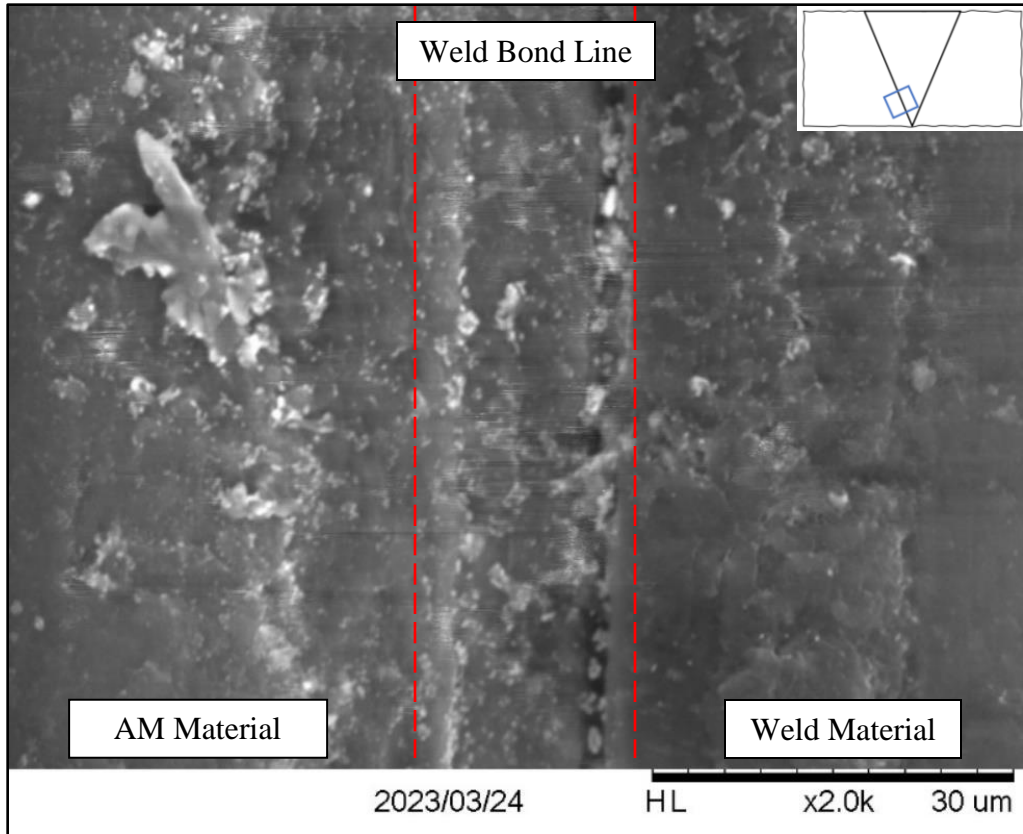


Figure 52: Weld Bond Line at the Root (x2000)

To compare the width of the weld bond line at the root and top of the weld, Figure 53 shows the weld line near the top of the weld surface. The lack of interphase at the weld line in top of the weld was observed across multiple specimens, suggesting that the heat-affected zone is smaller at the top of the weld than near the root.

Figure 53 shows a large porous region with small pores dotted vertically along the weld bond line near the top surface, indicating a lack of interphase.

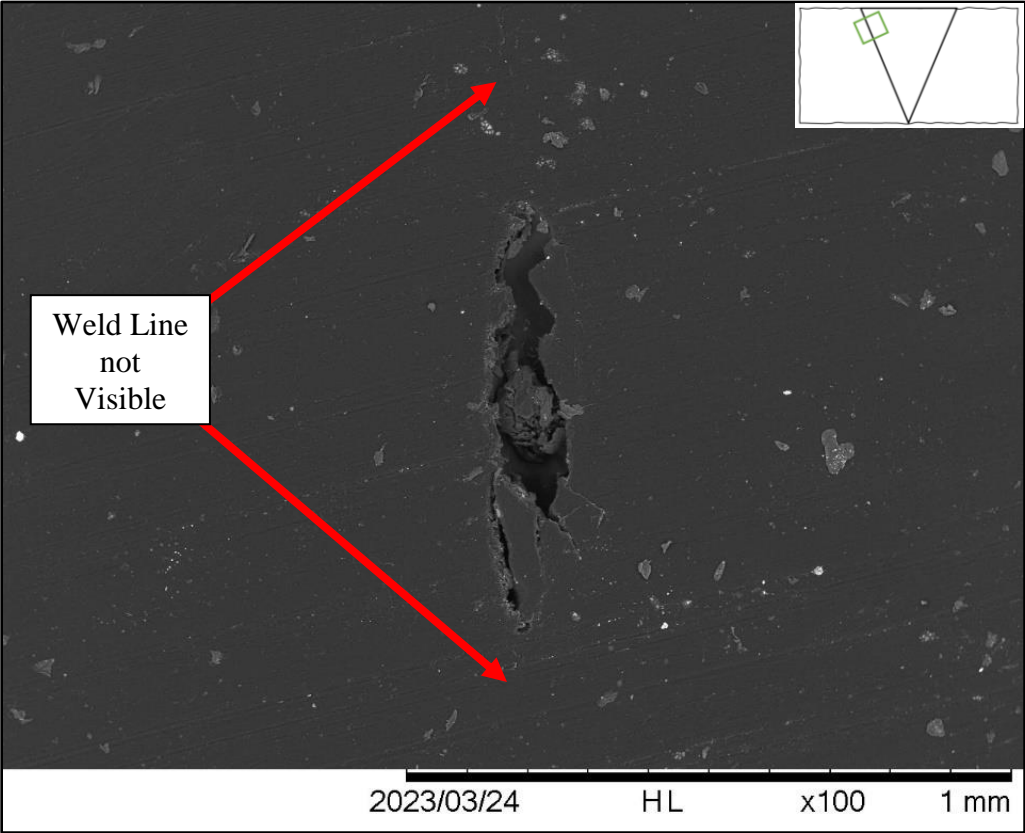


Figure 53: Porosity at Weld Bond Line near the Top Surface (x100)

Within this region, small pores can be seen dotted along the weld bond line, not a clear heat effected weld line. This difference in porosity and lack of interphase may have contributed to the strength difference between the root and top of the weld, possibly due to different temperature differentials during welding. The thinner fairing surface material at the root of the weld may have heated more thoroughly and uniformly, resulting in better fusion of material at the root than at the top of the welded surface.

4.4.3 Porosity Inspection within the Weld

The surface material of the welded joint had noticeably higher porosity than the AM surface and some large voids were found as shown below in Figure 54.

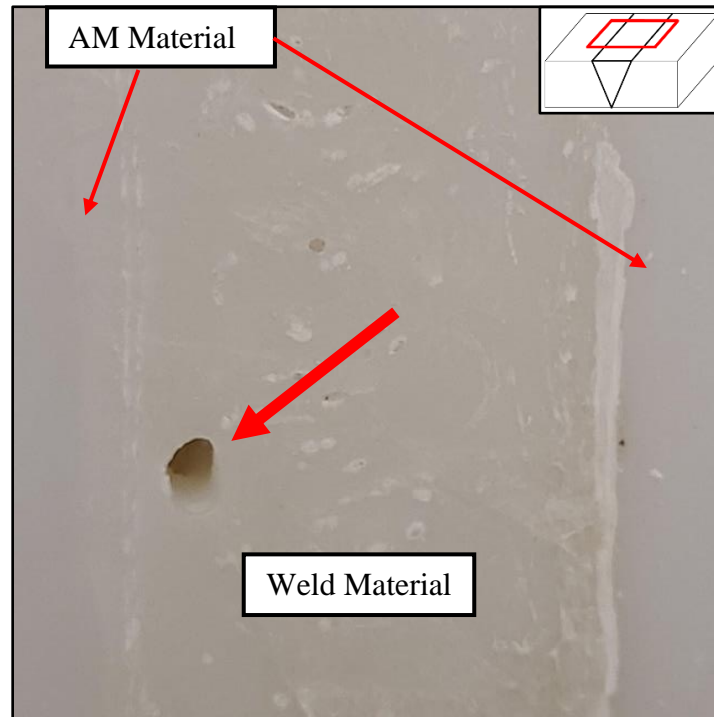


Figure 54: Porosity in Weld Surface & AM Surface

Despite the visible surface defects within the weld, there were no evident holes through the material. Overall, the welding process resulted in a strong permanent thermoplastic joint between the two AM plate surfaces. This inspect this porosity it is further imaged at 200 times magnification in Figure 55.

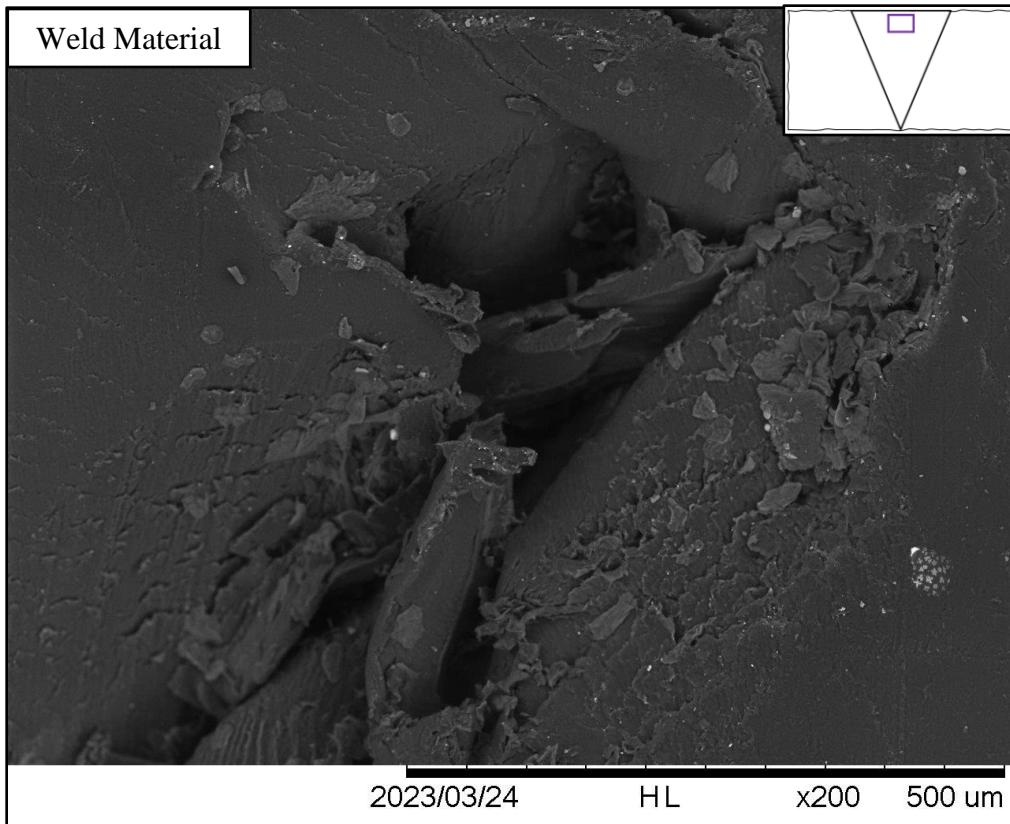


Figure 55: Porosity at the Root within Weld Material (x200)

The presence of porosity and voids within the welded material may be attributed to air within the extruder during the grinding and melting of the pelleted material. To address this issue, the use of smaller pelleted or granulated material could be explored. Additionally, voids between the fairing surfaces and the weld material could be caused by air trapped between the two materials during extrusion.

CHAPTER 5: CONCLUSIONS AND RECOMMENDATIONS

5.1 Conclusions

Thermoplastic extrusion welding is a feasible method for joining large-scale AM tooling components. With proper material selection and manufacturing of the joint a thermoplastic extrusion weld between mold segments can meet the tooling surface specifications of wind blade manufacturing.

5.1.1 Feasibility of the Joining Method Between Tooling Surfaces

The vacuum leakage testing of the welded AM plate at 20°C measured an average leak rate of 6.61 mbar over 30 minutes. This result met the surface vacuum integrity requirement of conventional thermoset mold surfaces for use in vacuum infusion of wind turbine blades. This was achieved by satisfying both the initial maximum vacuum requirement of less than 20 millibar and the maximum leak rate specification of 10 mbar over 30 minutes.

The thermoplastic joint yields a cohesive and continuous tooling surface across mold segments. However, without a coating, the welded and AM HIPS surfaces did not meet the hardness specification, with an average shore D hardness of 80.81 in the AM material and 72.86 in the weld material. Despite this, both the AM and welded HIPS surfaces exceeded the roughness specification, with a surface roughness of 50.18 μ in and 38.93 μ in respectively.

ASTM mechanical testing in tension and flexure demonstrated that the strength of the welded material was comparable to that of the printed material in the transverse direction. The specimen strength was approximately 80% of the ultimate tensile stress and 52% of the flexural stress of the AM Unigel HIPS base material used in this research. Additionally, the Welded AM specimen showed a significant loss in rigidity and a far lower percent elongation than an injection molded

counterpart. To reduce the risk of failure within the welded joint, proper undersurface reinforcement design in the mold is recommended for the intended application.

5.1.2 Recommendation of Full-Scale Welded Joint Design

This section covers the recommended design of the full-scale extrusion welded joint in AM tooling mold segments. The joint design involves a 60° bevel along the edge of each thermoplastic segment surface, as illustrated in Figure 56 below. Before welding, the tooling surfaces must be aligned and leveled with a gap of no more than $3/16$ in across the entire segment seam. This design has been represented throughout this work in the form of subscale welded plates with a 60° v-groove between them.

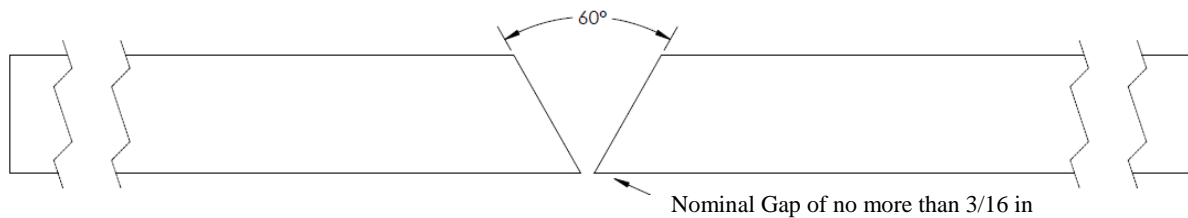


Figure 56: Joint Design Diagram [68]

The scalability of this joint is dependent on the thickness of the 3D-printed surface after machining. As shown above, the size of the welding foot must be determined based on the 3DP thickness. Thicker surfaces will require more material, therefore more time to complete the weld without the use of a larger extruder.

Once the weld is complete, the surface is manually finished to remove the extrusion bead fillet and create a cohesive tooling surface. Machining or a sliding router equipped with an end mill specialty jig can be used to achieve a smooth surface. Alternatively, an automatic hand planer or grinder can be used. After this step, the surface is hand-sanded to further refine the finish before coating.

5.2 Recommendations for Future Work

With the continued growth in scale of 3D printers, print area limitations on parts are becoming less of a concern. However, transportation challenges and long print times still hinder the commercialization of AM in many industries. Thermoplastic extrusion welding provides a simple and straightforward option for joining large-scale parts, emulating the 3D printing process. With the decreasing costs of 3D printers, parts can now be produced much faster than before. Moreover, large parts can be produced on two smaller printers and then welded together at the installation site, thereby increasing manufacturing speed and reducing transportation costs and challenges.

5.2.1 Thermoplastic Composite Materials

This study focused on a low-crystallinity or amorphous thermoplastic polymer, as described in Chapter 2. Now that manufacturing feasibility has been demonstrated for an amorphous material with high formability, future research should explore the feasibility of using more crystalline engineering-grade thermoplastic polymers.

Additionally, the effects of filler materials within the weld material should be investigated. While fillers in feedstock materials have been shown to improve mechanical properties in printed materials [34], [36], [47], they may have different effects on the bond strength between extrusion-welded components.

5.2.2 Further Testing of Welded Components

Two areas of further thermoplastic welding studies are recommended to improve the current results. Firstly, additional evaluation of vacuum integrity at elevated temperatures to determine the performance of the joint relative to the bag system would be valuable. A vacuum reservoir may be used instead of a vacuum bag to minimize leakage from the sealant tape and bag softening at high

temperatures. Secondly, it is recommended to carry out a porosity and density analysis of the extrusion welded material using different welding parameters. This analysis could yield valuable insights into further improving extrusion welds for this application.

5.2.3 Joining other Large-Scale AM Structures.

Future research on thermoplastic extrusion welding for joining additively manufactured structures should include mechanical testing of welded components in multiple bead directions in relation to the weld. Durability testing such as mechanical fatigue life and weatherability should also be performed to evaluate the feasibility of this welding technique in additional large-scale applications.

REFERENCES

- [1] B. K. Post *et al.*, “The Current State of Additive Manufacturing in Wind Energy Systems,” ORNL/TM--2017/479, 1415918, Dec. 2017. doi: 10.2172/1415918.
- [2] B. Post, B. Richardson, P. Lloyd, L. Love, S. Nolet, and J. Hannan, “Additive Manufacturing of Wind Turbine Molds,” ORNL/TM--2017/290, CRADA/NFE-16-06051, 1376487, Jul. 2017. doi: 10.2172/1376487.
- [3] R. Stewart, “Mould and tooling advances promising for composites,” *ElsevierScience Reinforced Plastics*, 2010. [Online]. Available: <https://www.reinforcedplastics.com/articles/mould-and-tooling-advances-promising-for-composites/>
- [4] Ferretti P, Santi GM, Leon-Cardenas C, Freddi M, Donnici G, Frizziero L, Liverani A., “Molds with Advanced Materials for Carbon Fiber Manufacturing with 3D Printing Technology,” *MDPI*, vol. 13, no. 21, p. 3700, 2021, doi: 10.3390/polym13213700.
- [5] B. K. Post, R. F. Lind, P. D. Lloyd, V. Kunc, J. M. Linhal, and L. J. Love, “The Economics of Big Area Additive Manufacturing,” in *Proceedings of the 26th Annual International Solid Freeform Fabrication Symposium – An Additive Manufacturing Conference*, Austin, Texas.
- [6] K.-T. Hsiao and D. Heider, “10 - Vacuum assisted resin transfer molding (VARTM) in polymer matrix composites,” in *Manufacturing Techniques for Polymer Matrix Composites (PMCs)*, S. G. Advani and K.-T. Hsiao, Eds., in Woodhead Publishing Series in Composites Science and Engineering. Woodhead Publishing, 2012, pp. 310–347. doi: 10.1533/9780857096258.3.310.
- [7] D. Heider and J. W. Gillespie, “VARTM Variability and Substantiation,” Center for Composite Materials, University of Delaware, Newark, 2008.
- [8] W. D. Brouwer, E. C. F. C. van Herpt, and M. Labor dus, “Vacuum injection moulding for large structural applications,” *Compos. Part Appl. Sci. Manuf.*, vol. 34, no. 6, pp. 551–558, Jun. 2003, doi: 10.1016/S1359-835X(03)00060-5.
- [9] “ASTM D 5687/D 5687M- 95 Standard Guide for Preparation of Flat Composite Panels with Processing Guidelines for Specimen Preparation.”
- [10] S. Nolet, *Large-scale Vacuum Infusion (TPI Composites Inc.)*.
- [11] “Sandia Report: Blade System Design Studies Volume I: I Composite Technologies for Large Wind Turbine Blades.” Accessed: May 03, 2022. [Online]. Available: <https://www.osti.gov/servlets/purl/800994>
- [12] G. Fernlund *et al.*, “Experimental and numerical study of the effect of cure cycle, tool surface, geometry, and lay-up on the dimensional fidelity of autoclave-processed composite

- parts,” *Compos. Part Appl. Sci. Manuf.*, vol. 33, no. 3, pp. 341–351, Mar. 2002, doi: 10.1016/S1359-835X(01)00123-3.
- [13] X. Zeng and J. Raghavan, “Role of tool-part interaction in process-induced warpage of autoclave-manufactured composite structures,” *Compos. Part Appl. Sci. Manuf.*, vol. 41, no. 9, pp. 1174–1183, Sep. 2010, doi: 10.1016/j.compositesa.2010.04.017.
- [14] V. Kaushik and J. Raghavan, “Experimental study of tool-part interaction during autoclave processing of thermoset polymer composite structures,” *Compos. Part Appl. Sci. Manuf.*, vol. 41, no. 9, pp. 1210–1218, Sep. 2010, doi: 10.1016/j.compositesa.2010.05.003.
- [15] K. D. Potter, M. Campbell, C. Langer, and M. R. Wisnom, “The generation of geometrical deformations due to tool/part interaction in the manufacture of composite components,” *Compos. Part Appl. Sci. Manuf.*, vol. 36, no. 2, pp. 301–308, Feb. 2005, doi: 10.1016/j.compositesa.2004.06.002.
- [16] “ASTM D696-16 Standard Test Method for Coefficient of Linear Thermal Expansion of Plastics Between –30°C and 30°C with a Vitreous Silica Dilatometer.”
- [17] “Process Modeling of Composite Materials: Residual Stress Development during Cure. Part I. Model Formulation,” *Sage Publ.*, vol. 26, no. 16, pp. 2330–2477, 1992.
- [18] D. B. Shah, K. M. Patel, A. I. Patel, V. Pariyal, and S. J. Joshi, “Experimental investigation on spring-back deformation during autoclave curing of parabolic antenna reflectors,” *Compos. Part Appl. Sci. Manuf.*, vol. 115, pp. 134–146, Dec. 2018, doi: 10.1016/j.compositesa.2018.09.017.
- [19] Y. Li, “A review on the tooling technologies for composites manufacturing of aerospace structures: materials, structures and processes,” *Compos. Part A*, p. 23, 2022.
- [20] “ISO 4287:1997 Surface texture: Profile method.” International Organization for Standardization. [Online]. Available: <https://www.iso.org/standard/10132.html>
- [21] “ASTM D2240 Standard Test Method for Rubber Property—Durometer Hardness.”
- [22] E. Ruiz, F. Trochu, and R. Gauvin, “Internal Stresses and Warpage of Thin Composite Parts Manufactured by RTM,” Jan. 01, 2004. <https://doi.org/10.1177/096369350401300105>
- [23] N. Amirth Jayasree, S. Omairey, and M. Kazilas, “Novel multi-zone self-heated composites tool for out-of-autoclave aerospace components manufacturing,” *Sci. Eng. Compos. Mater.*, Aug. 2020, doi: 10.1515/secm-2020-0033.
- [24] S. Black, “Tooling for composites: Evolutionary trajectory | CompositesWorld,” 2011. <https://www.compositesworld.com/articles/tooling-for-composites-evolutionary-trajectory>
- [25] R. Matsuzaki, S. Kobayashi, A. Todoroki, and Y. Mizutani, “Full-field monitoring of resin flow using an area-sensor array in a VaRTM process,” *Compos. Part Appl. Sci. Manuf.*, vol. 42, no. 5, pp. 550–559, May 2011, doi: 10.1016/j.compositesa.2011.01.014.

- [26] J.-M. Jeong *et al.*, “In-situ resin flow monitoring in VaRTM process by using optical frequency domain reflectometry and long-gauge FBG sensors,” *Compos. Struct.*, vol. 282, p. 115034, Feb. 2022, doi: 10.1016/j.compstruct.2021.115034.
- [27] “ASTM E1461 – 13 Standard Test Method for Thermal Diffusivity by the Flash Method.”
- [28] T. D. Ngo, A. Kashani, G. Imbalzano, K. T. Q. Nguyen, and D. Hui, “Additive manufacturing (3D printing): A review of materials, methods, applications and challenges,” *Compos. Part B Eng.*, vol. 143, pp. 172–196, Jun. 2018, doi: 10.1016/j.compositesb.2018.02.012.
- [29] L. J. Love *et al.*, “The importance of carbon fiber to polymer additive manufacturing,” *J. Mater. Res.*, vol. 29, no. 17, pp. 1893–1898, Sep. 2014, doi: 10.1557/jmr.2014.212.
- [30] “Thermoplastic 3D printer, MasterPrint® 3X | Ingersoll Machine Tools.” <https://en.machinetools.camozzi.com/products/additive-manufacturing/all-products/masterprint-.kl>
- [31] “BAAM - Big Area Additive Manufacturing,” *Cincinnati Incorporated*. <https://www.e-ci.com/baam>
- [32] B. K. Post, P. C. Chesser, R. F. Lind, M. R. Sallas, and L. J. Love, “Feasibility of using Big Area Additive Manufacturing to Directly Manufacture Boat Molds,” ORNL/TM--2017/709, 1427645, Jan. 2018. doi: 10.2172/1427645.
- [33] A. Roschli, B. K. Post, P. C. Chesser, M. Sallas, L. J. Love, and K. T. Gaul, “Precast Concrete Molds Fabricated with Big Area Additive Manufacturing,” presented at the International Solid Freeform Fabrication Symposium, 2018, p. 13. [Online]. Available: <https://www.osti.gov/servlets/purl/1471898>
- [34] L. J. Love *et al.*, “Breaking Barriers in Polymer Additive Manufacturing,” Oak Ridge National Lab. (ORNL), Oak Ridge, TN (United States). Manufacturing Demonstration Facility (MDF), Jan. 2015.
- [35] P. Pandey, V. R. Nallagundla, and S. Dhande, “Virtual hybrid-FDM system to enhance surface finish,” *Virtual Phys. Prototyp.*, pp. 101–116, Jun. 2006, doi: 10.1080/17452750600763905.
- [36] A. A. Hassen *et al.*, “The Durability of Large-Scale Additive Manufacturing Composite Molds,” presented at the CAMX – The Composites and Advanced Materials Expo, Anaheim, CA, Sep. 2016.
- [37] V. Kunc *et al.*, “Investigation of In-Autoclave Additive Manufacturing Composite Tooling,” presented at the CAMX – The Composites and Advanced Materials Expo., Anaheim, CA, Sep. 2016.
- [38] P. Wang, G. Kim, and R. Sterkenburg, “Investigating-the-Effectiveness-of-a-3D-Printed-Composite-Mold,” *World Academy of Science*, vol. 13, pp. 684–688, Oct. 2019, doi: 10.5281/zenodo.3566395.

- [39] T. Z. Sudbury, R. Springfield, V. Kunc, and C. Duty, “An assessment of additive manufactured molds for hand-laid fiber reinforced composites,” *Int. J. Adv. Manuf. Technol.*, vol. 90, no. 5, pp. 1659–1664, May 2017, doi: 10.1007/s00170-016-9464-9.
- [40] N. Northrup, J. Weaver, and A. R. George, “Vacuum Infusion of Composites: Durability of Hybrid Large Area Additive Tooling for Vacuum Infusion of Composites,” Peer-Reviewed Article, Brigham Young University, Provo, Utah, 2021.
- [41] Martin Spoerk, oamin Gonzalez-Gutierrez, Janak Sapkota, Stephan Schuschnigg, and Clemens Holzer, “Effect of the printing bed temperature on the adhesion of parts produced by fused filament fabrication,” *Plastics, Rubber and Composites*, vol. 47, pp. 17–24, 2018.
- [42] K. Sertoglu, “Ingersoll and Bell 3D printed a 22 foot-long rotor blade mold in 75 hours,” *3D Printing Industry*, Apr. 01, 2021. <https://3dprintingindustry.com/news/ingersoll-and-bell-3d-printed-a-22-foot-long-rotor-blade-mold-in-75-hours-188018/>
- [43] P. Malnati, “Hybrid, large-format additive tooling: Lighter, faster, less costly molds for big parts,” *Composites World*, Nov. 20, 2020. <https://www.compositesworld.com/articles/hybrid-large-format-additive-tooling-lighter-faster-less-costly-molds-for-big-parts>
- [44] “ASTM D648-18 Standard Test Method for Deflection Temperature of Plastics Under Flexural Load in the Edgewise Position.”
- [45] I. Fidan *et al.*, “The trends and challenges of fiber reinforced additive manufacturing,” *Int. J. Adv. Manuf. Technol.*, vol. 102, no. 5–8, pp. 1801–1818, Jun. 2019, doi: 10.1007/s00170-018-03269-7.
- [46] A. Gupta, S. Hasanov, F. Alifui-Segbaya, and I. Fidan, “Fiber-reinforced additively manufactured polymer composites.” Nov. 02, 2021. doi: 10.13140/RG.2.2.24688.99848.
- [47] N. Van de Werken, H. Tekinalp, P. Khanbolouki, S. Ozcan, A. Williams, and M. Tehrani, “Additively manufactured carbon fiber-reinforced composites: State of the art and perspective,” *Addit. Manuf.*, vol. 31, Nov. 2019, doi: 10.1016/j.addma.2019.100962.
- [48] K. M. M. Billah *et al.*, “Large-scale additive manufacturing of self-heating molds,” *Addit. Manuf.*, vol. 47, p. 102282, Nov. 2021, doi: 10.1016/j.addma.2021.102282.
- [49] M. J. Troughton, *Handbook of Plastics Joining: A Practical Guide*. Elsevier Science, 2008. [Online]. Available: https://books.google.com/books?id=BXL_mnDzW0QC
- [50] R. K. Flitney, *Seals and Sealing Handbook*, 6th ed. in *Seals and Sealing Handbook*. Elsevier Science, 2014.
- [51] A. Arabi Hassen *et al.*, “Joining Technique for In-Oven/Autoclave Molds Manufactured by Large Scale Polymer Additive Manufacturing,” *Manuf. Lett.*, Apr. 2022, doi: 10.1016/j.mfglet.2022.04.001.

- [52] A. Yousefpour, M. Hojjati, and J.-P. Immarigeon, "Fusion Bonding/Welding of Thermoplastic Composites," *J. Thermoplast. Compos. Mater.*, vol. 17, no. 4, pp. 303–341, Jul. 2004, doi: 10.1177/0892705704045187.
- [53] D. Grewell and A. Benatar, "Welding of Plastics: Fundamentals and New Developments," *Int. Polym. Process.*, vol. 22, no. 1, pp. 43–60, Mar. 2007, doi: 10.3139/217.0051.
- [54] O. Balkan, H. Demirer, A. Ezdeşir, and H. Yıldırım, "Effects of welding procedures on mechanical and morphological properties of hot gas butt welded PE, PP, and PVC sheets," *Polym. Eng. Sci.*, vol. 48, pp. 732–746, Apr. 2008, doi: 10.1002/pen.21014.
- [55] Ravi Ranjan *et al.*, "Classification and identification of surface defects in friction stir welding: An image processing approach," *Journal of Manufacturing Processes*, vol. 22, pp. 237–253, 2016, doi: <https://doi.org/10.1016/j.jmapro.2016.03.009>.
- [56] Ranvijay Kumar, Rupinder Singh, I.P.S. Ahuja, Rosa Penna, and Luciano Feo, "Weldability of thermoplastic materials for friction stir welding- A state of art review and future applications," *Composites Part B: Engineering*, vol. 137, pp. 1–15, 2018, doi: <https://doi.org/10.1016/j.compositesb.2017.10.039>.
- [57] "DIODE S." <https://www.leister.com/en/product/Diode-S#Details>
- [58] R. A. Grimm, "Welding processes for plastics," *Adv. Mater. Amp Process.*, vol. 147, no. 3, pp. 27–31, Mar. 1995.
- [59] "Abbeon.com - Your Source For Plastic Working Tools." <https://www.abbeon.com/index.aspx>
- [60] "Extrusion Welding of Thermoplastics." <https://www.twi-global.com/technical-knowledge/job-knowledge/extrusion-welding-of-thermoplastics-057.aspx>
- [61] T. Osswald and G. Menges, *Material Science of Polymers for Engineers*, 3rd ed. Hanser Publications.
- [62] Mendeleev, "Periodic Table of Thermoplastics." Tangram Technology, 2021. [Online]. Available: www.tangram.co.uk
- [63] C. Ageorges, L.Ye, and M. Hou, "Advances in fusion bonding techniques for joining thermoplastic matrix composites: a review," *Composites: Part A*, vol. 32, pp. 839–857, 2000, doi: 10.1016/S1359-835X(00)00166-4.
- [64] S. Prager and M. Tirrell, "The healing process at polymer–polymer interfaces," *J. Chem. Phys.*, vol. 75, no. 10, pp. 5194–5198, Nov. 1981, doi: 10.1063/1.441871.
- [65] J. Onken, S. Verwaayen, and C. Hopmann, "Evaluation of healing models to predict the weld line strength of the amorphous thermoplastic polystyrene by injection molding simulation," *Polymer Engineering and Science*, 2020, doi: 10.1002/pen.25614.

- [66] “Polystyrene HIPS (High Impact Polystyrene)|Boedeker.” <https://www.boedeker.com/Product/HIPS>
- [67] “PS ALTO IMPACTO M.I 2.8 U8884.” Unigel, 2013.
- [68] “HSK26 GSX Extrusion Welder midsize w/ Pellet feed, 230V and Case | Abbeon.” <https://www.abbeon.com/Item--i-HSK26GSX>
- [69] “JuggerBot 3D: Manufacturer of 3D printers.” <https://juggerbot3d.com/>
- [70] A. Segala and S. Nolet, “Shell Mold Specification.” TPI Composites.
- [71] “SM5142BY Vacuum Sealant Tape Technical Data Sheet.” POLYMERS SEALANTS NORTH AMERICA, INC., 2020.
- [72] “3577 Polyethylene Bagging Film.” Fibre Glast Developments Corporation, 2020.
- [73] “Breather and Bleeder,” *Fibre Glast Developments Corporation*. https://www.fibreglast.com/product/Breather_and_Bleeder_579
- [74] “DERAKANE 8084 Epoxy Vinyl Ester Resin Data Sheet.” Ashland, Composite Polymers, 2006.
- [75] “General Purpose Pressure Transducers with Adjustable Zero & Span,” *OMEGA ENGINEERING*.
- [76] “NI-9202 Datasheet,” *National Instruments*. <https://www.ni.com/docs/en-US/bundle/ni-9202-specs/page/overview.html>
- [77] “Electronic Durometer - Shore D Scale,” *Starrett*. <https://www.starrett.com/metrology/product-detail/3805D#Features>
- [78] “SJ-210 - Portable Surface Roughness Tester - Mitutoyo.” <https://www.mitutoyo.com/products/form-measurement-machine/surface-roughness/sj-210-portable-surface-roughness-tester-2/>
- [79] “ASTM D638-22 - Standard Test Method for Tensile Properties of Plastics,” Jul. 21, 2022.
- [80] “ASTM D790-17 - Standard Test Methods for Flexural Properties of Unreinforced and Reinforced Plastics and Electrical Insulating Materials,” Jul. 24, 2017.
- [81] “ASTM D618-21 - Standard Practice for Conditioning Plastics for Testing,” Jul. 22, 2021.
- [82] N. Zohdi and R. (Chunhui) Yang, “Material Anisotropy in Additively Manufactured Polymers and Polymer Composites: A Review,” *Polymers*, vol. 13, no. 19, 2021, doi: <https://doi.org/10.3390/polym13193368>.

- [83] M. Montero, S. Roundy, D. Odell, S.-H. Ahn, and P. Wright, "Material Characterization of Fused Deposition Modeling (FDM) ABS by Designed Experiments," *Proc. Rapid Prototyp. Manuf. Conf.*, Jul. 2001.
- [84] C. Savandaiah, B. Plank, J. Maurer, J. Leßlhumer, and G. Steinbichler, "COMPARATIVE STUDY OF FILLED AND UNFILLED POLYLACTIC ACID PRODUCED VIA INJECTION MOLDING AND 3D PRINTING," May 2021.
- [85] "TM3000 TableTop Scanning Electron Microscope," *Hitachi*. <https://www.hitachi-hightech.com/us/library/literature/brochure-tm3000-tabletop-scanning-electron-microscope.html>
- [86] "PRECISO CL50 - Low Speed Diamond Saw," *TOP TECH MACHINES*. https://toptech.tw/eng_product_detail.asp?Fid=F002516&Pid=201408050007
- [87] "L | Dyna-Purge." <https://dynapurge.com/project/l/>

APPENDIX A: LIST OF ABBREVIATIONS

AM	Additive Manufacturing
EERE	United States Department of Energy, Office of Energy Efficiency and Renewable Energy
AMO	Advanced Manufacturing Office
ASCC	University of Maine, Advanced Structures and Composites Center
ORNL	Oak Ridge National Laboratory
TPI	TPI Composites Inc.
SGRE	Siemens Gamesa Renewable Energy
ASTM	American Society for Testing and Materials
FRP	Fiber-Reinforced Polymer
VARTM	Vacuum-Assisted Resin Transfer Molding
SCRIMP	Seeman Composites Resin Infusion Molding Process
VOC	Volatile Organic Compounds
FVF	Fiber Volume Fraction
CTE	Coefficient of Thermal Expansion
HDT	Heat Deflection/Distortion Temperature
ISO	International Standard Organization
OOA	Out-of-Autoclave
FDM	Fused Deposition Modeling
BAAM	Big Area Additive Manufacturing
CNC	Computer Numerical Control
FRAM	Fiber-Reinforced Additive Manufacturing
ABS	Acrylonitrile Butadiene Styrene
PTFE	Polytetrafluoroethylene / Teflon
PP	Polypropylene
PE	Polyethylene
PVC	Polyvinyl Chloride
HIPS	High Impact Polystyrene
DAQ	Data Acquisition

APPENDIX B: CALIBRATION

The equipment used during this study was regularly calibrated; relevant calibration information for major testing equipment used is included in Table 22. Calibration information is given for the test frames used; load cells are also calibrated with the test frame.

Table 22: Relevant Calibration Information for Mechanical Testing

Equipment ID	Description	Relevant Calibration Dates
EM #3 (AS4397)	22.5-kip Instron Electro-Mechanical Actuator	February 2 nd , 2023
MTL Load Cell (AS 4396)	22.5-kip Instron Load Cell	
MTL #5 (AS 512)	Instron Servo-Hydraulic Actuator	November 16 th , 2022
Load Cell (AS 518)	25 kN Dynacell Load Cell	

APPENDIX C: RECOMMENDED MANUFACTURING PROCEDURE

Appendix C contains the full-scale polymer welding approach to joining AM thermoplastic mold segments. This will require pre-manufacture (3D printing) and placement of the fairing edges of two mold segments. The welding step will result in a permanent bond that would require routing or milling to reverse; thus, this step should be conducted when the molds are set in place in the production environment. The fairing edges of the 3D printed mold will need to be prepared with a 60° V-groove router bit. This will bevel each fairing surface with a full-thickness chamfer into which the weld material will flow. With the fairing edges cut, the tool surface should be fixed to the production floor and then aligned and adjusted as needed. Initial adjustment of the mold surface should occur before welding to reduce stresses at the weld seams. Once the mold is set, the weld joint fairing surfaces should be lightly sanded with 120 to 150-grit sandpaper and then thoroughly cleaned to ensure it is clear of obstructions and debris. At this point, a weld can be completed across the chord of the mold ensuring the process parameters are proper for the material being welded. Ideally, multiple tests of welds will be conducted and tested before joining large tooling segments. After the weld has cooled for at least thirty minutes, it can be finished to meet the specification of the tool surface. Figure 57 is a rendering showing the joint design in a tooling surface between two mold segments.

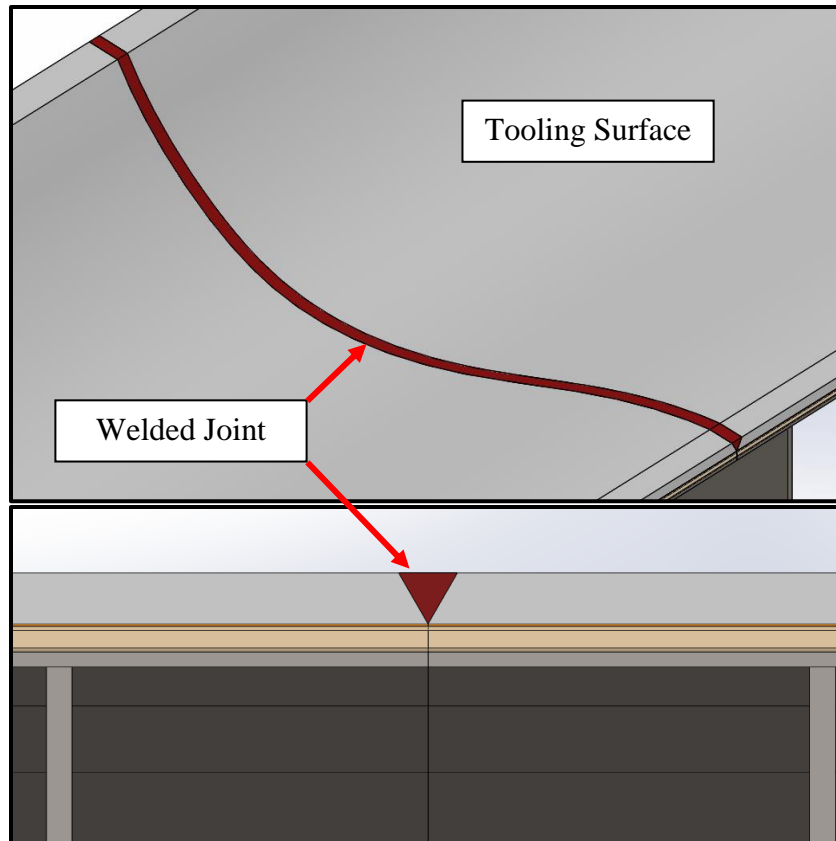


Figure 57: Render of Welded Joint Between Tooling Segments

The following section outlines the process of preparing, manufacturing and finishing the welded joint between two segments in a large-scale tooling mold.

1) Preparation:

- a) Begin by preparing a clean and clear workspace, removing flammable and explosive hazards.
- b) Acquire proper PPE including safety glasses and shield, weld gloves, and welding jacket.
- c) Acquire necessary tools, including the welder and its accessories, a 3-phase extension cable, pliers, a foil container, and a scraper.
- d) A weldability test is recommended to understand the process parameters of weld materials.

2) Material:

- a) For each meter of weld length, collect 2 kg of thermoplastic granulate in a clean 5-gallon bucket and a material scoop for filling the welder hopper.
 - b) Acquire roughly 0.5 kg of Dynapurge [87] or a similar granulate AM purging material.
 - c) Fill the hopper with 0.25 kg of Dynapurge and replace its plastic cap.
- 3) Alignment, Leveling, and Joint Prep:
- a) Smooth the fairing edges (not the mold surface) with 150+ grit sandpaper then again with 220 + sandpaper.
 - b) Clean the beveled fairing surfaces, removing dust accumulated from the sanding process.
 - c) Assuming the joint has been cut as designed, position the two mold segments so that the 60-degree beveled fairing surfaces are leveled, parallel, and aligned with a separation of no more than 4 mm.
- 4) Pre-heating (PPE Required):
- a) Plug in the welder on its stand, set temperatures, and preheat both the welder air and plasticizing temperatures to desired process temperatures of the material specified for the joint. This step may take roughly 15 minutes, the welder will indicate when it has reached the set temperature. Do NOT attempt to weld if the welder has not yet reached the set temperatures. It is recommended to turn on the blower air to keep the heating element from overheating during the preheating step.
 - b) Set the extruder screw speed (dial on the handle) to half of the maximum (half rotation). This depends on the weldability of the chosen material.
 - c) While the welder is heating, pull any old material from the weld nozzle and attach the welding trolley shown below in figure 04 designed for this butt joining process. The weld

feet will not remove with old material in the foot; thus, this must be done while the welder is heating.

5) Purging:

- a) Purge the extruder screw with Dynapurge until the extruded white Dynapurge comes out clean so that any over-heated or degraded material left in the barrel from the previous welding operation is cleared to prevent damage.
- b) Once the Dynapurge is cleared, stop extruding and fill the granulate hopper with weld material and replace the cap.
- c) Extrude again to ensure all Dynapurge is removed, then cut cleanly once sure the welder is clear.

6) Welding:

- a) Now that the fairing surfaces are prepared, place the welder at the edge of the joint and roll back and forth slowly over the first 50 mm, preheating the fairing surfaces to prep for the weld start.
- b) Once the weld is preheated, begin extrusion by pulling the welder trigger. As the screw pushes material, maintain downward pressure until a flow head is visible behind the welder.
- c) As the flow head builds, tilt the welder back slightly (toward the weld start) as shown below in Figure 58. This will allow the extrusion screw to push material and roll the welder forward with minimal user assistance. The welder will roll itself as the material extrudes but may require some adjustment to ensure proper alignment with the joint during the process. Do not over-tilt the welder, as the welding foot may dig into the fairing surfaces. Depending on the surface thickness, the weld should proceed at roughly 0.12 - 0.18 m/min or (0.4 – 0.6 ft/min).

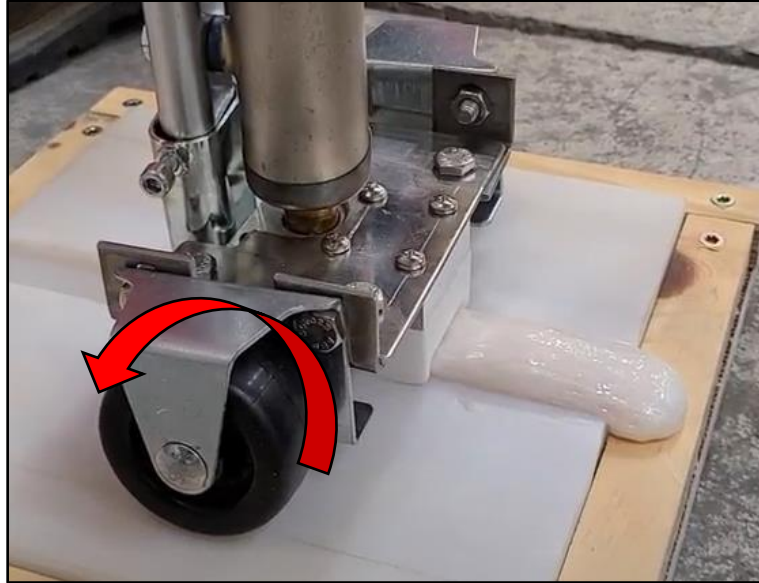


Figure 58: Rear Isometric of Welding Process with Slight Tilt from Operator

- d) As the welding proceeds, an assistant should use a silicone roller to apply downward pressure to the joint, rolling the cooling material forward and compressing the weld downward into the joint toward the welder.
 - e) As the weld completes, over-extrude beyond the surface for roughly 20 seconds or more, continue extruding off the fairing surfaces, and cut the weld bead to end the weld. This will ensure enough material is extruded at the joint terminations and reduce weld stretching.
- 7) After Welding is completed:
- a) It is recommended that the extruder should be purged with Dynapurge before cooling the welder so that any overheated or degraded material left in the barrel from the welding operation is cleared to prevent damage.
 - b) Remove the welding trolley if not intended for repeated use.
 - c) Allow the welder and finished joint to cool for a minimum of 30 minutes, ideally longer, before storing the welder and finishing joined surfaces.

APPENDIX D: TECHNICAL DATA SHEETS

Appendix D contains technical references and manufacturer's material and technical data sheets for the materials and equipment used in this thesis.

A brief outline is provided in the list below:

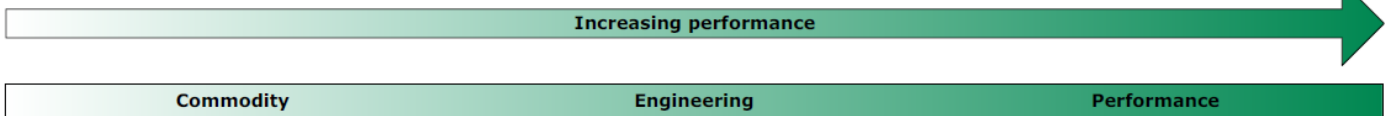
- C-1: Tangram Technology Periodic Table of Thermoplastics [62]
- Boedecker Plastics High Impact Polystyrene Sheet Material Data Sheet [66]
- Unigel High Impact Polystyrene Pellets Material Data Sheet [67]
- Derakane 8084 Epoxy Vinyl-Ester Resin Data Sheet [74]
- Abbeon Hand Welding Extruder HSK26 GSX [68]
- Starrett 3805D Shore D Durometer [77]
- Mitutoyo SJ-210 Portable Surface Roughness Tester [78]

Tangram Technology Periodic Table of Thermoplastics

The Periodic Table of the elements by Mendeleev was a historic achievement in chemistry and enabled chemists to see the relationship between structure and properties of the basic elements. Polymers also have a strong relationship between structure and properties and this 'Periodic Table of Polymers' is a first attempt to provide a simple codification of the basic polymer types and structures. The diversity of polymer types makes it impossible to include all of the variations in one simple table and this table only includes the most common polymers.

KEY
 TS = Tensile Strength at Yield @ 23°C
 EAB = Elongation at break
 TM = Tensile Modulus @ 23°C
 LTST = Long Term Service Temperature
 HDT = Heat Deflection Temperature @ 1.8 MPa
 Cost = Relative Cost

All properties are for the natural injection moulding grade resin only and do not include polymers with reinforcements or other functional fillers.



Amorphous

Increasing crystallinity

Semicrystalline

Random molecular orientation in both molten and solid phases.



General Characteristics
 Soften gradually. Generally transparent. Lower Tensile Strength and Tensile Modulus. Lower Density. Low Creep Resistance. High Dimensional Stability. Low fatigue resistance. Easy to bond using adhesives and solvents (high surface energy).

Random molecular orientation in molten phase, densely packed crystallites in solid phase.



General Characteristics
 Sharp melting point. Generally translucent or opaque. Higher Tensile Strength and Tensile Modulus. Higher Density. High Creep Resistance. Low Dimensional Stability. High fatigue resistance. Difficult to bond using adhesives and solvents (low surface energy).

Commodity	Engineering	Performance
<p>PO-HI High Impact Polyethylene TS: 19-33 MPa EAB: 40-50% TM: 1.0 GPa LTST: 95-100°C HDT: 60-80°C Cost: ●</p> <p>PVC-P Flexible Polyvinylchloride TS: 8-20 MPa EAB: 20-400% TM: 0.002-0.020 GPa LTST: 50°C HDT: 20°C Cost: ●</p> <p>PVC-U Unplasticized Polyvinylchloride TS: 45-55 MPa EAB: 25-80% TM: 2.50-3.02 GPa LTST: 60-70°C HDT: 64-70°C Cost: ●</p>	<p>PO-OP General Purpose Polyethylene TS: 40-50 MPa EAB: 3-3% TM: 2.3-3.0 GPa LTST: 70-80°C HDT: 72-82°C Cost: ●</p> <p>SBS Styrene-Butadiene-Styrene (Copolymer) TS: 45-52 MPa EAB: 40% TM: 1.8-2.0 GPa LTST: 80°C HDT: 65°C Cost: ●</p> <p>CA Cellulose Acetate TS: 30-55 MPa EAB: 8-50% TM: 1.5 GPa LTST: 45-70°C HDT: 48-55°C Cost: ●</p>	<p>ABC Acrylonitrile Butadiene Styrene (Copolymer) TS: 45-50 MPa EAB: 3-20% TM: 2.3-2.9 GPa LTST: 80-90°C HDT: 84-95°C Cost: ●</p> <p>SAN Styrene Acrylonitrile (Copolymer) TS: 47-72 MPa EAB: 2.0-10% TM: 2.3-3.0 GPa LTST: 85-90°C HDT: 84-95°C Cost: ●</p> <p>ASA Acrylonitrile Styrene Acrylate (Copolymer) TS: 50-70 MPa EAB: 1.5-4% TM: 2.3-2.9 GPa LTST: 85-100°C HDT: 82-100°C Cost: ●</p> <p>ASA Acrylonitrile Styrene Acrylate (Copolymer) TS: 50-70 MPa EAB: 1.5-4% TM: 2.3-2.9 GPa LTST: 85-100°C HDT: 82-100°C Cost: ●</p> <p>OB Styrene-Butadiene (Copolymer) TS: 20-30 MPa EAB: 20-80% TM: 1.5 GPa LTST: 85-70°C HDT: 70-77°C Cost: ●</p> <p>CP Cellulose Propionate TS: 30-45 MPa EAB: 40-50% TM: 0.7-1.0 GPa LTST: 60-70°C HDT: 45-70°C Cost: ●</p>
<p>PVC-U Unplasticized Polyvinylchloride TS: 45-55 MPa EAB: 25-80% TM: 2.50-3.02 GPa LTST: 60-70°C HDT: 64-70°C Cost: ●</p>	<p>PVC-U Unplasticized Polyvinylchloride TS: 45-55 MPa EAB: 25-80% TM: 2.50-3.02 GPa LTST: 60-70°C HDT: 64-70°C Cost: ●</p>	<p>PC Polycarbonate TS: 60-70 MPa EAB: 10-120% TM: 2.3-2.9 GPa LTST: 150-160°C HDT: 135-140°C Cost: ●</p> <p>PET-G Glycolated Polyethylene terephthalate TS: 80-100 MPa EAB: 10-15% TM: 2.5-3.0 GPa LTST: 120°C HDT: 130°C Cost: ●</p> <p>PVC-U/LX Crosslinked Unplasticized Polyvinylchloride TS: 20-40 MPa EAB: 150% TM: 0.5-1.0 GPa LTST: 70-100°C HDT: 120°C Cost: ●</p> <p>PVC-C Chlorinated Polyvinylchloride TS: 30-40 MPa EAB: 25-45% TM: 0.5-1.0 GPa LTST: 60-100°C HDT: 100°C Cost: ●</p>
<p>PE-HD High Density Polyethylene TS: 10-50 MPa EAB: 400-1000% TM: 1.0-1.4 GPa LTST: 80°C HDT: 40°C Cost: ●</p>	<p>PE-HD High Density Polyethylene TS: 10-50 MPa EAB: 400-1000% TM: 1.0-1.4 GPa LTST: 80°C HDT: 40°C Cost: ●</p>	<p>PAR Polycarbonate TS: 60-70 MPa EAB: 10-120% TM: 2.3-2.9 GPa LTST: 150-160°C HDT: 135-140°C Cost: ●</p> <p>PDU Polybutylene TS: 10-150 MPa EAB: 10-40% TM: 2.3-2.9 GPa LTST: 100-150°C HDT: 180-170°C Cost: ●</p> <p>PEI Polyetherimide TS: 100-150 MPa EAB: 40-60% TM: 2.3-2.9 GPa LTST: 200-210°C HDT: 200-210°C Cost: ●</p> <p>PAI Polyamideimide TS: 100-150 MPa EAB: 2-12% TM: 2.3-2.9 GPa LTST: 200-210°C HDT: 270-280°C Cost: ●</p> <p>PI Polyimide TS: 100-150 MPa EAB: 4-8% TM: 2.3-2.9 GPa LTST: 250-300°C HDT: 280-300°C Cost: ●</p> <p>PBI Polybenzimidazole TS: 100-150 MPa EAB: 2.8-3.0% TM: 4.0-6.0 GPa LTST: 290-400°C HDT: 220°C Cost: ●</p>
<p>PE-LD Low Density Polyethylene TS: 7-20 MPa EAB: 50-400% TM: 0.15-0.30 GPa LTST: 40-70°C HDT: 0°C Cost: ●</p> <p>PE-LD Linear Low Density Polyethylene TS: 14-20 MPa EAB: 50-300% TM: 0.2-1.0 GPa LTST: 44-50°C HDT: 0-14°C Cost: ●</p> <p>PE-HD Medium Density Polyethylene TS: 14-20 MPa EAB: 10-30% TM: 0.25-0.70 GPa LTST: 39-70°C HDT: 0-45°C Cost: ●</p> <p>PMP Polymethyl methacrylate TS: 20-28 MPa EAB: 10-30% TM: 1.0-2.0 GPa LTST: 55-60°C HDT: 45-50°C Cost: ●</p> <p>EVA Ethylene-vinyl Acetate (2-28% VA) TS: 10-18 MPa EAB: 50-700% TM: 0.04-0.14 GPa LTST: 20-22°C HDT: 0-20°C Cost: ●</p> <p>PE-X Crosslinked Polyethylene TS: 10-18 MPa EAB: 300% TM: 0.20-0.30 GPa LTST: 80°C HDT: 40°C Cost: ●</p> <p>PB Polybutene-1 (Polybutene) TS: 12-17 MPa EAB: 300-300% TM: 0.21-0.28 GPa LTST: 110°C HDT: 4-6°C Cost: ●</p> <p>PE-UHMW Ultra High Molecular Weight Polyethylene TS: 30 MPa EAB: 1000% TM: 0.5 GPa LTST: 90°C HDT: 4-6°C Cost: ●</p> <p>PA 11 Polyamide 11 (Nylon 11) TS: 80-90 MPa EAB: 30-40% TM: 1.0-2.0 GPa LTST: 74-140°C HDT: 130-150°C Cost: ●</p> <p>PA 12 Polyamide 12 (Nylon 12) TS: 90 MPa EAB: 20% TM: 1.0-1.8 GPa LTST: 70-80°C HDT: 130°C Cost: ●</p> <p>PPA Polyphosphazene TS: 85 MPa EAB: 2.0% TM: 2.4 GPa LTST: 140°C HDT: 140°C Cost: ●</p> <p>PA 46 Polyamide 46 (Nylon 46) TS: 100 MPa EAB: 10% TM: 3.0 GPa LTST: 130°C HDT: 140-150°C Cost: ●</p> <p>PEK Polyetherketone TS: 100-110 MPa EAB: 2.5-100% TM: 3.1-8.0 GPa LTST: 300-330°C HDT: 140-200°C Cost: ●</p> <p>PEEK Polyetheretherketone TS: 100-110 MPa EAB: 2.5-100% TM: 3.1-8.0 GPa LTST: 300-330°C HDT: 140-200°C Cost: ●</p>		
<p>PE-Chlorinated Chlorinated Polyethylene TS: 12.5 MPa EAB: 300% TM: 0.020 GPa LTST: 80°C HDT: 20°C Cost: ●</p> <p>PE-VLD Very Low Density Polyethylene TS: 3.4-4.0 MPa EAB: 600-700% TM: 0.10-0.30 GPa LTST: 80°C HDT: 0-10°C Cost: ●</p> <p>PP Polypropylene (Copolymer) TS: 33 MPa EAB: 100% TM: 1.0 GPa LTST: 100°C HDT: 40°C Cost: ●</p> <p>PP Polypropylene (Copolymer) TS: 20 MPa EAB: 300% TM: 1.0 GPa LTST: 80°C HDT: 40°C Cost: ●</p>	<p>PE-Chlorinated Chlorinated Polyethylene TS: 12.5 MPa EAB: 300% TM: 0.020 GPa LTST: 80°C HDT: 20°C Cost: ●</p> <p>PE-VLD Very Low Density Polyethylene TS: 3.4-4.0 MPa EAB: 600-700% TM: 0.10-0.30 GPa LTST: 80°C HDT: 0-10°C Cost: ●</p> <p>EMA Ethylene-methyl Acrylate TS: 9-12 MPa EAB: 150-300% TM: 0.03 GPa LTST: 50°C HDT: 0-20°C Cost: ●</p> <p>PBT Polybutylene terephthalate TS: 30-100 MPa EAB: 10-20% TM: 2.0-3.0 GPa LTST: 60-100°C HDT: 100°C Cost: ●</p> <p>PA 6 Polyamide 6 (Nylon 6) TS: 40-50 MPa EAB: 150-200% TM: 1.0-2.0 GPa LTST: 80-100°C HDT: 40-60°C Cost: ●</p> <p>PA 66 Polyamide 66 (Nylon 66) TS: 40-50 MPa EAB: 15-20% TM: 1.5-2.0 GPa LTST: 80-200°C HDT: 40-60°C Cost: ●</p> <p>PA 610 Polyamide 610 (Nylon 610) TS: 40-50 MPa EAB: 10-15% TM: 1.5-2.0 GPa LTST: 80-100°C HDT: 40-60°C Cost: ●</p> <p>PA 612 Polyamide 612 (Nylon 612) TS: 40-50 MPa EAB: 4-6% TM: 2.0-3.0 GPa LTST: 80-100°C HDT: 40-60°C Cost: ●</p> <p>POM Polyoxymethylene (Acetal Homopolymer) TS: 30-100 MPa EAB: 20-10% TM: 1.5-3.0 GPa LTST: 100°C HDT: 100°C Cost: ●</p> <p>POM Polyoxymethylene (Acetal Copolymer) TS: 30-100 MPa EAB: 20-10% TM: 1.5-3.0 GPa LTST: 100°C HDT: 100°C Cost: ●</p>	<p>LCP Liquid Crystalline Polymer (Thermotropic) TS: 90-160 MPa EAB: 30-100% TM: 2.0-3.0 GPa LTST: 200°C HDT: 40-60°C Cost: ●</p> <p>PFA Perfluoroalkoxy TS: 15-20 MPa EAB: 300% TM: 0.60 GPa LTST: 260°C HDT: 40-60°C Cost: ●</p> <p>ECTFE Ethylene-chlorotrifluoroethylene TS: 40-48 MPa EAB: 200% TM: 1.0 GPa LTST: 140-180°C HDT: 40-60°C Cost: ●</p> <p>PCTFE Polychlorotrifluoroethylene TS: 20-40 MPa EAB: 170% TM: 1.0 GPa LTST: 140-150°C HDT: 40-60°C Cost: ●</p> <p>PTFE Polytetrafluoroethylene TS: 17-21 MPa EAB: 140-400% TM: 0.35-0.75 GPa LTST: 260-280°C HDT: 40-60°C Cost: ●</p> <p>EVOH Ethylene-vinyl Alcohol TS: 37-200 MPa EAB: 100-200% TM: 1.0-1.5 GPa LTST: 80-100°C HDT: 40-60°C Cost: ●</p> <p>PEP Fluorinated ethylene-propylene TS: 90-104 MPa EAB: 1-5% TM: 2.0-3.0 GPa LTST: 180-200°C HDT: 40-60°C Cost: ●</p> <p>ETFE Ethylene-tetrafluoroethylene TS: 20-40 MPa EAB: 200-500% TM: 1.0 GPa LTST: 150°C HDT: 40-60°C Cost: ●</p> <p>PVDF Polyvinylidene fluoride TS: 30-50 MPa EAB: 50% TM: 1.0-1.5 GPa LTST: 150°C HDT: 40-60°C Cost: ●</p>

KEY TO MAJOR POLYMER FAMILIES: Styrenes, Polyolefins, Vinyls, Cellulosics, Polyesters, Polyamides, Acrylics, Polycarbonates, Acetals, Polyisophones, Imides, Fluoropolymers

This table is for comparison only and no responsibility can be taken for the accuracy or the use of the information contained herein. Copyright: Tangram Technology Ltd. (www.tangram.co.uk). The table may be freely reproduced for non-profit purposes provided full acknowledgement of the copyright is given. Comments and suggestions for improvement are welcome. Issue 7: February 2008

Typical Properties of Polystyrene HIPS (High Impact Polystyrene)

DETAIL

Description	Value
Material Type	Amorphous Thermoplastic
Chemical Name	PS Polystyrene
Additives	Unfilled
Color	Natural

PHYSICAL

Property	Test	Unit of Measure	Value
Density	ASTM D792	g/cm ³	1.04
	ASTM D792	lb/in ³	0.038
Water Absorption, 24 hrs, Immersion	ASTM D570	% by wt.	0.01

MECHANICAL

Property	Test	Unit of Measure	Value
Tensile Strength	ASTM D68	psi	4000
Tensile Modulus	ASTM D638	psi	260000
Tensile Elongation at Break	ASTM D638	%	55
Flexural Strength	ASTM D790	psi	8700
Flexural Modulus	ASTM D790	psi	280000
Compressive Strength	ASTM D695	psi	7500
Hardness	ASTM D785	NA	Rockwell L56
IZOD Impact-Notched	ASTM D256	ft-lb/in	2

THERMAL

Property	Test	Unit of Measure	Value
Coefficient of Linear Thermal Expansion	ASTM D696	x 10 ⁻⁵ in./in./°F	4.2
Heat Deflection Temp	ASTM D648	°C at 264 psi	92
	ASTM D648	°F at 264 psi	195
Max Continuous Operating Temp		°C	32
		°F	140
Flammability Rating	UL94	NA	HB

ELECTRICAL

Property	Test	Unit of Measure	Value
----------	------	-----------------	-------

Características del Producto

- Excelente desempeño en extrusión de bobinas y termoformage.
- Buenas propiedades mecánicas.
- Alto desempeño en mezcla con GPPS (cristal) en la extrusión de bobinas de uso general.
- Aprobado para uso en contacto con alimento ⁽¹⁾

Propiedades	ASTM				
	Norma	Inglés		Internacional	
		Unidades	Valores	Unidades	Valores
Índice de Fluidez ⁽²⁾	D-1238	g/10min	2.8	g/10min	2.8
Módulo de elasticidad (tracción)	D-638	psi	240.000	Mpa	1.600
Resistencia a la tracción (ruptura)	D-638	psi	3.000	Mpa	20
Elongación (ruptura)	D-638	%	>50	%	>50
Resistencia al impacto CHARPY ⁽³⁾ / IZOD ⁽⁴⁾ @ 23°C	D-256/A	Lbfxf/in	2 ⁽⁴⁾	J/m	105 ⁽⁴⁾
Punto de fusión VICAT ⁽⁵⁾ (B/50)	D-1525	°C	90	°C	90
Temperatura de inflexión (carga) ⁽⁶⁾ (A) @ 264psi / 1,82 MPa	D-648	°C	85	°C	85
Densidad	D-792	g/cm ³	1,06	g/cm ³	1,06
Absorción de agua	D-570	%	0,03	%	0,07

Clasificación conforme UL - 94HB

1. "Resoluciones 51 e 52 da la Agencia Nacional de Vigilancia Sanitaria (105/99 - Brazil e Mercosur)" e FDA USA 21 CFR 177.1640.

2. Ensayo bajo la condición: 200°C / 5 kg.

3. Cuerpo de prueba 127x13x6,3 mm.

4. Cuerpo de prueba moldeado por inyección de 63/12,6/3,5 mm (C/L/E); Rayo de entalle de 0,25R +/- 0,05; Profundidad 2,54 mm.

5. Testeo efectuado con carga de 5kg e temperatura creciente 50°C/h.

6. Cuerpo de proba moldado por inyección de 128/13/6,3 mm (C/L/E). Carga de teste de 264 psi.

OBSERVACIONES

1- Las descripciones, datos e informaciones contenidas en esta hoja técnica son de naturaleza meramente informativa sirviendo de apoyo para la aplicación técnicamente más adecuada del producto. Los datos proveídos son valores típicos para orientación de nuestros clientes no deben ser entendidos como límites de especificación, dado que muchos factores pueden influenciar en los parámetros de las propiedades. En ese sentido, no existe cualquier responsabilidad por su bueno o malo cumplimiento, aparte de que nos abstenemos de garantizar su infalibilidad, o de que su aplicación constituya infracción de cualquier privilegio industrial, propio o de terceros. Para cualquier información o aclaración adicionales, nuestro departamento técnico se pone a la disposición.

2- Este Producto está en conformidad con la Resolución 105/99 de la Agencia Nacional de Vigilancia Sanitaria - ANVISA (Brazil/Mercosur).

DERAKANE 8084 Epoxy Vinyl Ester Resin

January, 2006

High Elongation Tough Epoxy Vinyl Ester Resin

DERAKANE 8084 epoxy vinyl ester resin is an elastomer modified resin designed to offer increased adhesive strength, superior resistance to abrasion and severe mechanical stress, while giving greater toughness and elongation. DERAKANE 8084 and DERAKANE 8090 resins are the only vinyl esters available that offer this exceptional combination of properties.

Typical Liquid Resin Properties

Property ⁽¹⁾	Value
Density, 25°C/77°F	1.02 g/mL
Dynamic Viscosity, 25°C/77°F	360 mPa·s
Kinematic Viscosity	350 cSt
Styrene Content	40%
Shelf Life ⁽²⁾ , Dark, 25°C/77°F	6 months

- (1) Typical property values only, not to be construed as specifications.
 (2) Unopened drum with no additives, promoters, accelerators, etc. added. Shelf life specified from date of manufacture.

Applications and Fabrication Techniques

- DERAKANE 8084 resin is the resin of choice as a primer to prepare a substrate surface (steel or concrete) for application of a corrosion resistant lining.
- DERAKANE 8084 resin can be use for RTM, hand-lay, spray-up, filament winding and other industrial FRP applications.

Benefits

- DERAKANE 8084 resin has exhibited chemical resistance across a broad range of acids, bases and organic chemicals.
- Resin of choice as a primer to prepare a substrate surface for application of a corrosion resistant lining. It exhibits outstanding adhesive strength on different types of steel, aluminum and concrete.
- Superior elongation and toughness provides FRP equipment with better impact resistance and less cracking due to cyclic temperature, pressure fluctuations and mechanical shocks providing a safety factor against damage during process upsets or during shipping and installation.
- Has exhibited superior property retention under dynamic fatigue conditions.
- Approved for use in the manufacture of ships under a DNV (Det Norske Veritas) certificate.



Ashland is committed to the continuous evolution of technology and service solutions that promote health, safety and environmental protection around the world.

All statements, information and data presented herein are believed to be accurate and reliable but are not to be taken as a guarantee, express warranty or implied warranty of merchantability or fitness for a particular purpose, or representation, express or implied, for which seller assumes legal responsibility, and they are offered solely for your consideration, investigation and verification. Statements or suggestions concerning possible use of this product are made without representation or warranty that any such use is free of patent infringement and are not recommendations to infringe on any patent.

Distributed by
 Freeman Manufacturing & Supply Co.
 www.freemansupply.com (800) 321-8511
Registered trademark and TM trademark of Ashland Inc.
 * Registered service mark of the American Chemistry Council
 © 2002, 2004 Ashland Inc. All Rights Reserved. • CWT-DS-344 Rev. 1



ASHLAND

HSK

HSK - Hand Welding Extruders and Bending Technology

Hand welding extruder HSK26 GSX Pellet-Fed (Granulate)



BASIC EXTRUDER		
<ul style="list-style-type: none"> • Extrusion welding from PE, PP, PVC and PVDF • Temperature probe, location in the melt chamber • Control units for actual/ desired mass and air temperature and actual speed • Permanent speed control • Cold start protection • 1 pce nozzle blank included • Speedcontrol 		
TECHNICAL DATA		DIMENSIONS
Output	2.5 kg/h (with PE pellets)	600 x 200 x 430 mm
Heating extruder	700W / air 2300W	23.5 x 8 x 17 in
Drive	740W	
Air requirement	300 l/min	
Voltage	230V 50Hz	
Weight	7.4 kg or 16 lbs	
Guarantee	Screw and cylinder 24 months	
HSK26 GSX (WITH HOT AIR BLOWER)		
<ul style="list-style-type: none"> • Works as basic extruder, without external air supply • Hot air blower controlled (air quantity 300 l/min) • Technical data see basic extruder • Heating hot air blower 2300W 		
ADDITIONAL EQUIPMENT		
<ul style="list-style-type: none"> • Welding nozzles • Transportation box • Widen 	<ul style="list-style-type: none"> • Extruder nozzle preheating Prolongation 	<ul style="list-style-type: none"> • Angle adaptor • Air compactor
Technical execution subject to modifications		

8

HSK/PWS North America, Inc.
 at Abbeon Cal, Inc.
 1363 Donlon Street Unit 1, Ventura, CA 93003

805-676-0720 / 800-922-0977
 www.hsk-pws.com
 E-Mail: sales@abbeon.com

3805 ELECTRONIC DUROMETER

Starrett®

METROLOGY SOLUTIONS

The 3805 Durometers are designed to test the hardness of rubbers and plastics. These sleek hand held hardness testers are crafted and engineered to perform at the highest level of accuracy. An ergonomic, lightweight design assists in taking precise and consistent hardness measurements.

Shore A scale is for testing the following materials:

Rubber: Soft vulcanized (je tire), natural, nitrile Elastomeric materials (rubber & rubber like): GR-S, GR-1, neoprene, thiokol, flexible polyacrylic esters.

Other: Wax, felt, leather etc. (materials that normally yield under fingernail pressure, such as the heel on your shoe).

Shore D scale is for testing the following materials:

Rubber: Hard

Plastics: Harder grades such as rigid thermoplastics, plexiglass, thermoploystrene, vinyl sheet, cellulose acetate, thermosetting, laminates (je formica)

Other: Printing rolls, densified wood, etc. (materials that would not normally indent under fingernail pressure, such as a pocket comb or bowling ball).

FEATURES AND SPECIFICATIONS (3805B & 3805D)

- Measuring range: 0-100
- Deviation: <1%H
- Resolution: 0.5H
- Digital read out
- Auto Hold feature
- Accurate and repetitive deviation = 20-90HSA HSA<+/-1grade
- Uses 1-SR44 Button Cell Battery
- Storage case

3805 Electronic Durometer

Description	Cat. No.	EDP
3805B Shore A Scale Electronic Durometer in plastic case	3805B	69882
Shore A 3 Rubber Test Block Certified Set	SRB-3	68200
3805D Shore D Scale Electronic Durometer in plastic case	3805D	02069



Bulletin 400

Starrett

PDF 07/19 specifications subject to change.

starrett.com

SJ-210 Series Specifications

Specifications

Type of detector	Standard drive unit type		Retractable drive unit type		Transverse tracing drive unit type	
	SJ-210 (0.75 mN type)	SJ-210 (4 mN type)	SJ-210 (0.75 mN type)	SJ-210 (4 mN type)	SJ-210 (0.75 mN type)	SJ-210 (4 mN type)
Model No.	inch/mm	178-561-11A	178-561-12A	178-563-11A	178-563-12A	178-565-11A 178-565-12A
X axis		.63" (16.0mm)			.22" (5.6mm)	
Measuring range	Range	14400 μm (-7900 μm to +6300 μm) [360 μm (-200 μm to +160 μm)]				
	Z axis (Detector) Range/Resolution	14400 μm / .8 μm (360 μm / 0.02 μm) 4000 μm / .2 μm (100 μm / 0.005 μm) 1000 μm / .08 μm (25 μm / 0.002 μm)				
Measuring speed		When measuring: 0.01, 0.02, 0.03 in/s (0.25mm/s, 0.5mm/s, 0.75mm/s) When returning: 04 in/s (1mm/s)				
Measuring force/Stylus tip		0.75 mN / 2 μmR 60°, 4 mN / 5 μmR 90°				
Skid force		Less than 400 mN				
Applicable standards		JIS '82/JIS '94/JIS '01/ISO '97/ANSI/VDA				
Assessed profiles		Primary profile, Roughness profile, DF profile, Roughness profile-Motif				
Parameters		Ra, Rc, Ry, Rz, Rq, Rt, Rmax ¹ , Rp, Rv, Rz, Rsk, Rku, Rv, Rq, Rsm, Rz1max ² , S, HSC, RzIS ³ , Rppi, R Δ a, R Δ q, Rf, Rmc, Rmr(c), R Δ c, Rk, Rpk, Rvk, Mr1, Mr2, A1, A2, Vo, Rpm, tp ⁴ , Htp ⁴ , R, Rx, AR, Possible Customize				
Graph analysis		Beating area curve/Amplitude distribution curve				
Filters		Gaussian, 2CR75, PC75				
Cut off length	λ c	0.003, 0.01, 0.03, 0.1" (0.08, 0.25, 0.8, 2.5mm)				
	λ s ⁵	100, 300μm (2.5, 8μm)				
Sampling length		0.003, 0.01, 0.03, .1" (0.08, 0.25, 0.8, 2.5mm)				
Number of sampling lengths (xn)		x1, x2, x3, x4, x5, x6, x7, x8, x9, x10, Arbitrary 0.01~.63" (.0001" interval) [0.3~16.0mm: 0.01mm interval]			x1, x2, x3, x4, x5, x6, x7, x8, x9, x10, Arbitrary .0118 ~ .22" (.0001" interval) [(0.3 ~ 5.6mm: 0.01mm interval)]	
LCD dimensions		1.45 x 1.93" (36.7x48.9 mm)				
Display languages		Japanese, English, German, French, Italian, Spanish, Portuguese, Korean, Traditional Chinese, Simplified Chinese, Czech, Polish, Hungarian, Turkish, Swedish, Dutch				
Measurement result display		Vertical display: 1-parameter display/3-parameter display/Trace display Horizontal display: 1-parameter display/4-parameter display/Trace display (Horizontal display is invertible)				
Printing function ⁶ (Dedicated printer is required separately.)		Measurement conditions/Calculation results/GO/NG judgement result/Calculation results for each sampling length/ Assessed profile/Bearing area curve/Amplitude distribution curve/Environment setting information				
External I/O		USB I/F, Digimatic Output, Printer Output, RS-232C I/F, Foot SW I/F				
Functions	Customization	Desired parameters can be selected for calculation and display				
	GO/NG judgment ⁷	By max value/16 % /Standard deviation				
	Storage of measurement condition	Save the conditions at power OFF				
Storage		Internal memory: Measurement condition (10 sets) Memory card (Option): 500 measurement conditions, 10000 measured profiles, 500 display images Text file (Measurement conditions/Measured profile/Assessed profile/ Bearing area curve/Amplitude distribution curve)				
	Calibration	Auto-calibration with the entry of numerical value/ Average calibration with multiple measurement (Max.5 times) is available				
Power-saving function		Auto-sleep off function (10~600 sec) ⁸				
Power supply		Two-way power supply: battery (rechargeable Ni-MH battery) and AC adapter Note 1: Charging time: about 4 hours (may vary due to ambient temperature) Note 2: Endurance: about 1000 measurements (differs slightly due to use conditions/environment)				
Size (WxDxH)	Display unit	2.05 x 2.6" x 6.3" (52.1x65.8x160mm) (sliding cover closed, detector not mounted)				
	Drive unit	4.5 x .9 x 1.02" (115x23x26mm) (detector not mounted)				
Mass		About 1.1lbs (500g) (Display unit + Drive unit + Standard detector)				
Standard accessories		12BA303 Connecting cable ⁹ 178-601 Roughness specimen Ra (3 μm) 12BAR344 Carrying case 12BAK700 Calibration stage Protective sheets for display, AC Adapter, Operation manual, Quick reference manual, Warranty			12BA303 Connecting cable ⁹ 178-606 Roughness specimen Ra (1 μm) 12AAE643 Point-contact adapter 12AAE644 V-type adapter 12BAR344 Carrying case 12BAK700 Calibration stage Protective sheets for display AC Adapter, Operation manual, Quick reference manual, Warranty	

*1 Calculation is available only when selecting the VDA, ANSI or JIS '82 standard.
 *2 Calculation is available only when selecting the ISO '97 standard.
 *3 Calculation is available only when selecting the JIS '01 standard.
 *4 Calculation is available only when selecting the ANSI standard.
 *5 Not available when selecting the JIS '82 standard.
 *6 Order the SJ-210 printer (178-421, optional accessory) separately. See page 19 for details about the SJ-210 printer.
 *7 Standard deviation only can be selected in ANSI. 16 % rule cannot be selected in VDA.
 *8 Auto-sleep function is invalid when AC adaptor is used.
 *9 For connecting the calculation display unit and drive unit.
 Note: To denote your AC line voltage add the following suffixes (e.g. 178-560-11A).
 A for 120 V, C for 100 V, D for 230 V, E for 230 V (for UK), DC for 220 V (for China), K for 220 V (for Korea)

Members of the Committee

Dr. Wilhelm Friess, Advisor

Dr. Friess is a Professor of Mechanical Engineering at the University of Maine where he directs the capstone experience and teaches courses in aircraft design and engineering mechanics. He received his Ph.D. in Aeronautical Engineering from Rensselaer Polytechnic Institute in 1997. His primary research areas include engineering design, with applications in unmanned aerial vehicles, aerodynamics, energy, and sports, as well as engineering education.



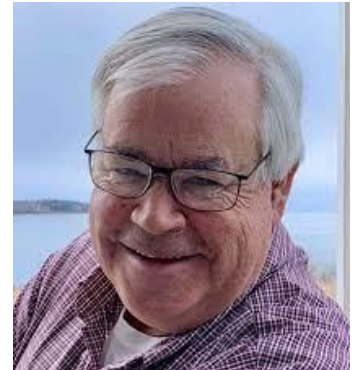
Dr. Bashir Khoda

Dr. Khoda is an Associate Professor of Mechanical Engineering at the University of Maine where he teaches computer-aided design and manufacturing. He received his Ph.D. in Industrial and Systems Engineering at the University at Buffalo in 2013. His primary research areas include additive manufacturing, digital manufacturing, computer-aided design, and bio-manufacturing.



Mr. Steve Nolet

Mr. Nolet is Senior Director, Innovation & Technology and Principal Engineer at TPI Composites in Warren, Rhode Island. Steve received his M.S. in Aeronautical Engineering from the Massachusetts Institute of Technology in 1984. He manages the research and development of low-cost composite structures for the TPI's three primary business units: wind energy, military ground vehicles, and transportation systems.



EERE Project Principal Investigator

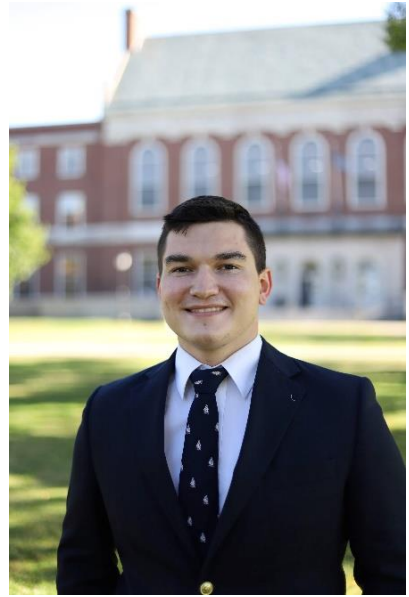
John Arimond, Principal Investigator

Mr. Arimond is the Business Development Manager at the Advanced Structures and Composites Center at the University of Maine. He received his M.S. in Mechanical Engineering from the Massachusetts Institute of Technology in 1984. John leads EERE-funded research in the application of large-scale AM to the fabrication of rapid, low-cost wind blade tooling.



Biography of the Author

Chase Colby Flaherty was born in Damariscotta, Maine on December 17th, 1998, and was raised in Tenants Harbor, Maine. He graduated from Oceanside High School in 2017. He attended the University of Maine and graduated in 2021 with a bachelor's degree in mechanical engineering. Upon graduation, he continued at the University of Maine within the Mechanical Engineering graduate program and pursued his M.S. at the Advanced Structures and Composites Center (ASCC). After receiving his degree, Chase will be joining Compotech, Inc., a leading defense manufacturing and technology company based out of Brewer, Maine, to begin his career in the field of composites manufacturing research and development.



Chase is a candidate for the Master of Science degree in Mechanical Engineering from the University of Maine in May of 2023.